

Copy 274
RM E50J26a

NACA RM E50J26a

E 50 J 26a

NACA



RESEARCH MEMORANDUM

6399

FORCE AND PRESSURE CHARACTERISTICS FOR A SERIES OF NOSE
INLETS AT MACH NUMBERS FROM 1.59 TO 1.99

II - ISENTROPIC-SPIKE ALL-EXTERNAL COMPRESSION INLET

By L. J. Obey and G. W. Englert

Lewis Flight Propulsion Laboratory
Cleveland, Ohio

REF ID: A6471
~~CLASSIFIED DOCUMENT~~
This document contains neither recommendations nor conclusions of the National Defense Research Commission or the Defense Department. It is the property of the United States Government and is loaned to your agency; it and its contents are not to be distributed outside your agency without the express permission of the Director, Defense Research Commission. Distribution outside your agency by your agency or by any other person, without the express permission of the Director, Defense Research Commission, is illegal under Title 18, United States Code, Section 793 and 794, and is subject to prosecution under the law.
Information so classified may be imparted only to persons in the military and naval services of the United States and of the Commonwealth of Australia who have a legitimate interest thereon.

NATIONAL ADVISORY COMMITTEE
FOR AERONAUTICS

WASHINGTON
February 9, 1951

519.98/13



0143211

1

NACA RM E50J26a

2035

~~CONFIDENTIAL~~

NATIONAL ADVISORY COMMITTEE FOR AERONAUTICS

RESEARCH MEMORANDUMFORCE AND PRESSURE CHARACTERISTICS FOR A SERIES OF NOSE
INLETS AT MACH NUMBERS FROM 1.59 TO 1.99

II - ISENTROPIC-SPIKE ALL-EXTERNAL COMPRESSION INLET

By L. J. Oberry and G. W. Englert

SUMMARY

An experimental investigation to determine the external and internal flow characteristics of a typical ram-jet-inlet configuration of an external-compression type utilizing an isentropic spike and a subsonic diffuser was conducted in the NACA Lewis 8- by 6-foot supersonic wind tunnel. The model was investigated over a range of mass-flow ratios at angles of attack up to 10° , free-stream Mach numbers of 1.59, 1.79, and 1.99, and a Reynolds number of approximately 2.4×10^6 based on inlet diameter.

Comparison of the results at zero angle of attack with various theories shows that the skin-friction and additive-drag components were predicted at all mass-flow ratios and extrapolation of the experimental pressure-drag curves showed close agreement with the theoretical value predicted at a mass-flow ratio of unity. The variation of the lift- and pitching-moment coefficients with angle of attack were predicted reasonably well at the critical mass-flow ratios; however, the incremental drag due to angle of attack was considerably underestimated.

The experimental investigation showed that the drag coefficient decreased with increasing mass-flow ratio, increased with free-stream Mach number at a given mass-flow ratio, and decreased with increasing free-stream Mach number at critical mass-flow ratios. These trends were largely due to the variation of the additive drag component with mass-flow ratio and free-stream Mach number.

Longitudinal pressure distributions measured over the external surface of the model at various mass-flow ratios and several angles of attack show that the most severe effects of these variables on the pressure distributions extend approximately 1.5 diameters downstream of the cowl lip.

Shock oscillation occurred at the two higher Mach numbers and increased in severity with angle of attack and free-stream Mach number.

~~CONFIDENTIAL~~

C-4/2 81

2035

INTRODUCTION

Internal and external aerodynamic characteristics of a series of supersonic inlets operating without heat addition were investigated in the NACA Lewis 8- by 6-foot supersonic wind tunnel.

The data presented herein were obtained from the investigation of an all-external, isentropic-compression-type inlet operating over a range of mass-flow ratios, at angles of attack from 0° to 10° , Mach numbers 1.59, 1.79, and 1.99, and an average Reynolds number of 2.4×10^6 based on inlet diameter.

The purposes of this investigation were: (1) to experimentally determine the pressure, force, and moment characteristics of a typical inlet configuration, and (2) to correlate these results with existing theory where possible.

SYMBOLS

The following symbols are used in this report:

- | | |
|-------|----------------------------------------------------------------|
| C_D | drag coefficient, $D/q_0 S_m$ |
| C_F | skin-friction drag coefficient based on wetted area |
| C_L | lift coefficient, $L/q_0 S_m$ |
| C_M | pitching-moment coefficient about base of model, $G/q_0 S_m l$ |
| C_p | pressure coefficient, $\frac{p-p_0}{q_0}$ |
| D | drag |
| d | diameter at area of maximum cross section, 0.677 foot |
| G | pitching moment about base of model |
| L | lift |
| l | length of model, 4.96 feet |
| M | Mach number |
| m | mass flow |

2035

P total pressure
p static pressure
q $\gamma p M^2 / 2$
S cross-sectional area
 S_c inlet capture area defined by cowl lip, 0.1920 square foot
 S_m maximum cross-sectional area, 0.3601 square foot
U velocity
u velocity in boundary layer
 x, r, θ cylindrical coordinates
y distance from model surface
 α angle of attack
 γ ratio of specific heats, 1.40
 δ boundary-layer thickness

Subscripts:

a additive
f friction
l local
p pressure
0 free stream
1 cowl lip
2 station at $x = 7.558$ inches
3 combustion-chamber inlet
5 minimum area at plug

APPARATUS AND PROCEDURE

A photograph of the pressure model is shown in figure 1. The force model was geometrically identical to the pressure model except that the pressure-tube conduits and the boundary-layer rake were removed. Aft of station 7.875 (fig. 2(a)), the model and the apparatus used in this investigation were identical to the equipment reported in reference 1. The spike (fig. 2(c)) was designed to produce an infinite number of infinitesimal compression waves and was so placed that the point of coalescence of the compression waves would occur ahead of the cowl lip at Mach number 1.8. (See reference 2.) The cowl (fig. 2(b)) had a blunt, subsonic leading edge as shown in detail A in figure 2. Coordinates for the model are presented in table I.

The axial variation of geometric area ratio was calculated in the manner described in reference 1 and is shown in figure 3. The reduction in area ratio from $x/D = 0$ to 0.375 was associated with the design condition of subsonic flow entering the inlet and the constant-area region from $x/D = 0.375$ to 0.500 was included to permit stabilization of the boundary layer before the beginning of subsonic compression. Reference stations throughout the model and other terms are defined in figure 4.

The instrumentation of both force and pressure models was identical to that of reference 1, except that the total-pressure rakes at the leading edge of the struts were omitted. The locations of the various pressure tubes are given in table II.

Both models were investigated at Mach numbers of 1.59, 1.79, and 1.99, angles of attack from 0° to 10° , and over a range of mass-flow ratios. The Reynolds number based on inlet diameter (0.495 ft) varied from 2.3×10^6 to 2.5×10^6 .

One of the basic parameters for the analysis of the data is considered to be the mass-flow ratio. The mass-flow ratio is defined as the ratio of the air entering the engine to the air in a free-stream tube having a diameter equal to the cowl diameter of 5.912 inches.

Calculation of the mass flow through the engine was based on choking at the exit plug at the geometric exit area and the total pressure measured in the combustion chamber. A correction factor of 0.98, based on subsequent calibration of the diffuser and on the mass flow calculated by the method of reference 3, was then applied to the data.

RESULTS AND DISCUSSION

External-Flow Characteristics

Zero angle of attack. - The variation of the drag coefficient with mass-flow ratio is presented in figure 5 for three Mach numbers and zero angle of attack. The drag coefficient was defined to include all the forces parallel to the flight direction acting on the external body surface and on the outermost entering streamline. As figure 5 shows, the drag coefficient increased rapidly at all Mach numbers as the mass-flow ratio decreased, and at a given mass-flow ratio the drag coefficient increased with Mach number. The drag at critical mass flow, however, decreased with increasing Mach number. This decrease is shown more clearly in figure 6 by the variation of minimum drag coefficient with Mach number. In order to provide an understanding of the variations noted in the total drag, the variations of the components of pressure, skin friction, and additive drags are separately analyzed.

The variation of the pressure-drag coefficient with mass-flow ratio for three Mach numbers and zero angle of attack is presented in figure 7. The pressure-drag coefficient was obtained by graphical integration of measured static pressures over the external portion of the body. Theoretical values for a mass-flow ratio of 1 were determined from theoretical pressure distributions obtained by the method of references 4 and 5, with the assumption that the small region of transonic flow about the 0.016-inch radius of the cowl lip had a negligible effect on the remaining flow field. Extrapolation of the experimental curves to a mass-flow ratio of unity indicates good agreement between experiment and theory.

The experimental pressure-drag coefficients increased with free-stream Mach number at a given mass-flow ratio and decreased with decreasing mass-flow ratio, all having attained a negative value at mass-flow ratios less than 0.65. The negative pressure drag resulted from regions of high acceleration about the inlet, the extent and the magnitude of which are shown in figure 8 where the axial pressure distributions for a range of mass-flow ratios and three Mach numbers are presented. Figure 8 shows that the low pressures produced by the high acceleration extended approximately 1.5 diameters downstream of the lip. The decrease in the pressure coefficients between diameter ratios x/d of 4 and 5 resulted from the change in slope of the external surface, whereas the decrease at $x/d \approx 2$ and 3.25 for free-stream Mach numbers of 1.79 and 1.99, respectively, were due to weak tunnel disturbances. Also plotted in figure 8 are the theoretical pressure distributions calculated for mass-flow ratios of 1.0. These

curves indicate the limiting value of the pressure loading as the mass-flow ratio approached unity. Additional pressure-distribution data are presented in tables III to VI.

The variation of skin-friction drag coefficient with mass-flow ratio is presented in figure 9. The friction drag was computed by the method of reference 6 based on the change in momentum in the boundary layer corrected for the loss across the inlet shock. Sample calculations showed that, for high mass-flow ratios, exclusion of the effect of the pressure gradient over the forward portion of the model surface increased the momentum decrement by an amount corresponding to approximately 1.5 percent of the friction-drag coefficient. In view of this small quantity, no pressure-gradient corrections were applied to the data.

As shown in figure 9, the skin-friction drag coefficient was essentially independent of mass-flow ratio and decreased only slightly between Mach numbers 1.59 and 1.79. The measured friction-drag coefficients are compared in figure 10 with values calculated by the method of reference 7. The good agreement indicates that two-dimensional theory predicts the friction drag on this model.

Representative boundary-layer profiles are plotted in figure 11. For a given free-stream Mach number, the decrease in local Mach number as the mass-flow ratio decreased corresponded to the increased losses across the bow wave, as discussed in reference 6.

The boundary layer was assumed to extend to the points marked on the curves of figure 11 in the vicinity of $y = 0.6$. Reducing the data in the assumed boundary layer to the more usual form, as presented in figure 12, shows that the profiles follow closely the $1/7$ th power law.

The variation of additive drag coefficient with mass-flow ratio is presented in figure 13. The additive drag was calculated as the momentum change from free-stream conditions to station 7.558 (flow stations 0 to 2). The theoretical curves were obtained from the one-dimensional analysis presented in reference 8, modified at Mach number 1.59 to account for supersonic additive drag. The theoretical calculations were based on a 20° conical spike instead of the actual curvature of the spike. As figure 13 shows, the additive drag rapidly increased with decreasing mass-flow ratio and increased with free-stream Mach number for a fixed mass-flow ratio. Except in the region of shock oscillation, the agreement with the theoretical curve is reasonable.

2035

A comparison of the sum of the drag components determined from the pressure data with the measured total drag from the balance is presented in figure 14 and shows excellent agreement in all but the shock-oscillation region. The components of drag show that the increase in drag with decreasing mass-flow ratio is largely caused by the increase in additive drag. Also, most of the increase in drag with Mach number for a constant mass-flow ratio can be attributed to an increase in additive drag.

Angle of attack. - The variation of total-drag coefficient with mass-flow ratio for various angles of attack and for three Mach numbers is shown in figure 15. For a given free-stream Mach number and mass-flow ratio, the drag coefficient increased with angle of attack. This trend was largely due to an increase in the drag component of the normal force, inasmuch as calculations not included in this report show that the axial force coefficient was approximately constant and thus contributed little to the change in drag coefficient with angle of attack. Shock oscillation increased in severity with angle of attack and Mach number and apparently caused a decrease in drag coefficient; however, because of the unreliability of the data (particularly the mass flow) in this region, no conclusions are warranted.

The lift and pitching-moment coefficients were defined to include only the effects of the external flow over the body and were calculated by subtracting the internal forces and moments from the measured data. The lift-and pitching-moment coefficients are presented in figures 16 and 17, respectively, as functions of mass-flow ratio.

An additive lift and thus also an additive pitching moment are present when there is spillage over the cowl at angles of attack. These components are due to deflection of the entering streamlines in the region between the inlet-shock configuration and the cowl lip. The additive effects are included in both coefficients, inasmuch as it was impossible to determine them with the existing instrumentation. The measured pitching-moment coefficient was reduced by assuming that the turning of the internal flow from the free-stream direction to the angle of attack of the body occurred at the cowl lip, thus determining the location of the normal force produced by the internal flow. Although this assumption is not strictly true, it is probably within the accuracy of the measurements. Both lift and pitching moment tended to decrease slightly with decreasing mass-flow ratio at all angles of attack. This decrease is due to the change in mass flow spilled over the engine because only the external flow contributed to either coefficient.

As with other data, shock oscillation at times produced erratic variations in both lift and pitching moment and no conclusions were drawn from the data in these regions. The center of pressure locations, as shown in figure 18, were quite erratic in the oscillation regions, but generally were located approximately 4.5 to 5 diameters ahead of the base.

The variation of the aerodynamic characteristics with angle of attack at critical mass flow is presented in figure 19; also presented for a mass-flow ratio of 1.00 is the theoretical variation of lift, increment of drag, and pitching moment with angle of attack, as calculated by the method of reference 9, modified for an open-nose body and assuming no end effects. Theory reasonably well predicted the lift and pitching moment variation but appreciably underestimated the increment of drag due to angle of attack.

A typical variation of pressure distribution over the top and bottom surfaces of the model is shown in figure 20 for the four angles of attack at critical conditions. The increased pressure coefficient over the bottom surface of the body due to angle of attack extends over the length of the body; however, cross-flow separation over the top surface starting at $x/D = 1.5$ to 2.0 is indicated because the pressure coefficient is approximately zero and independent of angle of attack. The dip in the curves between $x/D = 4$ and 5 resulted from the change in slope of the body. Pressure coefficients for other operating conditions are presented in tables III to VI.

Representative schlieren photographs shown in figure 21 illustrate the change in shock configuration with angle of attack for the three Mach numbers at critical mass-flow ratios. The bow wave at radii greater than the cowl lip shows little change in curvature or orientation with respect to the free stream as the angle of attack is varied. The shock configuration on the cone and at radii less than the cowl radius is appreciably changed and regions of separation on the upper part of the cone surface are apparent.

Oscillation of the normal shock ahead of the cowl occurred at Mach numbers of 1.79 and 1.99 in the subcritical regime, as shown in the schlieren high-speed motion picture films of figure 22. At zero angle of attack and a mass-flow ratio of approximately 0.42 (fig. 22(a)), one type of oscillation is shown. Some of the frames in the sequence shown have been deleted. The actual cycles consisted of a movement of the normal shock to the tip, as shown in frames 1 to 4, three short pulses of the type shown in frames 4 to 8, and a return of the shock to its original position (frames 9 to 23). The frequency of this cycle has been estimated at 50 oscillations per second. At an angle of attack of 3° and a lower mass-flow ratio, a single pulse oscillating at approximately 230 cycles per second was observed (fig. 22(b)). No

2035

frames have been omitted from this sequence. Both figures 22(a) and 22(b) show that separation occurred at the spike and increased in magnitude as the bow wave progressively moved forward of the cowl lip. The oscillation data are not considered numerically reliable, but were presented as dashed lines in the figures to show some of the qualitative effects of shock oscillation. The occurrence of shock oscillation differed in the two models. For example, at zero angle of attack and Mach numbers 1.79 and 1.99, shock oscillation occurred in the pressure model but not in the force model. Slight differences in instrumentation and test conditions may account for this phenomenon.

Internal-Flow Characteristics

Zero angle of attack. - The variation of total-pressure recovery and combustion-chamber Mach number with mass-flow ratio is shown in figure 23. The measured total pressure P_3 was corrected to conform with the static pressure measured in the combustion chamber and the mass flow. The combustion-chamber Mach number presented was calculated assuming isentropic expansion from the annular area of the combustion chamber to the cross-sectional area of the combustion chamber with the sting removed. The total-pressure recovery was approximately constant with mass-flow ratio in the subcritical range at Mach number 1.59, but decreased slightly for the higher Mach numbers due to shock oscillation.

The peak recovery was somewhat lower than that obtained in reference 2, because the spike location of this inlet was not optimized for maximum pressure recovery but was compromised to obtain low drag and reasonably high pressure recovery.

A breakdown of the measured total-pressure losses into inlet and subsonic-diffuser losses is presented in figure 24 as a function of mass-flow ratio. The almost constant pressure recovery in the subcritical regime may be attributed to the fact that as the mass flow was decreased, the supersonic losses $\Delta P_{0,2}/P_0$ increased at approximately the same rate that the subsonic losses $\Delta P_{2,3}/P_0$ decreased. At critical mass flow, the subsonic losses accounted for approximately 5 percent of the available total pressure for all Mach numbers.

The performance of the subsonic diffuser is presented in figure 25 in terms of total-, static-, and dynamic-pressure parameters. The total-pressure recovery for the subsonic diffuser P_3/P_2 was approximately independent of Mach number in the stable portion of the subcritical regime; however, the total-pressure loss expressed in

terms of the dynamic pressure $\Delta P/q_2$ increased with free-stream Mach number. This increase is believed to result from differences in inlet boundary-layer conditions (reference 10). Subsequent subsonic-diffuser studies indicate that approximately 4 percent of the total available pressure was lost due to the support struts.

The Mach-number profiles, as determined by the combustion-chamber rakes, are shown in figure 26 at six circumferential stations. As the mass flow decreased the profiles measured by the four side rakes approached the profiles determined by the top and bottom rakes, indicating that the wake effects of the support struts decreased with decreasing mass-flow ratio.

Angle of attack. - The total-pressure recovery and the combustion-chamber Mach number were independent of angle of attack up to 6° (fig. 27) at Mach number 1.59. At an angle of attack of 10° and a Mach number of 1.59, the pressure recovery was reduced approximately 1 percent and no effect was noted in the combustion-chamber Mach number. At Mach numbers 1.79 and 1.99 and moderate angles of attack, however, shock oscillation was encountered and a severe reduction in total-pressure recovery resulted. Angles of attack up to and including 6° reduced the maximum amount of mass flow available to the diffuser by the reduction in inlet area (that is, by the cosine of the angle of attack). At an angle of attack of 10° , however, a reduction in mass flow larger than that due to the reduction in projected inlet area was attained, probably due to choking in the upper quadrant, as mentioned in reference 1.

The internal-pressure distribution curves presented in figure 28 show that the pressure coefficient over the bottom surface of the diffuser was approximately independent of angle of attack up to and including 6° , but a pronounced variation is noted at an angle of attack of 10° similar to the tendency previously noted in the mass-flow ratio. The distribution over the top surface shows that the tendency to choke in the region of the struts ($x/D = 1.35$) increased with increasing angle of attack. As shown in figure 29, the total pressure, in general, was higher over the top half of the combustion-chamber inlet than over the bottom half. Measurements obtained with wall orifices located on the bottom of the spike ($r/r_3 = 0.38$) were nearly the same as the static-pressure measurements made near the center of the flow channel. As the static pressure was nearly constant at this survey station, the trends of the total-pressure curves are an indication of the relative amounts of mass flow per unit area at various parts of the survey. This criterion also indicated a greater mass flow through the top half of the combustion-chamber inlet than through the bottom.

2035
SUMMARY OF RESULTS

The external- and internal-flow characteristics of an isentropic spike all-external compression inlet were investigated in the NACA Lewis 8- by 6-foot supersonic wind tunnel. The investigation was conducted through a range of mass-flow ratios and angles of attack at Mach numbers of 1.59, 1.79, and 1.99 and at an average Reynolds number of 2.4×10^6 based on inlet diameter. From this investigation the following results were obtained:

1. The total-drag coefficient of the inlet rapidly increased with decreasing mass-flow ratio, increased with free-stream Mach number at a given mass-flow ratio, and decreased with increasing free-stream Mach number at critical mass-flow ratio, largely due to the contribution of the additive drag coefficient.
2. Extrapolation of the experimental pressure-drag coefficient to the condition of no mass-flow spillage indicated close agreement with the value determined by linearized potential theory at zero angle of attack.
3. The skin-friction drag showed good agreement with the theoretical value obtained from von Kármán's turbulent boundary-layer theory assuming two-dimensional compressible flow.
4. The additive drag was reasonably well predicted from one-dimensional flow considerations.
5. Lift and pitching moment slightly decreased with decreased mass flow at all angles of attack. The lift and pitching-moment coefficients at critical mass-flow ratio were predicted reasonably well; however, the increment of drag due to angle of attack was considerably underestimated. Calculations show that the experimentally determined axial-force coefficient was independent of angle of attack.
6. Mass-flow ratio markedly affected the pressure distribution over the external cowl surface for the first 1.5 diameters downstream of the cowl lip. Cross-flow separation due to angle of attack was experienced over the rearward portion of the top surface of the body.
7. Increasing angle of attack and Mach number increased the severity of the shock oscillations with the apparent increases in total-pressure losses.

Lewis Flight Propulsion Laboratory,
National Advisory Committee for Aeronautics,
Cleveland, Ohio.

REFERENCES

1. Esenwein, Fred T., and Valerino, Alfred S.: Force and Pressure Characteristics for a Series of Nose Inlets at Mach numbers from 1.59 to 1.99. I - Conical Spike All-External Compression Inlet with Subsonic Cowl Lip. NACA RM E50J26.
2. Moeckel, W. E., and Connors, J. F.: Investigation of Shock Diffusers at Mach number 1.85. III - Multiple-Shock and Curved-Contour Projecting Cones. NACA RM E7F13, 1947.
3. Moeckel, W. E.: Approximate Method for Predicting Form and Location of Detached Waves Ahead of Plane and Axially Symmetric Bodies. NACA TN 1921, 1949.
4. Brown, Clinton E., and Parker, Hermon M.: A Method for the Calculation of External Lift, Moment, and Pressure Drag of Slender Open-Nosed Bodies of Revolution at Supersonic Speeds. NACA Rep. 808, 1945.
5. Sauer, Robert: Introduction to Theoretical Gas Dynamics. J. W. Edwards (Ann Arbor), 1947, pp. 77-81.
6. Luidens, Roger W., and Madden, Robert T.: Interpretation of Boundary-Layer Pressure-Rake Data in Flow with a Detached Shock. NACA RM E50I29a.
7. de Karman, Th.: The Problem of Resistance in Compressible Fluids. Quinto Convegno "Volta", Reale Accademia d'Italia (Roma), Sett. 30-Ott. 6, 1935, pp. 3-57.
8. Dailey, C. L., and McFarland, H. W.: Development of Ramjet Components. Prog. Rep. 9961-8, Univ. Southern Calif. Aero. Lab., USCIA, Feb. 7, 1950. (Bi-monthly Prog. Rep. Dec. 1949-Jan. 1950 under Navy Contract Noa(s) 9961.)
9. Allen, Julian H.: Estimation of the Forces and Moments Acting on Inclined Bodies of Revolution of High Fineness Ratio. NACA RM A9I26, 1949.
10. Copp, Martin R., and Klevatt, Paul L.: Investigation of High-Subsonic Performance Characteristics of a 12° 21-Inch Conical Diffuser, Including Effects of Change in Inlet-Boundary-Layer Thickness. NACA RM L9H10, 1950.

TABLE I

TABLE OF COORDINATES FOR 8-INCH RAM-JET CONFIGURATION

2035

(a) Center-body coordinates

Station	Diameter (in.)
-1.750	1.275
-1.500	1.474
-1.250	1.687
-1.000	1.902
- .750	2.137
- .500	2.410
- .250	2.715
0	3.005
.250	3.285
.500	3.533
.750	3.750
1.000	3.910
1.500	4.130
2.000	4.250
3.000	4.390
4.000	4.470
5.000	4.530
6.000	4.565
7.000	4.590
7.750	4.600
7.875	4.606
10.000	4.585
12.000	4.545
14.000	4.486
16.000	4.415
18.000	4.327
20.000	4.220
22.000	4.084
24.000	3.922
26.000	3.715
30.031	3.340

(b) Outer-shell coordinates

Station	Diameter (in.)	
	External	Internal
0.050	5.992	5.875
.100	6.040	5.876
.150	6.080	5.884
.200	6.113	5.899
.250	6.140	5.915
.375	6.198	5.960
.500	6.245	6.000
1.000	6.389	6.139
1.500	6.496	6.246
2.000	6.564	6.314
2.500	6.610	6.360
3.000	6.648	6.398
9.875	6.998	6.748
14.000	7.210	6.960
22.000	7.616	7.366
30.000	8.024	7.774
32.000	8.125	7.875
56.000	8.125	7.875



TABLE II

LOCATION OF STATIC-PRESSURE ORIFICES FOR PRESSURE MODEL

(a) Location of static tubes
along shell contour.

Station		
External ^a	Internal ($\theta=0^\circ$)	
0.50	11.00	0.50
1.00	12.00	1.00
1.50	14.00	1.50
2.00	16.00	2.00
2.50	18.00	2.50
3.00	21.00	3.00
4.00	24.00	4.00
5.00	27.00	5.00
6.00	31.00	6.00
7.00	35.00	7.00
8.00	40.00	8.00
9.00	45.00	9.00
10.00		

(b) Location of static
tubes ($\theta=0^\circ$).

Station	
Spike	Island
-1.50	8.00
-1.00	9.00
-0.50	10.00
0	11.00
0.50	12.00
1.00	14.00
1.50	16.00
2.00	18.00
2.50	21.00
3.00	24.00
4.00	27.00
5.00	31.00
6.00	37.00
7.00	

^aTwo rows of orifices at
 $\theta = 180^\circ$ and 270° .



TABLE III - EXTERNAL AND INTERNAL PRESSURE COEFFICIENTS OF NACA 8-INCH RAM-JET CONFIGURATION
FOR FOUR ANGLES OF ATTACK AT FREE-STREAM MACH NUMBER OF 1.59



Station	$\alpha = 0^\circ; m_3/m_0 = 0.720$				$\alpha = 0^\circ; m_3/m_0 = 0.612$				$\alpha = 0^\circ; m_3/m_0 = 0.508$				$\alpha = 0^\circ; m_3/m_0 = 0.394$				$\alpha = 0^\circ; m_3/m_0 = 0.283$							
	Outer shell		Center body	Outer shell		Center body	Outer shell		Center body	Outer shell		Center body	Outer shell		Center body	Outer shell		Center body	Outer shell					
	External	Internal		External	Internal		External	Internal		External	Internal		External	Internal		External	Internal		External	Internal				
$\alpha \rightarrow$	180°	270°	0°	180°	270°	0°	180°	270°	0°	180°	270°	0°	180°	270°	0°	180°	270°	0°	180°	270°	0°			
-1.5	0.533			1.049			1.034			1.155			1.196			1.840			1.870					
-1.0	-0.016	-0.019		.942	.742		-0.083	-0.086	1.819	1.070	-0.144	-0.150	1.558	1.246	-0.214	-0.220	1.456	1.379	-0.270	-0.280	1.619	1.468		
-0.5	-0.052	-0.051		.877	.715		-0.083	-0.085	1.199	1.061	-0.131	-0.131	1.346	1.273	-0.184	-0.188	1.447	1.408	-0.231	-0.237	1.610	1.486		
0	1.030			1.102			1.154			1.189			1.356			1.333			1.459	1.415	-0.205	-0.221	1.603	1.494
0.5	0.056	0.063	1.044	.929	-0.063	-0.060	1.263	1.184	-0.149	-0.157	1.391	1.260	-0.247	-0.257	1.480	1.565	-0.327	-0.336	1.655	1.445				
1.0	-0.016	-0.019	.942	.742	-0.083	-0.086	1.819	1.070	-0.144	-0.150	1.558	1.246	-0.214	-0.220	1.456	1.379	-0.270	-0.280	1.619	1.468				
1.5	-0.052	-0.051	.877	.715	-0.083	-0.085	1.199	1.061	-0.131	-0.131	1.346	1.273	-0.184	-0.188	1.447	1.408	-0.231	-0.237	1.610	1.486				
2.0	-0.062	-0.065	.801	.708	-0.096	-0.104	1.175	1.114	-0.129	-0.141	1.351	1.290	-0.171	-0.185	1.459	1.415	-0.205	-0.221	1.603	1.494				
2.5	-0.072	-0.071	.774	.735	-0.101	-0.103	1.163	1.157	-0.189	-0.189	1.333	1.394	-0.167	-0.166	1.456	1.426	-0.193	-0.194	1.603	1.500				
3.0	-0.065	-0.077	.726	.712	-0.091	-0.101	1.154	1.140	-0.119	-0.126	1.380	1.310	-0.150	-0.162	1.433	1.428	-0.174	-0.177	1.603	1.500				
4.0	-0.049	-0.059	.618	.600	-0.071	-0.078	1.144	1.189	-0.096	-0.100	1.512	1.512	-0.118	-0.115	1.429	1.429	-0.158	-0.156	1.603	1.500				
5.0	-0.059	-0.045	.534	.517	-0.056	-0.060	1.151	1.148	-0.070	-0.070	1.517	1.517	-0.086	-0.088	1.452	1.452	-0.108	-0.103	1.603	1.500				
6.0	-0.052	-0.037	.441	.448	-0.045	-0.052	1.163	1.162	-0.064	-0.064	1.384	1.384	-0.069	-0.070	1.436	1.436	-0.082	-0.083	1.604	1.504				
7.0	-0.026	-0.031	.420	.343	-0.059	-0.059	1.184	1.180	-0.044	-0.045	1.555	1.553	-0.055	-0.056	1.441	1.441	-0.065	-0.065	1.507	1.507				
8.0	-0.035	-0.039	.288	.250	-0.032	-0.027	1.198	1.196	-0.056	-0.056	1.345	1.345	-0.047	-0.045	1.446	1.447	-0.056	-0.056	1.610	1.610				
9.0	-0.034	-0.028	.234	.201	-0.031	-0.021	1.802	1.802	1.201	-0.036	1.348	1.348	-0.045	-0.036	1.448	1.449	-0.048	-0.040	1.618	1.610				
10.0	-0.016	-0.015	.514	.514	-0.022	-0.021	1.196	1.196	-0.026	-0.026	1.346	1.346	-0.034	-0.035	1.442	1.442	-0.058	-0.058	1.612	1.612				
11.0	-0.011	-0.004	.357	.357	-0.015	-0.015	1.200	1.200	-0.030	-0.031	1.553	1.553	-0.035	-0.037	1.454	1.454	-0.050	-0.050	1.613	1.613				
12.0	-0.008	-0.006	.830	.830	-0.018	-0.015	1.288	1.288	-0.015	-0.019	1.566	1.566	-0.021	-0.025	1.461	1.461	-0.024	-0.027	1.617	1.617				
14.0	-0.008	-0.004	.595	.595	-0.011	-0.009	1.281	1.281	-0.013	-0.013	1.395	1.395	-0.017	-0.017	1.494	1.494	-0.020	-0.018	1.605	1.595				
16.0	-0.008	-0.009	.788	.788	-0.011	-0.013	1.524	1.524	-0.015	-0.016	1.423	1.423	-0.016	-0.020	1.490	1.490	-0.019	-0.019	1.582	1.582				
18.0	-0.004	-0.009	.913	.913	-0.006	-0.012	1.558	1.558	-0.008	-0.013	1.443	1.443	-0.012	-0.017	1.503	1.503	-0.013	-0.018	1.588	1.588				
21.0	-0.006	-0.013	1.044	1.044	-0.008	-0.015	1.407	1.407	-0.010	-0.016	1.473	1.473	-0.012	-0.020	1.580	1.580	-0.012	-0.020	1.547	1.547				
24.0	-0.003	-0.008	1.156	1.156	-0.006	-0.012	1.446	1.446	-0.005	-0.013	1.499	1.499	-0.008	-0.015	1.554	1.554	-0.008	-0.015	1.556	1.556				
27.0	-0.009	-0.013	1.195	1.195	-0.011	-0.015	1.474	1.474	-0.011	-0.016	1.517	1.517	-0.012	-0.018	1.545	1.545	-0.013	-0.018	1.561	1.561				
31.0	-0.013	-0.018	1.238	1.238	-0.013	-0.019	1.490	1.490	-0.013	-0.020	1.587	1.587	-0.017	-0.021	1.551	1.551	-0.015	-0.020	1.564	1.564				
35.0	-0.044	-0.039		1.288	-0.015	-0.039		1.512	-0.045	-0.040		1.545	-0.047	-0.041		1.559	-0.048	-0.040		1.567				
40.0	-0.023	-0.021			-0.024	-0.020			-0.018	-0.018			-0.027	-0.021			-0.085	-0.085						
45.0	-0.016	-0.021			-0.018	-0.020							-0.018	-0.021			-0.017	-0.020						

Station	(b) Circumferential distribution of C_p							
	Outer shell, external				Outer shell, internal			
$\alpha \rightarrow$	198°	216°	234°	252°	198°	216°	234°	252°
0.5	0.062	0.062	0.061	0.056	-0.062	-0.047	-0.044	-0.053
14.0	-0.013	-0.014	-0.013	-0.004	-0.015	-0.019	-0.018	-0.008
45.0	-0.081	-0.081	-0.081	-0.083	-0.083	-0.083	-0.083	-0.083

TABLE III - EXTERNAL AND INTERNAL PRESSURE COEFFICIENTS OF NACA 8-INCH RAM-JET CONFIGURATION
FOR FOUR ANGLES OF ATTACK AT FREE-STREAM MACH NUMBER OF 1.59 - Continued



Station	$\alpha = 5^\circ; m_2/m_0 = 0.719$				$\alpha = 5^\circ; m_2/m_0 = 0.617$				$\alpha = 5^\circ; m_2/m_0 = 0.551$				$\alpha = 5^\circ; m_2/m_0 = 0.412$				$\alpha = 5^\circ; m_2/m_0 = 0.280$							
	(a) Continued. Longitudinal distribution of C_p .																							
	Outer shell		Center body	Outer shell		Center body	Outer shell		Center body	Outer shell		Center body	Outer shell		Center body	Outer shell		Center body	Outer shell		Center body			
	External	Internal		External	Internal		External	Internal		External	Internal		External	Internal		External	Internal		External	Internal				
$\theta \rightarrow$	180°	270°	0°	0°	180°	270°	0°	0°	180°	270°	0°	0°	180°	270°	0°	0°	180°	270°	0°	0°	180°	270°	0°	
-1.0					0.692				1.036				1.121				1.215						1.283	
-1.0					1.062				1.164				1.209				1.280						1.327	
-0.5					1.119				1.193				1.258				1.312						1.367	
0					1.086				1.150				1.197				1.310						1.396	
0.5	-0.070	0.067	0.957	0.886	-0.149	-0.034	1.177	1.063	-0.211	-0.105	1.287	1.170	-0.319	-0.236	1.439	1.331	-0.406	-0.345	1.524	1.458				
1.0	-0.108	-0.014	.855	.655	-0.162	-0.069	1.142	.984	-0.204	-0.116	1.261	1.132	-0.293	-0.204	1.418	1.335	-0.352	-0.283	1.508	1.461				
1.5	-0.107	-0.205	.811	.640	-0.151	-0.067	1.182	1.015	-0.187	-0.102	1.254	1.164	-0.254	-0.175	1.415	1.364	-0.316	-0.242	1.504	1.481				
2.0	-0.119	-0.058	.743	.643	-0.151	-0.088	1.109	1.047	-0.179	-0.116	1.241	1.191	-0.233	-0.172	1.408	1.382	-0.267	-0.222	1.501	1.491				
2.5	-0.126	-0.051	.737	.700	-0.154	-0.087	1.124	1.081	-0.179	-0.108	1.236	1.218	-0.228	-0.152	1.408	1.397	-0.267	-0.194	1.501	1.497				
3.0	-0.120	-0.064	.711	.688	-0.148	-0.087	1.100	1.098	-0.166	-0.106	1.254	1.224	-0.210	-0.141	1.407	1.400	-0.244	-0.178	1.501	1.499				
4.0	-0.101	-0.055	.598	.885	-0.123	-0.070	1.098	1.096	-0.141	-0.065	1.232	1.231	-0.164	-0.107	1.407	1.407	-0.196	-0.184	1.503	1.501				
5.0	-0.081	-0.045	.820	.510	-0.102	-0.058	1.112	1.118	-0.108	-0.062	1.242	1.242	-0.151	-0.088	1.412	1.418	-0.155	-0.104	1.506	1.506				
6.0	-0.066	-0.040	.439	.444	-0.076	-0.046	1.132	1.132	-0.084	-0.060	1.256	1.256	-0.104	-0.059	1.418	1.420	-0.123	-0.083	1.508	1.508				
7.0	-0.052	-0.036	.417	.341	-0.069	-0.036	1.160	1.160	-0.066	-0.044	1.273	1.272	-0.081	-0.057	1.430	1.428	-0.097	-0.070	1.514	1.512				
8.0	-0.046	-0.028	.287	.258	-0.044	-0.031	1.178	1.180	-0.062	-0.058	1.287	1.287	-0.065	-0.049	1.435	1.435	-0.077	-0.069	1.517	1.517				
9.0	-0.035	-0.018	.244	.218	-0.039	-0.028	1.186	1.188	-0.045	-0.034	1.293	1.293	-0.055	-0.043	1.441	1.441	-0.062	-0.061	1.519	1.519				
10.0	-0.024	-0.021		.498	-0.028	-0.028		1.188	-0.033	-0.032		1.295	-0.040	-0.041		1.443	-0.047	-0.047		1.520				
11.0	-0.016	-0.020		.368	-0.019	-0.024		1.203	-0.023	-0.028		1.306	-0.028	-0.036		1.447	-0.033	-0.042		1.522				
12.0	-0.011	-0.020		.219	-0.013	-0.024		1.226	-0.016	-0.027		1.320	-0.021	-0.034		1.454	-0.026	-0.039		1.526				
14.0	-0.009	-0.015		.668	-0.011	-0.019		1.276	-0.012	-0.021		1.355	-0.016	-0.028		1.469	-0.018	-0.031		1.532				
16.0	-0.008	-0.018		.828	-0.010	-0.021		1.318	-0.012	-0.023		1.388	-0.015	-0.028		1.484	-0.014	-0.031		1.558				
18.0	-0.004	-0.017		.987	-0.006	-0.020		1.362	-0.007	-0.021		1.411	-0.008	-0.025		1.497	-0.010	-0.027		1.542				
21.0	-0.006	-0.021		.879	-0.005	-0.021		1.402	-0.007	-0.024		1.448	-0.009	-0.028		1.515	-0.010	-0.029		1.550				
24.0	-0.006	-0.017		1.144	-0.005	-0.019		1.445	-0.007	-0.020		1.477	-0.009	-0.022		1.529	-0.010	-0.023		1.558				
27.0	-0.009	-0.020		1.203	-0.011	-0.021		1.472	-0.012	-0.023		1.501	-0.013	-0.023		1.542	-0.014	-0.026		1.563				
31.0	-0.014	-0.028		1.242	-0.016	-0.026		1.490	-0.016	-0.028		1.513	-0.018	-0.028		1.549	-0.018	-0.029		1.567				
35.0	-0.044	-0.046			-0.044	-0.046		1.513	-0.046	-0.048		1.531	-0.047	-0.048		1.557	-0.047	-0.049		1.570				
37.0	-0.021			1.275	-0.023				-0.025				-0.023			-0.024				-0.016	-0.050			
40.0	-0.013	-0.027			-0.014	-0.028			-0.015	-0.028			-0.018	-0.029		-0.024								
45.0	-0.013	-0.027																						

Station	(b) Continued. Circumferential distribution of C_p .																							
	Outer shell, external				Outer shell, external				Outer shell, external				Outer shell, external				Outer shell, external				Outer shell, external			
$\theta \rightarrow$	198°	216°	234°	252°	198°	216°	234°	252°	198°	216°	234°	252°	198°	216°	234°	252°	198°	216°	234°	252°	198°	216°	234°	252°
0.5	-0.061	-0.059	-0.014	0.017	-0.141	-0.115	-0.068	-0.064	-0.204	-0.182	-0.156	-0.132	-0.316	-0.295	-0.267	-0.254	-0.402	-0.386	-0.361	-0.356				
14.0	-0.013	-0.020	-0.014	-0.016	-0.023	-0.021	-0.019	-0.018	-0.025	-0.025	-0.022	-0.022	-0.022	-0.029	-0.030	-0.027	-0.024	-0.030	-0.032	-0.030				
43.0	-0.021	-0.021	-0.025	-0.016	.021	-0.021	-0.026	-0.012	-0.021	-0.021	-0.026	.012	-0.022	-0.022	-0.026	.015	-0.023	-0.023	-0.027	.015				

2035

TABLE III - EXTERNAL AND INTERNAL PRESSURE COEFFICIENTS OF NACA 8-INCH RAM-JET CONFIGURATION
FOR FOUR ANGLES OF ATTACK AT FREE-STREAM MACH NUMBER OF 1.69 - Continued.



Station	$\alpha = 6^\circ; m_2/m_0 = 0.716$				$\alpha = 6^\circ; m_2/m_0 = 0.608$				$\alpha = 6^\circ; m_2/m_0 = 0.494$				$\alpha = 6^\circ; m_2/m_0 = 0.386$			
	(a) Continued. Longitudinal distribution of C_p .															
	Outer shell		Center body	Outer shell		Center body	Outer shell		Center body	Outer shell		Center body	Outer shell		Center body	
	External	Internal		External	Internal		External	Internal		External	Internal		External	Internal		
$\theta \rightarrow$	180°	270°	0°	0°	180°	270°	0°	0°	180°	270°	0°	0°	180°	270°	0°	0°
-1.5			0.734				1.068					1.185				1.264
-1.0			1.092				1.192					1.258				1.383
-0.5			1.138				1.216					1.280				1.354
0			1.026				1.142					1.244				1.364
0.5	-0.184	0.068	0.860	.841	-0.268	-0.056	1.151	1.058	-0.355	-0.183	1.386	1.224	-0.435	-0.303	1.481	1.393
1.0	-.199	.009	.764	.541	-.259	-.075	1.138	.979	-.326	-.154	1.515	1.205	-.369	-.252	1.467	1.411
1.5	-.188	-.004	.721	.512	-.840	-.065	1.140	1.023	-.297	-.157	1.515	1.241	-.360	-.205	1.467	1.434
2.0	-.191	-.046	.664	.536	-.230	-.084	1.124	1.063	-.275	-.132	1.510	1.270	-.387	-.193	1.466	1.449
2.5	-.193	-.054	.708	.673	-.228	-.082	1.128	1.101	-.267	-.119	1.511	1.295	-.315	-.169	1.467	1.460
3.0	-.183	-.061	.693	.670	-.214	-.063	1.128	1.115	-.264	-.109	1.515	1.305	-.291	-.152	1.468	1.466
4.0	-.182	-.058	.688	.577	-.174	-.070	1.134	1.128	-.208	-.086	1.518	1.515	-.239	-.118	1.472	1.471
5.0	-.134	-.053	.518	.506	-.142	-.061	1.151	1.150	-.164	-.076	1.329	1.328	-.193	-.097	1.478	1.478
6.0	-.091	-.055	.439	.445	-.112	-.059	1.172	1.171	-.127	-.070	1.341	1.341	-.152	-.084	1.484	1.484
7.0	-.059	-.044	.422	.342	-.079	-.057	1.198	1.194	-.093	-.065	1.356	1.354	-.112	-.077	1.492	1.490
8.0	-.044	-.045	.288	.265	-.056	-.056	1.217	1.217	-.067	-.065	1.369	1.369	-.081	-.075	1.496	1.496
9.0	-.038	-.047	.293	.263	-.045	-.057	1.228	1.228	-.051	-.065	1.375	1.377	-.060	-.073	1.501	1.500
10.0	-.026	-.055		.498	-.032	-.061		1.252	-.035	-.098		1.379	-.040	-.076		1.502
11.0	-.018	-.053		.372	-.021	-.060		1.244	-.022	-.065		1.367	-.026	-.073		1.507
12.0	-.010	-.054		.209	-.018	-.061		1.265	-.015	-.068		1.398	-.017	-.075		1.509
14.0	-.005	-.053		.689	-.010	-.059		1.307	-.012	-.065		1.421	-.012	-.069		1.518
16.0	-.005	-.050		.833	-.007	-.054		1.344	-.009	-.060		1.441	-.008	-.065		1.525
18.0	-.002	-.047		.938	-.005	-.052		1.373	-.005	-.055		1.457	-.005	-.059		1.531
21.0	-.005	-.049		1.051	-.006	-.058		1.417	-.006	-.053		1.483	-.006	-.056		1.541
24.0	-.005	-.042		1.137	-.007	-.044		1.455	-.007	-.046		1.507	-.008	-.047		1.550
27.0	-.011	-.045		1.195	-.012	-.046		1.483		-.047		1.524	-.013	-.047		1.556
31.0	-.014	-.049		1.255	-.016	-.050		1.499	-.016	-.058		1.553	-.016	-.052		1.562
35.0	-.017	-.070			-.046	-.070		1.518	-.046	-.072		1.544	-.044	-.070		1.565
37.0				1.269												
40.0	-.019				-.020				-.080				-.020			
45.0	-.012	-.054			-.013	-.054			-.013	-.054			-.013	-.052		

(b) Continued. Circumferential distribution of C_p .

Station	Outer shell, external															
	198°	216°	234°	252°	198°	216°	234°	252°	198°	216°	234°	252°	198°	216°	234°	252°
0.5	-0.172	-0.134	-0.075	-0.010	-0.256	-0.225	-0.179	-0.123	-0.347	-0.383	-0.283	-0.237	-0.428	-0.404	-0.368	-0.342
14.0	-.016	-.030	-.036	-.048	-.020	-.035	-.044	-.056	-.021	-.036	-.048	-.061	-.021	-.037	-.052	-.066
43.0	-.023	-.029	-.034	-.001	-.026	-.029	-.036	-.006	-.026	-.029	-.036	-.004	-.024	-.028	-.036	-.004

TABLE III - EXTERNAL AND INTERNAL PRESSURE COEFFICIENTS OF NACA 8-INCH RAM-JET CONFIGURATION
FOR FOUR ANGLES OF ATTACK AT FREE-STREAM MACH NUMBER OF 1.59 - Concluded



Station	$\alpha = 10^\circ; m_3/m_0 = 0.705$				$\alpha = 10^\circ; m_3/m_0 = 0.604$				$\alpha = 10^\circ; m_3/m_0 = 0.495$				$\alpha = 10^\circ; m_3/m_0 = 0.325$			
	(a) Concluded. Longitudinal distribution of C_p .															
	Outer shell		Center body	Outer shell		Center body	Outer shell		Center body	Outer shell		Center body	Outer shell		Center body	
	External	Internal		External	Internal		External	Internal		External	Internal		External	Internal		
0 →	180°	270°	0°	0°	180°	270°	0°	0°	180°	270°	0°	0°	180°	270°	0°	0°
-1.5			0.904				1.087			1.159						1.249
-1.0			1.124				1.215			1.236						1.305
-0.5			1.165				1.235			1.250						1.325
0			1.036				1.134			1.186						1.311
0.5	-0.273	0.135	0.758	.789	-0.360	-0.051	1.056	1.004	-0.584	-0.118	1.187	1.116	-0.447	-0.251	1.387	1.508
1.0	-.291	.019	.649	.424	-.348	-.036	1.071	.905	-.373	-.107	1.195	1.087	-.424	-.210	1.384	1.510
1.5	-.280	.004	.554	.328	-.328	-.025	1.089	.967	-.357	-.081	1.206	1.115	-.404	-.168	1.380	1.541
2.0	-.276	-.036	.430	.372	-.310	-.064	1.084	1.025	-.336	-.085	1.204	1.159	-.375	-.156	1.390	1.566
2.5	-.270	-.043	.432	.357	-.305	-.068	1.098	1.074	-.335	-.079	1.212	1.195	-.373	-.132	1.395	1.587
3.0	-.263	-.058	.469	.451	-.291	-.074	1.105	1.094	-.319	-.087	1.219	1.212	-.356	-.120	1.400	1.596
4.0	-.251	-.055	.593	.580	-.254	-.067	1.119	1.117	-.276	-.061	1.251	1.231	-.307	-.100	1.408	1.410
5.0	-.166	-.060	.538	.527	-.187	-.071	1.140	1.142	-.222	-.081	1.243	1.249	-.253	-.097	1.418	1.420
6.0	-.095	-.068	.444	.440	-.126	-.077	1.163	1.163	-.153	-.067	1.261	1.263	-.193	-.100	1.426	1.428
7.0	-.068	-.076	.418	.340	-.075	-.082	1.189	1.186	-.101	-.089	1.277	1.275	-.124	-.102	1.433	1.453
8.0	-.045	-.081	.287	.258	-.050	-.080	1.210	1.211	-.062	-.095	1.282	1.284	-.077	-.107	1.434	1.457
9.0	-.035	-.081	.314	.328	-.036	-.099	1.221	1.222	-.045	-.104	1.294	1.286	-.052	-.116	1.434	1.436
10.0	-.020	-.103		.619	-.021	-.109		1.226	-.087	-.117		1.284	-.081	-.127		1.435
11.0	-.010	-.108		.354	-.012	-.114		1.238	-.016	-.120		1.291	-.018	-.132		1.436
12.0	-.003	-.118		.215	-.005	-.123		1.257	-.008	-.128		1.307	-.009	-.141		1.445
14.0	-.000	-.127		.701	-.003	-.133		1.300	-.005	-.138		1.340	-.005	-.150		1.459
16.0	-.000	-.135		.830	-.001	-.141		1.336	-.005	-.146		1.371	-.003	-.158		1.474
18.0	-.004	-.137		.924	-.003	-.145		1.368	-.002	-.158		1.395	-.003	-.163		1.484
21.0	-.001	-.119		1.037	-.000	-.123		1.408	-.000	-.132		1.432	-.001	-.159		1.504
24.0	-.001	-.101		1.124	-.002	-.105		1.446	-.000	-.105		1.465	-.001	-.107		1.580
27.0	-.005	-.106		1.185	-.006	-.106		1.473	-.010	-.107		1.485	-.011	-.108		1.530
31.0	-.007	-.103		1.221	-.008	-.105		1.491	-.012	-.103		1.496	-.012	-.104		1.553
35.0	-.048	-.123			-.049	-.122		1.510	-.051	-.123		1.505	-.051	-.124		1.558
37.0				1.254												
40.0	-.013				-.013				-.017				-.018			
45.0	-.013	-.103			-.015	-.103			-.017	-.103			-.018	-.103		
	(b) Concluded. Circumferential distribution of C_p .															
Station	Outer shell, external				Outer shell, external				Outer shell, external				Outer shell, external			
0 →	198°	216°	234°	252°	198°	216°	234°	252°	198°	216°	234°	252°	198°	216°	234°	252°
0.5	-0.244	-0.221	-0.158	-0.051	-0.351	-0.309	-0.231	-0.147	-0.371	-0.355	-0.279	-0.209	-0.437	-0.407	-0.364	-0.319
14.0	-.020	-.048	-.084	-.049	-.020	-.050	-.087	-.147	-.021	-.082	-.095	-.155	-.083	-.055	-.100	-.167
43.0	-.035	-.050	-.052	-.019	-.036	-.051	-.053	-.025	-.035	-.061	-.054	-.021	-.053	-.051	-.053	-.020

TABLE IV - EXTERNAL AND INTERNAL PRESSURE COEFFICIENTS OF NACA 8-INCH RAM-JET CONFIGURATION
FOR FOUR ANGLES OF ATTACK AT FREE-STREAM MACH NUMBER OF 1.79



Station	$\alpha = 0^\circ; m_3/m_0 = 0.790$				$\alpha = 0^\circ; m_3/m_0 = 0.772$				$\alpha = 0^\circ; m_3/m_0 = 0.670$				$\alpha = 0^\circ; m_3/m_0 = 0.544$				$\alpha = 3^\circ; m_3/m_0 = 0.789$							
	(a) Longitudinal distribution of C_p .																							
	Outer shell		Center body	Outer shell		Center body	Outer shell		Center body	Outer shell		Center body	Outer shell		Center body	Outer shell		Center body	Outer shell		Center body			
	External	Internal		External	Internal		External	Internal		External	Internal		External	Internal		External	Internal		External	Internal				
$\theta \rightarrow$	180°	270°	0°	0°	180°	270°	0°	0°	180°	270°	0°	0°	180°	270°	0°	0°	180°	270°	0°	180°	270°	0°		
-1.5				0.430			0.429			0.432			0.432			0.749						0.500		
-1.0				.504			.514			1.122			1.334									.579		
-0.5				1.158			1.256			1.323			1.375									1.173		
0				1.160			1.187			1.263			1.348									1.139		
0.5	0.130	0.181	1.163	1.054	0.100	0.089	1.244	1.099	0.010	-0.002	1.382	1.297	-0.096	-0.104	1.497	1.368	0.080	0.126	1.080	1.002				
1.0	.064	.046	1.076	.843	.038	.028	1.172	.849	-.017	-.027	1.343	1.168	-.094	-.093	1.470	1.344	-.027	.048	.975	.719				
1.5	.031	.024	1.009	.886	.019	.011	1.133	.968	-.020	-.027	1.526	1.205	-.070	-.078	1.468	1.380	-.041	.026	.921	.712				
2.0	-.005	-.015	.958	.889	-.009	-.024	1.091	1.000	-.036	-.068	1.304	1.239	-.075	-.068	1.450	1.407	-.084	-.015	.860	.728				
2.5	-.023	-.027	.917	.880	-.029	-.033	1.076	1.040	-.051	-.066	1.294	1.270	-.079	-.084	1.448	1.431	-.080	-.025	.872	.841				
3.0	-.031	-.036	.882	.858	-.054	-.041	1.060	1.039	-.053	-.060	1.288	1.275	-.078	-.083	1.444	1.435	-.082	-.055	.851	.825				
4.0	-.050	-.035	.760	.745	-.032	-.038	1.040	1.006	-.046	-.053	1.280	1.275	-.064	-.068	1.440	1.438	-.074	-.034	.744	.728				
5.0	-.026	-.030	.657	.658	-.029	-.033	1.057	1.056	-.041	-.044	1.287	1.295	-.055	-.056	1.444	1.444	-.063	-.030	.657	.648				
6.0	-.080	-.024	.590	.591	-.024	-.026	1.088	1.085	-.053	-.056	1.299	1.299	-.045	-.041	1.450	1.450	-.068	-.025	.584	.564				
7.0	-.025	-.018	.563	.482	-.019	-.020	1.129	1.124	-.026	-.029	1.319	1.316	-.032	-.031	1.460	1.460	-.042	-.020	.552	.478				
8.0	-.011	-.014	.450	.394	-.014	-.015	1.159	1.160	-.031	-.035	1.332	1.333	-.035	-.031	1.468	1.470	-.032	-.030	.423	.385				
9.0	-.008	-.009	.380	.321	-.009	-.011	1.164	1.163	-.017	-.014	1.337	1.336	-.019	-.016	1.472	1.472	-.019	-.009	.386	.332				
10.0	.004	-.008		.668	.005	-.009		1.156	-.006	-.009	1.334	-.008	-.016	1.478	-.007	-.008					.645			
11.0	.017	-.002		.490	.016	.001		1.176	-.009	-.002	1.345	-.006	-.008	1.480	-.008	0					.497			
12.0	.012	.011		.365	.009	.011		1.216	-.002	-.004	1.357	0	-.008	1.492	-.011	-.005					.360			
14.0	-.006	.007		.001	-.007	.005		1.294	-.018	0	1.412	-.016	-.004	1.517	-.020	-.008					.897			
16.0	-.016	-.003		.958	-.019	-.008		1.353	-.023	-.009	1.460	-.085	-.014	1.539	-.016	-.015					1.017			
18.0	.009	-.003		1.065	.009	-.004		1.395	-.006	-.006	1.480	-.008	-.011	1.558	-.006	-.014					1.107			
21.0	.011	.001		1.193	.010	.001		1.455	-.008	-.004	1.581	-.004	-.006	1.587	-.008	-.009					1.210			
24.0	.009	-.001		1.869	.009	-.001		1.501	-.006	-.004	1.586	-.008	-.006	1.613	-.006	-.010					1.285			
27.0	.002	.004		1.356	.001	.005		1.558	-.002	-.002	1.585	-.003	-.001	1.653	-.008	-.005					1.348			
31.0	.003	.005		1.381	.001	.004		1.560	-.002	-.002	1.597	-.002	-.002	1.642	-.001	-.004					1.389			
35.0	-.020	-.021			-.020	-.022			-.024	-.025			-.022	-.024		-.023	-.022							
37.0				1.489				1.606				1.629			1.660						1.434			
40.0	-.010	-.009			-.011	-.010			-.013	-.013			-.012	-.011		-.012	-.012							
45.0	-.010	-.009			-.009	-.010			-.020	-.015			-.012	-.011		-.010	-.020							

(b) Circumferential distribution of C_p .

Station	Outer shell, external				Outer shell, external				Outer shell, external				Outer shell, external				Outer shell, external			
	198°	216°	234°	252°	198°	216°	234°	252°	198°	216°	234°	252°	198°	216°	234°	252°	198°	216°	234°	252°
0.5	0.134	0.136	0.152	0.127	0.104	0.104	0.103	0.095	0.010	0.013	0.015	0.006	-0.024	-0.021	-0.024	-0.024	0.027	0.042	0.064	0.093
14.0	-.005	-.005	-.006	.004	-.007	-.006	-.006	.003	-.012	-.011	-.009	-.001	-.016	-.016	-.015	-.006	-.021	-.022	-.017	-.018
45.0	-.011	-.010	-.010	-.011	-.018	-.009	-.011	-.011	-.014	-.012	-.013	-.013	-.014	-.012	-.012	-.014	-.013	-.017	-.020	

TABLE IV - EXTERNAL AND INTERNAL PRESSURE COEFFICIENTS OF MAGA 6-INCH RAM-JET CONFIGURATION
FOR FOUR ANGLES OF ATTACK AT FREE-STREAM MACH NUMBER OF 1.79 - Continued



Station	$\alpha = 3^\circ; m_3/m_0 = 0.766$				$\alpha = 3^\circ; m_3/m_0 = 0.596$				$\alpha = 5^\circ; m_3/m_0 = 0.542$				$\alpha = 6^\circ; m_3/m_0 = 0.786$			
	(a) Continued. Longitudinal distribution of C_p .															
	Outer shell		Center body	Outer shell		Center body	Outer shell		Center body	Outer shell		Center body	Outer shell		Center body	
	External	Internal		External	Internal		External	Internal		External	Internal		External	Internal		
$\theta \rightarrow$	180°	270°	0°	0°	180°	270°	0°	0°	180°	270°	0°	0°	180°	270°	0°	0°
-1.5			0.501				0.556			0.736			0.577			
-1.0			0.598				1.325			1.359			.701			
-0.5			1.252				1.362			1.588			1.188			
0			1.179				1.303			1.346			1.189			
0.5	-0.016	0.089	1.174	1.081	-0.143	-0.053	1.405	1.270	-0.183	-0.101	1.468	1.357	-0.089	0.156	0.985	0.959
1.0	-.049	.028	1.120	.989	-.134	-.058	1.383	1.231	-.161	-.091	1.448	1.319	-.110	.059	.867	.826
1.5	-.056	.012	1.101	.953	-.120	-.051	1.378	1.278	-.141	-.075	1.444	1.362	-.113	.057	.769	.527
2.0	-.073	-.023	1.075	.986	-.120	-.069	1.369	1.315	-.136	-.086	1.437	1.395	-.123	-.003	.726	.584
2.5	-.087	-.032	1.072	1.039	-.125	-.069	1.367	1.347	-.139	-.081	1.437	1.423	-.133	-.019	.842	.830
3.0	-.090	-.041	1.087	1.047	-.121	-.070	1.367	1.357	-.133	-.080	1.437	1.429	-.129	-.031	.845	.827
4.0	-.079	-.038	1.084	1.056	-.104	-.060	1.369	1.367	-.114	-.067	1.439	1.439	-.113	-.032	.743	.726
5.0	-.066	-.033	1.086	1.086	-.090	-.051	1.380	1.380	-.094	-.051	1.449	1.460	-.096	-.032	.666	.658
6.0	-.054	-.028	1.180	1.118	-.071	-.038	1.396	1.396	-.072	-.040	1.461	1.461	-.086	-.031	.596	.589
7.0	-.044	-.024	1.162	1.157	-.064	-.029	1.413	1.411	-.058	-.034	1.476	1.475	-.055	-.027	.564	.486
8.0	-.035	-.020	1.184	1.196	-.041	-.025	1.428	1.428	-.043	-.027	1.488	1.488	-.024	-.024	.431	.400
9.0	-.021	-.009	1.206	1.206	-.026	-.019	1.437	1.439	-.028	-.028	1.495	1.497	-.025	-.024	.453	.404
10.0	-.008	-.010		1.208	-.014	-.019		1.442	-.016	-.022		1.500	-.023	-.027		.649
11.0	-.008	-.001		1.227	-.017	-.012		1.452	-.018	-.013		1.508	-.021	-.024		.550
12.0	-.012	-.003		1.259	-.019	-.012		1.466	-.020	-.013		1.519	-.021	-.032		.850
14.0	-.021	-.009		1.325	-.027	-.016		1.494	-.026	-.015		1.539	-.025	-.040		.980
16.0	-.017	-.015		1.376	-.020	-.028		1.517	-.020	-.022		1.558	-.003	-.046		1.081
18.0	.006	-.014		1.416	-.002	-.017		1.643	-.002	-.018		1.572	.008	-.045		1.159
21.0	.008	-.009		1.468	-.003	-.014		1.562	-.003	-.013		1.591	.009	-.034		1.248
24.0	.005	-.010		1.509	-.002	-.014		1.585	-.003	-.015		1.610	.007	-.036		1.317
27.0	-.002	-.005		1.545	-.005	-.007		1.603	-.003	-.006		1.637	.001	-.029		1.378
31.0	-.001	-.003		1.568	-.003	-.006		1.615	-.003	-.006		1.637	.002	-.025		1.409
35.0	-.023	-.029			-.025	-.032		1.639	-.025	-.031			-.023	-.055		
37.0												1.656		-.008	-.042	
40.0	-.011	-.017			-.014	-.019			-.012	-.019				-.007	-.043	
45.0	-.009	-.019			-.011	-.019			-.010	-.019						1.461

(b) Continued. Circumferential distribution of C_p .																
Station	Outer shell, external				Outer shell, external				Outer shell, external				Outer shell, external			
$\theta \rightarrow$	198°	216°	234°	252°	198°	216°	234°	252°	198°	216°	234°	252°	198°	216°	234°	252°
0.5	-0.009	0.008	0.030	0.055	-0.158	-0.123	-0.099	-0.080	-0.180	-0.165	-0.143	-0.125	-0.076	-0.038	0.008	0.065
14.0	-.021	-.022	-.017	-.012	-.028	-.030	-.025	-.020	-.029	-.029	-.025	-.021	-.029	-.037	-.040	-.048
43.0	-.013	-.013	-.016	-.016	-.014	-.014	-.017	-.019	-.014	-.013	-.017	-.018	-.015	-.019	-.024	-.036

TABLE IV - EXTERNAL AND INTERNAL PRESSURE COEFFICIENTS OF NACA 8-INCH RAM-JET CONFIGURATION
FOR FOUR ANGLES OF ATTACK AT FREE-STREAM MACH NUMBER OF 1.79 - Concluded



Station	$\alpha = 5^\circ; m_3/m_0 = 0.768$				$\alpha = 6^\circ; m_3/m_0 = 0.716$				$\alpha = 10^\circ; m_3/m_0 = 0.768$				$\alpha = 10^\circ; m_3/m_0 = 0.749$				
	Outer shell		Center body	Outer shell		Center body	Outer shell		Center body	Outer shell		Center body	Outer shell		Center body	Outer shell	
	External	Internal		External	Internal		External	Internal		External	Internal		External	Internal		External	Internal
$\theta \rightarrow$	180°	270°	0°	0°	180°	270°	0°	0°	180°	270°	0°	0°	180°	270°	0°	180°	270°
-1.5				0.576			0.576			0.685			0.686				
-1.0				.688			.829			.894			.925				
-0.5				1.242			1.298			1.222			1.330				
0				1.157			1.201			1.120			1.128				
0.5	-0.117	0.100	1.069	1.001	-0.145	0.050	1.176	1.077	-0.194	0.172	0.872	.899	-0.205	0.144	0.882	.909	
1.0	-.129	.041	1.032	.759	-.147	.015	1.157	.943	-.204	.074	.761	.519	-.213	.072	.779	.534	
1.5	-.128	.024	1.052	.856	-.140	.006	1.161	1.009	-.194	.044	.655	.388	-.023	.040	.787	.418	
2.0	-.132	-.013	1.019	.928	-.140	-.026	1.150	1.074	-.196	.001	.505	.451	-.201	-.001	.908	.855	
2.5	-.139	-.025	1.031	.998	-.147	-.034	1.157	1.150	-.198	-.011	.471	.431	-.205	-.014	.947	.919	
3.0	-.135	-.035	1.036	1.015	-.143	-.041	1.162	1.147	-.189	-.022	.500	.418	-.198	-.025	.960	.944	
4.0	-.120	-.057	1.044	1.035	-.125	-.041	1.172	1.157	-.155	-.030	.741	.759	-.172	-.032	.981	.973	
5.0	-.104	-.056	1.074	1.072	-.106	-.041	1.196	1.196	-.147	-.035	.694	.694	-.145	-.037	1.019	1.018	
6.0	-.078	-.055	1.110	1.108	-.086	-.036	1.223	1.222	-.079	-.041	.593	.583	-.084	-.042	1.065	1.062	
7.0	-.055	-.025	1.154	1.149	-.064	-.030	1.254	1.252	-.056	-.046	.558	.495	-.061	-.046	1.116	1.112	
8.0	-.033	-.025	1.189	1.191	-.039	-.030	1.281	1.281	-.051	-.048	.392	.396	-.052	-.049	1.158	1.160	
9.0	-.031	-.027	1.205	1.205	-.054	-.030	1.292	1.293	-.044	-.032	.509	.532	-.045	-.052	1.181	1.184	
10.0	-.025	-.028		1.206	-.030	-.030		1.298	-.035	-.067		.658	-.037	-.066		1.191	
11.0	-.023	-.027		1.225	-.027	-.050		1.311	-.029	-.075		.487	-.029	-.076		1.212	
12.0	-.024	-.035		1.259	-.027	-.036		1.355	-.035	-.085		.779	-.025	-.087		1.244	
14.0	-.024	-.042		1.523	-.027	-.043		1.385	-.002	-.099		.936	.001	-.100		1.306	
16.0	-.001	-.048		1.375	-.001	-.049		1.427	-.005	-.114		1.036	.006	-.114		1.355	
18.0	.008	-.045		1.414	-.005	-.047		1.450	.012	-.128		1.113	.012	-.127		1.393	
21.0	.009	-.036		1.467	-.007	-.038		1.503	.013	-.121		1.205	.012	-.122		1.445	
24.0	-.006	-.037		1.508	-.004	-.038		1.538	.012	-.109		1.279	.011	-.110		1.489	
27.0	-.001	-.050		1.542	-.003	-.030		1.565	.007	-.101		1.337	.007	-.104		1.524	
31.0	0	-.025		1.560	0	-.026		1.570	.008	-.077		1.374	.008	-.079		1.544	
35.0	-.025	-.055			-.025	-.055			-.024	-.106			-.023	-.106			
37.0				1.606	-.009	-.045		1.617	-.004	-.058		1.420	-.003	-.097			
40.0	-.009	-.043			-.008	-.045			-.002	-.055			-.008	-.095			1.583
45.0	-.008	-.043															

(b) Concluded. Circumferential distribution of C_p .

Station	Outer shell, external				Outer shell, external				Outer shell, external				Outer shell, external			
$\theta \rightarrow$	198°	216°	234°	252°	198°	216°	234°	252°	198°	216°	234°	252°	198°	216°	234°	252°
0.5	-0.103	-0.068	-0.026	0.030	-0.130	-0.103	-0.061	-0.032	-0.181	-0.145	-0.066	-0.041	-0.196	-0.164	0.091	0.014
14.0	-.031	-.058	-.042	-.048	-.032	-.040	-.045	-.052	-.018	-.049	-.084	-.132	-.019	-.050	-.086	-.132
43.0	-.015	-.019	-.025	-.036	-.017	-.019	-.026	-.036	-.029	-.043	-.044	-.080	-.028	-.042	-.044	-.060

TABLE V - EXTERNAL AND INTERNAL PRESSURE COEFFICIENTS OF NACA 8-INCH RAM-JET CONFIGURATION FOR FOUR ANGLES OF ATTACK AT FREE-STREAM MACH NUMBER OF 1.79 WITH MODEL ROTATED 180°



Station	$\alpha = 0^\circ; m_3/m_0 = 0.790$				$\alpha = 0^\circ; m_3/m_0 = 0.750$				$\alpha = 0^\circ; m_3/m_0 = 0.680$				$\alpha = 0^\circ; m_3/m_0 = 0.553$			
	Outer shell		Center body	Outer shell		Center body	Outer shell		Center body	Outer shell		Center body	Outer shell		Center body	
	External	Internal		External	Internal		External	Internal		External	Internal		External	Internal		
$\theta \rightarrow$	0°	90°	180°	180°	0°	90°	180°	180°	0°	90°	180°	180°	0°	90°	180°	180°
-1.5				0.451			0.431			0.435			0.700			
-1.0				.509			.534			1.115			1.537			
-0.5				1.287			1.277			1.327			1.580			
0				1.177			1.206			1.261			1.348			
0.5	0.103	0.115	1.279	1.069	0.073	0.083	1.337	1.141	0.007	0.018	1.426	1.228	-0.091	-0.081	1.586	1.358
1.0	.058	.044	1.391	.982	.082	.028	1.427	1.021	-.019	-.014	1.484	1.163	-.082	-.077	1.550	1.341
1.5	.018	.023	1.036	.939	.006	.013	1.141	1.051	-.023	-.016	1.290	1.200	-.070	-.062	1.455	1.380
2.0	-.011	-.013		.973	-.018	-.022		1.089	-.040	-.043		1.237	-.072	-.077	1.674	1.409
2.5	-.051	-.025	.962	1.016	-.037	-.030	1.070	1.126	-.055	-.046	1.228	1.269	-.081	-.074	1.409	1.433
3.0	-.058	-.034	1.449	1.015	-.043	-.039	1.477	1.129	-.057	-.052	1.521	1.273	-.078	-.075	1.682	1.436
4.0	-.036	-.033	.920	1.008	-.039	-.036	1.025	1.126	-.052	-.046	1.194	1.274	-.067	-.062	1.387	1.439
5.0	-.050	-.028	.890	1.088	-.032	-.030	.974	1.143	-.045	-.038	1.102	1.285	-.054	-.051	1.311	1.446
6.0	-.025	-.023	1.471	1.057	-.027	-.025	1.470	1.162	-.034	-.030	1.494	1.299	-.043	-.036	1.556	1.453
7.0	-.018	-.016		1.099	-.021	-.017		1.192	-.028	-.024		1.315	-.036	-.028	1.673	1.463
8.0	-.014	-.013	1.248	1.144	-.015	-.013	1.313	1.223	-.021	-.019	1.411	1.356	-.028	-.018	1.526	1.474
9.0	-.012	-.006		1.149	-.014	-.007		1.228	-.019	-.011		1.340	-.024	-.011	1.688	1.477
10.0	-.004	-.005		1.140	-.005	-.006		1.223	-.010	-.005		1.358	-.014	-.009		1.477
11.0	.007	-.001		1.159	-.006	0		1.238	-.002	-.005		1.348	-.003	-.004		1.482
12.0	.006	.011		1.200	-.005	.013		1.269	-.002	-.008		1.370	-.005	.002		1.494
14.0	-.004	.011		1.279	-.005	.008		1.334	-.007	.005		1.416	-.011	-.001		1.519
16.0	-.013	-.008		1.340	-.014	-.008		1.385	-.016	-.011		1.451	-.019	-.016		1.543
18.0	.010	-.008		1.384	-.010	-.007		1.424	-.008	-.008		1.481	-.004	-.009		1.561
21.0	.013	.003		1.444	-.013	.003		1.475	-.009	.001		1.522	-.007	-.002		1.590
24.0	.010	.001		1.492	-.010	0		1.518	-.007	-.002		1.556	-.005	-.003		1.618
27.0	.001	.002		1.580	-.001	.003		1.552	-.001	.001		1.584	-.001	-.001		1.636
31.0	.002	.002		1.553	-.003	.003		1.570	0	.001		1.598	-.001	0		1.647
35.0	-.020	-.025			-.018	-.024		1.613	-.019	-.026		1.630	-.021	-.026		
37.0				1.599								1.630	-.011	-.016		1.685
40.0	-.008	-.015			-.008	-.014			-.011	-.016			-.011	-.016		
45.0	-.013	-.013			-.012	-.012			-.014	-.014			-.014	-.014		

(b) Circumferential distribution of C_p .

Station	Outer shell, external				Outer shell, external				Outer shell, external				Outer shell, external			
	18°	36°	54°	72°	18°	36°	54°	72°	18°	36°	54°	72°	18°	36°	54°	72°
0.5	0.109	0.115	0.113	0.114	0.079	0.084	0.086	0.084	0.012	0.017	0.021	0.019	-0.066	-0.077	-0.067	-0.074
14.0	-.007	-.011	-.006	-.010	-.008	-.010	-.005	-.010	-.011	-.013	-.008	-.004	-.015	-.018	-.014	-.001
43.0	-.011	-.010	-.011	-.013	-.011	-.009	-.011	-.012	-.012	-.011	-.012	-.014	-.013	-.013	-.014	-.014

TABLE V - EXTERNAL AND INTERNAL PRESSURE COEFFICIENTS OF NACA 8-INCH RAM-JET CONFIGURATION FOR FOUR ANGLES OF ATTACK AT FREE-STREAM MACH NUMBER OF 1.79 WITH MODEL ROTATED 180° - Continued



Station	$\alpha = 3^\circ; m_3/m_0 = 0.789$			$\alpha = 3^\circ; m_3/m_0 = 0.728$			$\alpha = 3^\circ; m_3/m_0 = 0.617$			$\alpha = 3^\circ; m_3/m_0 = 0.563$		
	(a) Continued. Longitudinal distribution of C_p .											
	Outer shell		Center body	Outer shell		Center body	Outer shell		Center body	Outer shell		Center body
	External	Internal		External	Internal		External	Internal		External	Internal	
$\theta \rightarrow$	0°	90°	180°	0°	90°	180°	0°	90°	180°	0°	90°	180°
-1.5			0.369			0.370			0.410			0.860
-1.0			.430			.635			1.209			1.267
-0.5			1.224			1.285			1.345			1.370
0			1.201			1.244			1.323			1.363
0.5	0.224	0.107	1.065	1.154	0.174	0.059	1.159	1.219	0.072	-0.053	1.392	1.387
1.0	.126	.040	1.371	1.038	.101	.013	1.375	1.146	.043	-.045	1.412	1.312
1.5	.094	.025	1.244	1.041	.064	.005	1.382	1.165	.038	-.058	1.563	.341
2.0	.055	-.016	1.834	1.058	.042	-.029	1.791	1.188	.016	-.058	1.709	1.565
2.5	.028	-.026	.832	1.084	.018	-.036	.993	1.212	-.003	-.060	1.215	1.385
3.0	.016	-.033	1.445	1.074	.008	-.043	1.485	1.209	-.008	-.082	1.548	1.585
4.0	.012	-.031	.818	1.052	.007	-.040	.964	1.195	-.008	-.053	1.182	1.379
5.0	.015	-.028	.841	1.065	.008	-.034	.964	1.202	-.001	-.045	1.162	1.380
6.0	.018	-.024	1.351	1.082	.007	-.030	1.331	1.211	-.001	-.053	1.390	1.385
7.0	.013	-.019	1.834	1.112	.008	-.022	1.785	1.225	-.001	-.025	1.720	1.388
8.0	.016	-.013	1.034	1.139	.010	-.014	1.154	1.239	-.004	-.019	1.338	1.399
9.0	.014	-.005	1.802	1.113	.010	-.007	1.755	1.219	-.006	-.012	1.703	1.377
10.0	.020	-.006		1.069	.015	-.008		1.189	.011	-.014		1.358
11.0	.024	-.002		1.086	.020	-.004		1.199	.016	-.009		1.382
12.0	.031	.001		1.142	.029	-.002		1.237	.025	-.006		1.383
14.0	.019	0		1.242	.015	-.003		1.314	.014	-.006		1.431
16.0	.004	-.017		1.316	.005	-.019		1.375	-.001	-.021		1.472
18.0	.011	-.017		1.371	.009	-.019		1.421	.007	-.020		1.505
21.0	.021	-.006		1.445	.018	-.007		1.485	.016	-.008		1.552
24.0	.019	-.008		1.502	.017	-.009		1.534	.015	-.009		1.590
27.0	.007	-.007		1.540	.007	-.008		1.586	.004	-.007		1.612
31.0	.008	-.004		1.565	.008	-.005		1.584	.007	-.008		1.625
35.0	-.017	-.031			-.017	-.031			-.018	-.051		-.018
37.0				1.608				1.621			1.652	
40.0	-.006	-.021			-.007	-.022			-.006	-.021		-.006
45.0	-.011	-.019			-.012	-.019			-.011	-.019		-.011

(b) Continued. Circumferential distribution of C_p .

Station	Outer shell, external				Outer shell, external				Outer shell, external				Outer shell, external			
	18°	36°	54°	72°	18°	36°	54°	72°	18°	36°	54°	72°	18°	36°	54°	72°
0.5	0.228	0.211	0.184	0.148	0.177	0.161	0.134	0.099	0.073	0.065	0.043	0.007	0.020	0.006	-0.012	-0.047
14.0	.012	.004	.002	.008	.010	.005	-.001	.005	.007	-.001	-.004	.002	.004	-.003	-.007	.001
43.0	-.008	-.009	-.014	-.019	-.009	-.011	-.016	-.019	-.008	-.011	-.018	-.019	-.008	-.011	-.015	-.020

TABLE V - EXTERNAL AND INTERNAL PRESSURE COEFFICIENTS OF NACA 8-INCH RAM-JET CONFIGURATION FOR FOUR ANGLES OF ATTACK AT FREE-STREAM MACH NUMBER OF 1.79 WITH MODEL ROTATED 180° - Concluded



Station	$\alpha = 6^\circ; m_3/m_0 = 0.786$				$\alpha = 6^\circ; m_3/m_0 = 0.734$				$\alpha = 10^\circ; m_3/m_0 = 0.768$			
	(a) Concluded. Longitudinal distribution of C_p .											
	Outer shell		Center body	Outer shell		Center body	Outer shell		Center body	Outer shell		Center body
	External	Internal		External	Internal		External	Internal		External	Internal	
0 →	0°	90°	180°	180°	0°	90°	180°	180°	0°	0°	90°	180°
-1.5			0.304				0.303					0.561
-1.0			.411				.506					.687
-0.5			1.106				1.151					.739
0			1.219				1.260					.942
0.5	0.337	0.100	0.957	1.214	0.328	0.075	1.052	1.273	0.487	0.139	1.258	1.104
1.0	.212	.041	1.398	1.117	.202	.025	1.377	1.218	.358	.070	1.456	1.212
1.5	.177	.026	1.221	1.098	.167	.016	1.381	1.214	.285	.044	1.147	1.217
2.0	.126	-.011		1.094	.123	-.018	1.388	1.218	.222	-.001	1.973	1.182
2.5	.095	-.021		1.04	.092	-.026	.742	1.228	.187	-.013	1.014	1.186
3.0	.077	-.032	1.415	1.082	.074	-.038	1.490	1.217	.168	-.023	1.380	1.134
4.0	.067	-.032	.815	1.043	.064	-.038	.747	1.192	.146	-.004	1.586	1.076
5.0	.050	-.030	.815	1.047	.059	-.035	.873	1.190	.184	-.033	.951	1.050
6.0	.066	-.027	1.284	1.064	.054	-.028	1.279	1.193	.124	-.039	1.326	1.064
7.0	.053	-.025	1.202	1.090	.050	-.025	1.260	1.205	.115	-.043	1.999	1.085
8.0	.049	-.023	1.023	1.110	.048	-.025	1.126	1.207	.107	-.048	1.329	1.100
9.0	.046	-.023	1.237	1.057	.045	-.025	1.507	1.162	.099	-.051	1.973	1.038
10.0	.051	-.027		.944	.050	-.028		1.098	.101	-.060		.864
11.0	.054	-.025		.972	.052	-.025		1.105	.105	-.068		.620
12.0	.054	-.027		1.059	.053	-.026		1.151	.106	-.077		.971
14.0	.050	-.029		1.191	.050	-.030		1.263	.105	-.091		1.137
16.0	.032	-.047		1.279	.051	-.048		1.388	.087	-.110		1.242
18.0	.021	-.048		1.347	.081	-.049		1.397	.070	-.128		1.320
21.0	.036	-.032		1.435	.036	-.033		1.475	.078	-.119		1.421
24.0	.036	-.034		1.500	.035	-.035		1.554	.074	-.108		1.497
27.0	.022	-.033		1.840	.023	-.033		1.587	.060	-.104		1.534
31.0	.021	-.028		1.563	.021	-.027		1.583	.049	-.086		1.555
35.0	-.005	-.053			-.004	-.054		1.618	.022	-.109		1.593
37.0				1.605								
40.0	.006	-.045			.004	-.046			.027	-.101		
45.0	-.001	-.042			-.002	-.043			.018	-.098		

Station	Outer shell, external				Outer shell, external				Outer shell, external				
	0 →	18°	36°	54°	72°	18°	36°	54°	72°	18°	36°	54°	72°
	0.5	0.340	0.305	0.254	0.165	0.532	0.298	0.240	0.159	0.477	0.433	0.360	0.274
14.0	.041	.023	.004	-.005	.040	.023	.004	-.006	.093	.058	.014	-.028	
43.0	.001	-.013	-.027	-.048	-.001	-.011	-.026	-.042	.014	-.017	-.056	-.094	

TABLE VI - EXTERNAL AND INTERNAL PRESSURE COEFFICIENTS OF NACA 8-INCH RAM-JET CONFIGURATION
FOR FOUR ANGLES OF ATTACK AT FREE-STREAM MACH NUMBER OF 1.99



Station	$\alpha = 0^\circ; m_3/m_0 = 0.860$			$\alpha = 0^\circ; m_3/m_0 = 0.839$			$\alpha = 0^\circ; m_3/m_0 = 0.783$			$\alpha = 0^\circ; m_3/m_0 = 0.644$		
	(a) Longitudinal distribution of C_p .											
	Outer shell		Center body	Outer shell		Center body	Outer shell		Center body	Outer shell		Center body
	External	Internal		External	Internal		External	Internal		External	Internal	
$\theta \rightarrow$	180°	270°	0°	0°	180°	270°	0°	0°	0°	180°	270°	0°
-1.5			0.409				0.403			0.409		
-1.0			.479				.480			.480		
-0.5			.715				.722			1.241		
0			1.291				1.334			1.353		
0.5	0.194	-0.001	1.233	1.158	0.171	-0.002	1.312	1.182	0.119	-0.010	1.392	1.209
1.0	.097	.001	1.150	.845	.067	.002	1.241	.960	.062	.056	1.344	1.102
1.5	.065	.056	1.097	.876	.058	.058	1.206	1.018	.045	.038	1.321	1.155
2.0	.086	.016	1.033	.892	.026	.011	1.168	1.069	.014	0	1.297	1.200
2.5	.003	.194	1.018	.998	-.001	.169	1.153	1.128	-.009	.115	1.286	1.255
3.0	-.007	-.012	.986	.963	-.010	-.015	1.140	1.119	-.018	-.019	1.276	1.257
4.0	-.010	-.015	.869	.850	-.013	-.017	1.116	1.107	-.018	-.021	1.262	1.255
5.0	-.009	-.013	.769	.762	-.012	-.015	1.129	1.151	-.016	-.018	1.270	1.262
6.0	-.007	-.012	.699	.696	-.010	-.012	1.156	1.158	-.014	-.016	1.286	1.285
7.0	-.003	-.007	.651	.563	-.007	-.006	1.197	1.192	-.010	-.013	1.310	1.308
8.0	-.004	-.008	.529	.476	-.008	-.008	1.225	1.230	-.012	-.010	1.328	1.328
9.0	-.006	-.005	.515	.428	-.007	-.005	1.230	1.232	-.010	-.007	1.332	1.319
10.0	-.003	-.006	.741	-.006	-.006	1.222	-.009	-.007			-.011	-.011
11.0	.001	-.005	.577	-.003	-.005	1.244	-.007	-.004			-.006	-.008
12.0	.003	-.003	.471	-.008	-.008	1.284	-.005	-.007			1.345	-.006
14.0	.003	.001	.328	.001	.001	1.359	-.008	0			1.373	-.003
16.0	.005	.005	.835	.005	.005	1.414	-.003	.003			1.451	-.003
18.0	.010	.006	.944	.011	.004	1.458	-.010	.006			1.475	-.001
21.0	.014	.007	1.065	.014	.007	1.518	-.014	.015			1.580	-.009
24.0	.017	.016	1.181	.018	.016	1.569	-.017	.005			1.605	-.013
27.0	-.007	.004	1.267	-.007	.006	1.614	-.009	.006			1.645	-.012
31.0	.004	-.021	1.323	.006	-.017	1.639	-.005	-.019			1.666	-.002
35.0	-.031	-.034		-.017	-.032		-.005	.034			1.714	-.020
37.0			1.400			1.695					1.714	-.034
40.0	-.018	-.026		-.011	-.026		-.001	-.028			1.749	-.025
45.0	-.011	-.025		-.010	-.025		-.010	-.026			1.749	-.025

(b) Circumferential distribution of C_p .

Station	Outer shell, external															
	198°	216°	234°	252°	198°	216°	234°	252°	198°	216°	234°	252°	198°	216°	234°	252°
0.5	0.200	0.203	0.199	0.197	0.176	0.178	0.178	0.172	0.122	0.127	0.122	0.119	0.012	0.014	0.016	0.009
14.0	.003	.001	.001	.001	-.001	-.002	-.002	-.001	-.004	-.005	-.005	-.003	-.003	-.005	-.005	-.005
45.0	-.011	-.008	-.011	-.018	-.010	-.008	-.010	-.011	-.009	-.007	-.010	-.010	-.011	-.009	-.011	-.012

TABLE VI - EXTERNAL AND INTERNAL PRESSURE COEFFICIENTS OF NACA 8-INCH RAM-JET CONFIGURATION
FOR FOUR ANGLES OF ATTACK AT FREE-STREAM MACH NUMBER OF 1.99 - Continued



Station	$\alpha = 5^\circ; m_3/m_0 = 0.859$				$\alpha = 5^\circ; m_3/m_0 = 0.837$				$\alpha = 5^\circ; m_3/m_0 = 0.789$				$\alpha = 6^\circ; m_3/m_0 = 0.855$			
	(a) Continued. Longitudinal distribution of C_p .															
	Outer shell		Center body	Outer shell		Center body	Outer shell		Center body	Outer shell		Center body	Outer shell		Center body	
	External	Internal		External	Internal		External	Internal		External	Internal		External	Internal		
$\theta \rightarrow$	180°	270°	0°	0°	180°	270°	0°	0°	180°	270°	0°	0°	180°	270°	0°	0°
-1.5			0.480				0.479					0.481				0.558
-1.0			.575				.559					.559				.675
-0.5			.807				.824					1.163				.927
0			1.387				1.306					1.325				1.227
0.5	0.094	0.005	1.130	1.106	0.068	-0.006	1.228	1.131	0.054	-0.007	1.306	1.176	0.005	0.007	1.147	1.058
1.0	.028	.095	1.053	.749	.014	.084	1.158	.826	-.003	.068	1.261	1.002	-.058	.102	.847	.671
1.5	.004	.062	.953	.651	-.006	.055	1.144	.944	-.017	.044	1.263	1.080	-.054	.067	.826	.554
2.0	-.025	.018	.972	.928	-.017	.013	1.122	1.015	-.036	.007	1.234	1.148	-.073	.023	.677	.593
2.5	-.044	.199	.972	.889	-.048	.173	1.122	1.092	-.065	.136	1.234	1.207	-.088	.209	.704	.586
3.0	-.050	-.009	.950	.899	-.056	-.016	1.117	1.097	-.080	-.015	1.231	1.217	-.095	-.006	.921	.985
4.0	-.050	-.011	.849	.816	-.052	-.016	1.111	1.099	-.055	-.018	1.231	1.226	-.088	-.012	.855	.832
5.0	-.044	-.011	.760	.754	-.048	-.016	1.136	1.134	-.050	-.017	1.249	1.249	-.076	-.013	.771	.762
6.0	-.039	-.011	.694	.689	-.044	-.016	1.187	1.165	-.044	-.016	1.271	1.273	-.066	-.017	.705	.694
7.0	-.033	-.009	.661	.584	-.036	-.014	1.210	1.215	-.038	-.015	1.303	1.299	-.056	-.016	.657	.593
8.0	-.029	-.009	.528	.485	-.031	-.014	1.247	1.249	-.038	-.015	1.328	1.330	-.054	-.016	.529	.494
9.0	-.025	-.006	.559	.457	-.029	-.009	1.262	1.262	-.032	-.010	1.337	1.340	-.045	-.017	.647	.666
10.0	-.020	-.006		.703	-.024	-.009		1.262	-.029	-.008		1.340	-.019	-.024		.776
11.0	-.018	-.004		.620	-.022	-.009		1.284	-.016	-.006		1.369	-.012	-.026		.593
12.0	-.015	-.006		.440	-.013	-.011		1.319	-.006	-.011		1.386	-.007	-.031		.461
14.0	.001	-.007		.359	.002	-.011		1.384	-.002	-.010		1.441	-.002	-.033		.324
16.0	.007	-.006		.880	.008	-.009		1.432	-.002	-.008		1.482	-.005	-.034		.865
18.0	.011	-.002		.989	.011	-.007		1.489	-.008	-.006		1.518	.011	-.035		.975
21.0	.027	-.002		1.115	.026	-.006		1.518	.024	-.003		1.561	.021	-.032		1.104
24.0	.009	.010		1.202	.008	.007		1.559	.008	.008		1.599	.005	-.021		1.192
27.0	-.012	0		1.281	-.012	-.004		1.601	-.013	-.003		1.658	-.012	-.026		1.269
31.0	.005	-.024		1.333	.005	-.025		1.627	.004	-.025		1.682	.005	-.050		1.321
35.0	-.018	-.040			-.024	-.039			-.020	-.040			-.020	-.064		
37.0				1.409				1.685				1.710				1.393
40.0	-.008	-.034			-.011	-.033			-.010	-.035			-.006	-.058		
45.0	-.008	-.038			-.011	-.032			-.008	-.032			-.008	-.057		

(b) Continued. Circumferential distribution of C_p .

Station	Outer shell, external															
$\theta \rightarrow$	198°	216°	234°	252°	198°	216°	234°	252°	198°	216°	234°	252°	198°	216°	234°	252°
0.5	0.105	0.123	0.141	0.168	0.071	0.094	0.115	0.141	0.048	0.060	0.083	0.107	0.019	0.045	0.083	0.142
14.0	-.002	-.006	-.007	-.006	-.003	-.008	-.008	-.007	-.005	-.010	-.011	-.017	-.007	-.020	-.031	-.037
43.0	-.008	-.011	-.013	-.015	-.013	-.014	-.016	-.022	-.008	-.011	-.015	-.017	-.012	-.017	-.022	-.034

TABLE VI - EXTERNAL AND INTERNAL PRESSURE COEFFICIENTS OF NACA 8-INCH RAM-JET CONFIGURATION
FOR FOUR ANGLES OF ATTACK AT FREE-STREAM MACH NUMBER OF 1.99 - Concluded



Station	$\alpha = 6^\circ; m_3/m_0 = 0.840$				$\alpha = 6^\circ; m_3/m_0 = 0.784$				$\alpha = 10^\circ; m_3/m_0 = 0.837$				$\alpha = 10^\circ; m_3/m_0 = 0.818$			
	(a) Concluded. Longitudinal distribution of C_p .															
	Outer shell		Center body	Outer shell		Center body	Outer shell		Center body	Outer shell		Center body	Outer shell		Center body	
	External	Internal		External	Internal		External	Internal		External	Internal		External	Internal		
$\theta \rightarrow$	180°	270°	0°	0°	180°	270°	0°	0°	180°	270°	0°	0°	180°	270°	0°	0°
-1.5			0.560				0.558					0.686				0.674
-1.0			.680				.674					.798				.801
-0.5			.933				1.261					1.139				1.187
0			1.257				1.291					1.190				1.199
0.5	-0.025	0.008	1.513	1.075	-0.059	-0.003	1.548	1.189	-0.103	0.011	1.028	.989	-0.138	0.009	1.491	.897
1.0	-.055	.091	1.054	.720	-.074	.072	1.205	.909	-.116	.111	.850	.570	-.145	.107	.868	.885
1.5	-.064	.060	1.076	.898	-.079	.049	1.216	1.043	-.119	.075	.728	.429	-.143	.070	.869	.461
2.0	-.079	.017	1.080	.987	-.088	.023	1.211	1.137	-.129	.028	.568	.472	-.145	.025	.964	.920
2.5	-.093	.182	1.097	1.087	-.102	.140	1.222	1.196	-.139	.235	.507	.483	-.157	.202	1.012	.987
3.0	-.098	-.011	1.104	1.088	-.104	-.015	1.228	1.214	-.137	-.002	.513	.422	-.153	-.006	1.041	1.020
4.0	-.083	-.015	1.112	1.103	-.097	-.020	1.240	1.255	-.122	-.011	.808	.555	-.156	-.013	1.095	1.089
5.0	-.081	-.017	1.145	1.145	-.084	-.020	1.266	1.268	-.110	-.019	.805	.820	-.124	-.020	1.145	1.146
6.0	-.070	-.018	1.182	1.180	-.076	-.022	1.294	1.295	-.095	-.025	.704	.691	-.093	-.028	1.188	1.189
7.0	-.064	-.020	1.227	1.224	-.071	-.023	1.329	1.326	-.058	-.030	.655	.620	-.087	-.034	1.240	1.236
8.0	-.058	-.020	1.266	1.270	-.048	-.020	1.357	1.360	-.048	-.036	1.002	.514	-.050	-.039	1.556	1.283
9.0	-.054	-.020	1.286	1.286	-.036	-.020	1.374	1.376	-.037	-.042	.751	.541	-.039	-.047	1.306	1.309
10.0	-.024	-.025		1.293	-.027	-.029		1.383	-.024	-.051		.725	-.028	-.057		1.323
11.0	-.017	-.028		1.314	-.020	-.030		1.400	-.013	-.064		.598	-.015	-.063		1.342
12.0	-.012	-.033		1.346	-.015	-.034		1.423	-.007	-.082		.437	-.008	-.072		1.367
14.0	-.005	-.037		1.404	-.006	-.037		1.468	.001	-.075		.511	.001	-.081		1.415
16.0	-.002	-.037		1.448	0	-.039		1.506	.007	-.082		.854	.007	-.093		1.454
18.0	-.009	-.037		1.483	.007	-.057		1.553	.028	-.085		.964	.024	-.089		1.483
21.0	.019	-.035		1.523	.018	-.036		1.568	.012	-.094		1.069	.009	-.110		1.521
24.0	.002	-.024		1.556	0	-.025		1.597	.001	-.094		1.180	.001	-.114		1.552
27.0	-.013	-.028		1.588	-.015	-.028		1.625	-.002	-.080		1.253	-.002	-.102		1.578
31.0	.003	-.051		1.609	.003	-.053		1.644	.010	-.098		1.302	.009	-.111		1.594
35.0	-.022	-.065			-.022	-.066			-.019	-.123			-.020	-.137		
37.0	-.006	-.061		1.666	-.006	-.060		1.689	-.002	-.098		1.368	-.005	-.106		1.643
40.0	-.008	-.058			-.006	-.058			-.009	-.097			-.012	-.104		
(b) Concluded. Circumferential distribution of C_p .																
Station	Outer shell, external				Outer shell, external				Outer shell, external				Outer shell, external			
$\theta \rightarrow$	198°	216°	234°	252°	198°	216°	234°	252°	198°	216°	234°	252°	198°	216°	234°	252°
0.5	-0.013	0.015	0.059	0.113	-0.048	-0.019	0.026	0.076	-0.086	-0.032	0.055	0.115	-0.122	-0.072	-0.005	0.080
14.0	-.010	-.022	-.034	-.039	-.012	-.024	-.036	-.041	-.011	-.039	-.075	-.091	-.013	-.043	-.085	-.106
43.0	-.013	-.018	-.024	-.037	-.015	-.018	-.024	-.035	-.026	-.036	-.038	-.052	-.026	-.044	-.043	-.054

1970-1971

1970-1971

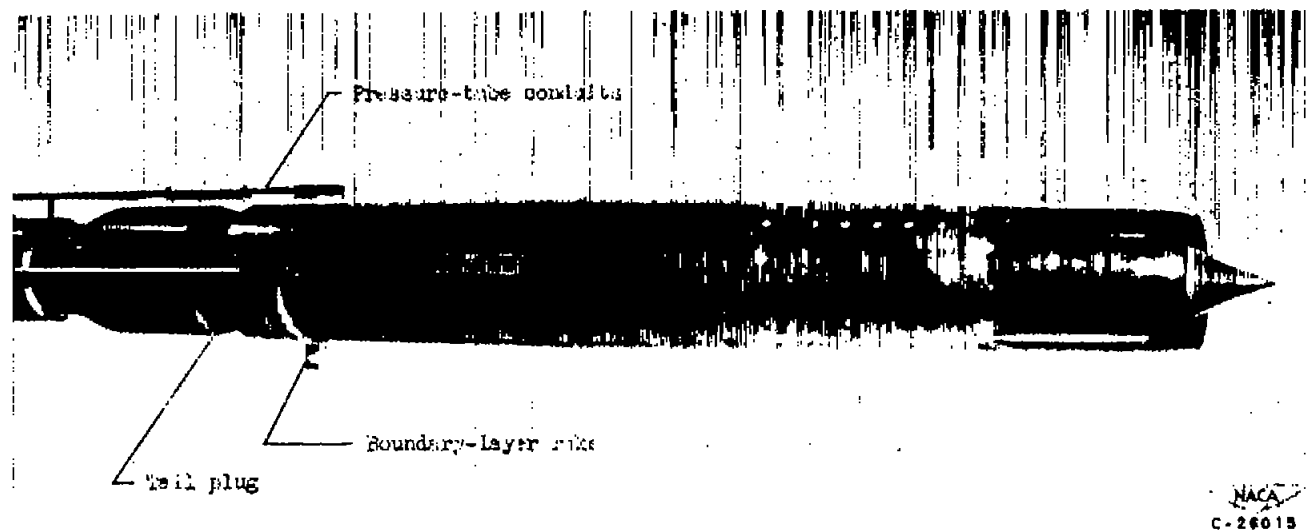
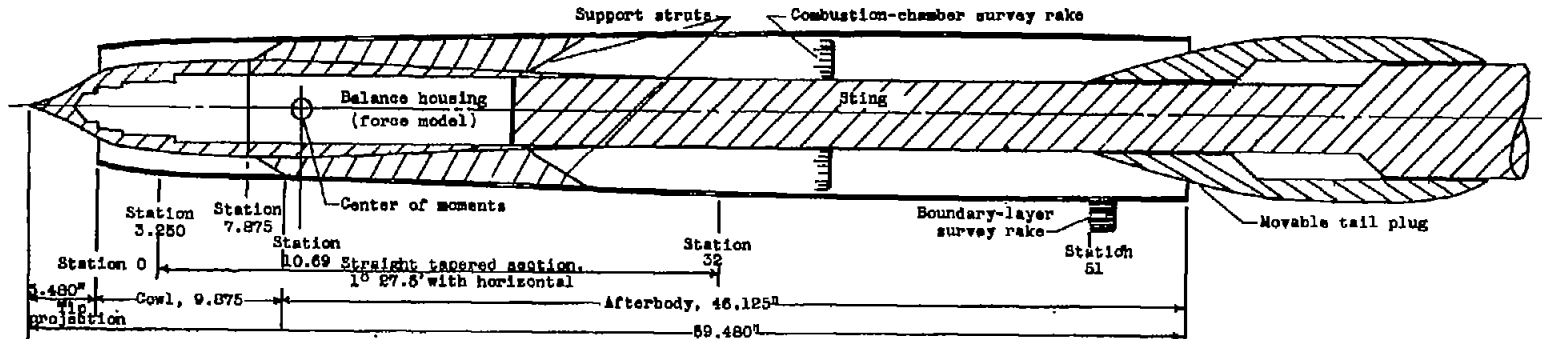


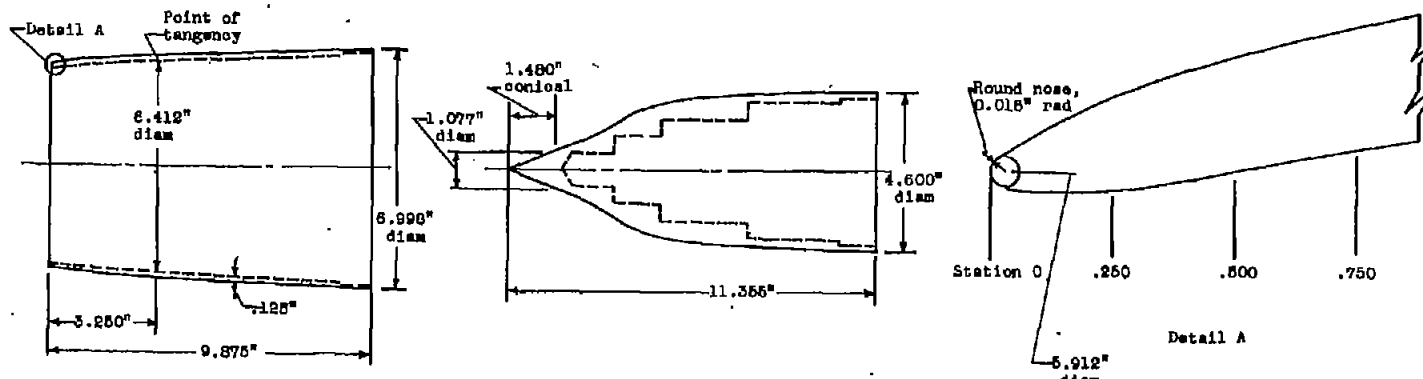
Figure 1. - 8-inch ram-jet configuration.

██████████

██████████



(a) NACA 8-inch ram-jet configuration.



(b) Details of cowl.

(c) Details of spike.

Figure 2. - Schematic diagram of NACA 8-inch ram-jet configuration showing principal dimensions of model and details of all-external isentropic compression inlet.

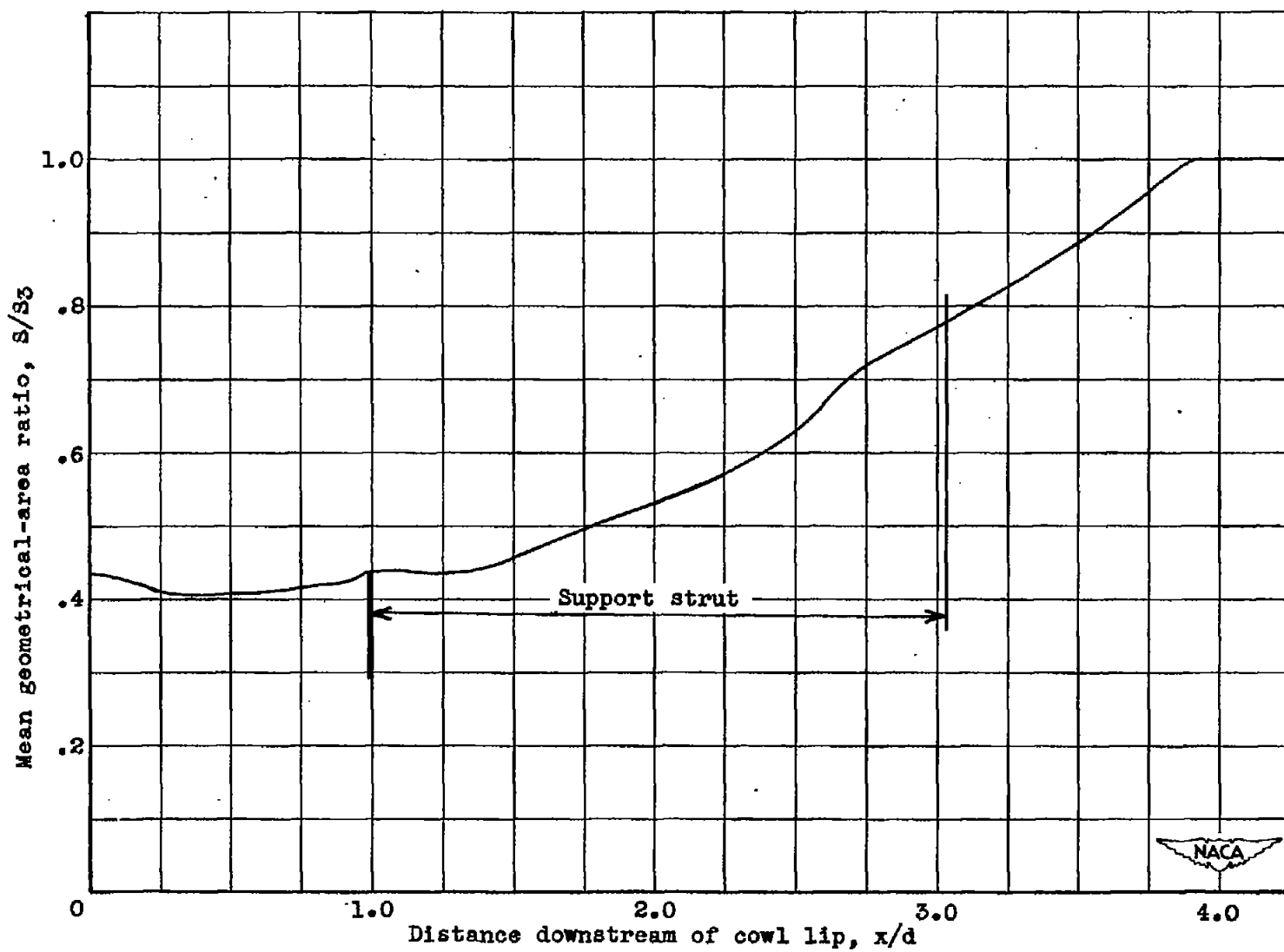


Figure 3. - Longitudinal variation of mean geometric area.

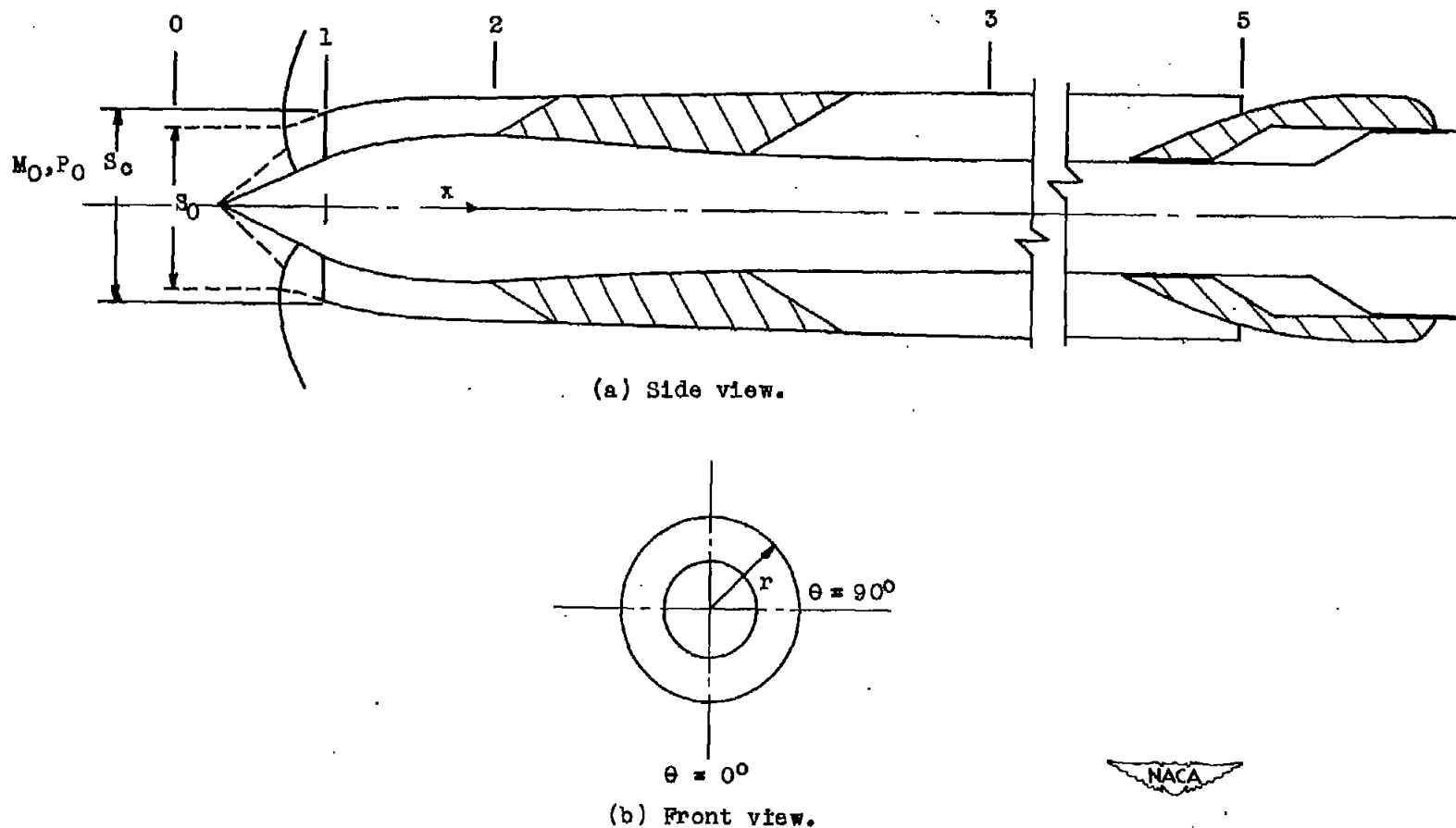


Figure 4. - Notation for 8-inch ram-jet configuration.

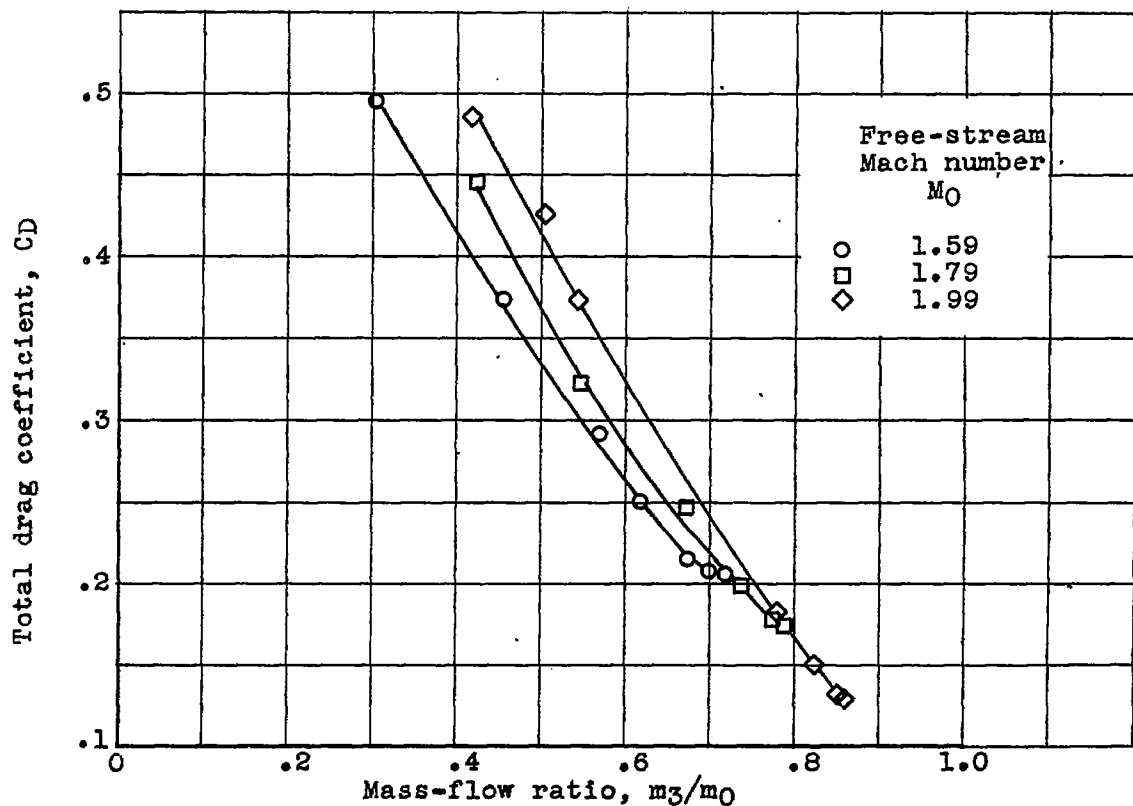
~~CONFIDENTIAL~~

Figure 5. - Variation of total drag coefficient with mass-flow ratio at zero angle of attack for three Mach numbers.

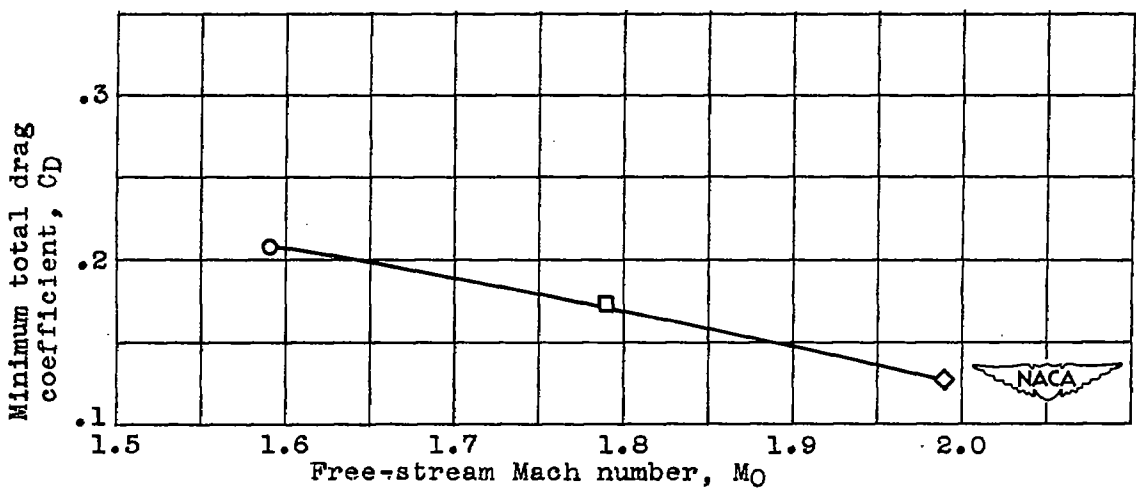


Figure 6. - Variation of minimum total drag coefficient with free-stream Mach number at zero angle of attack.

~~CONFIDENTIAL~~

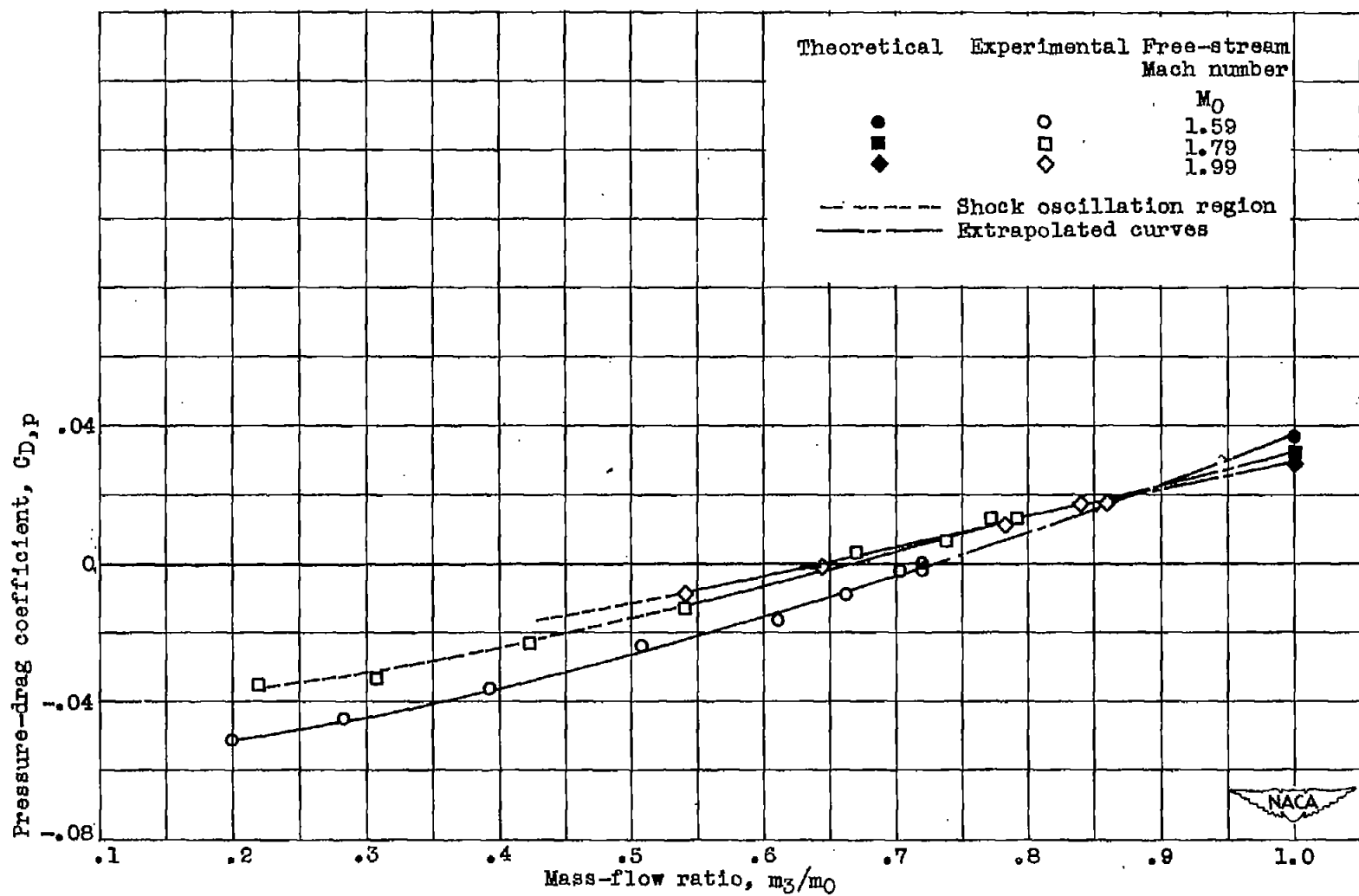
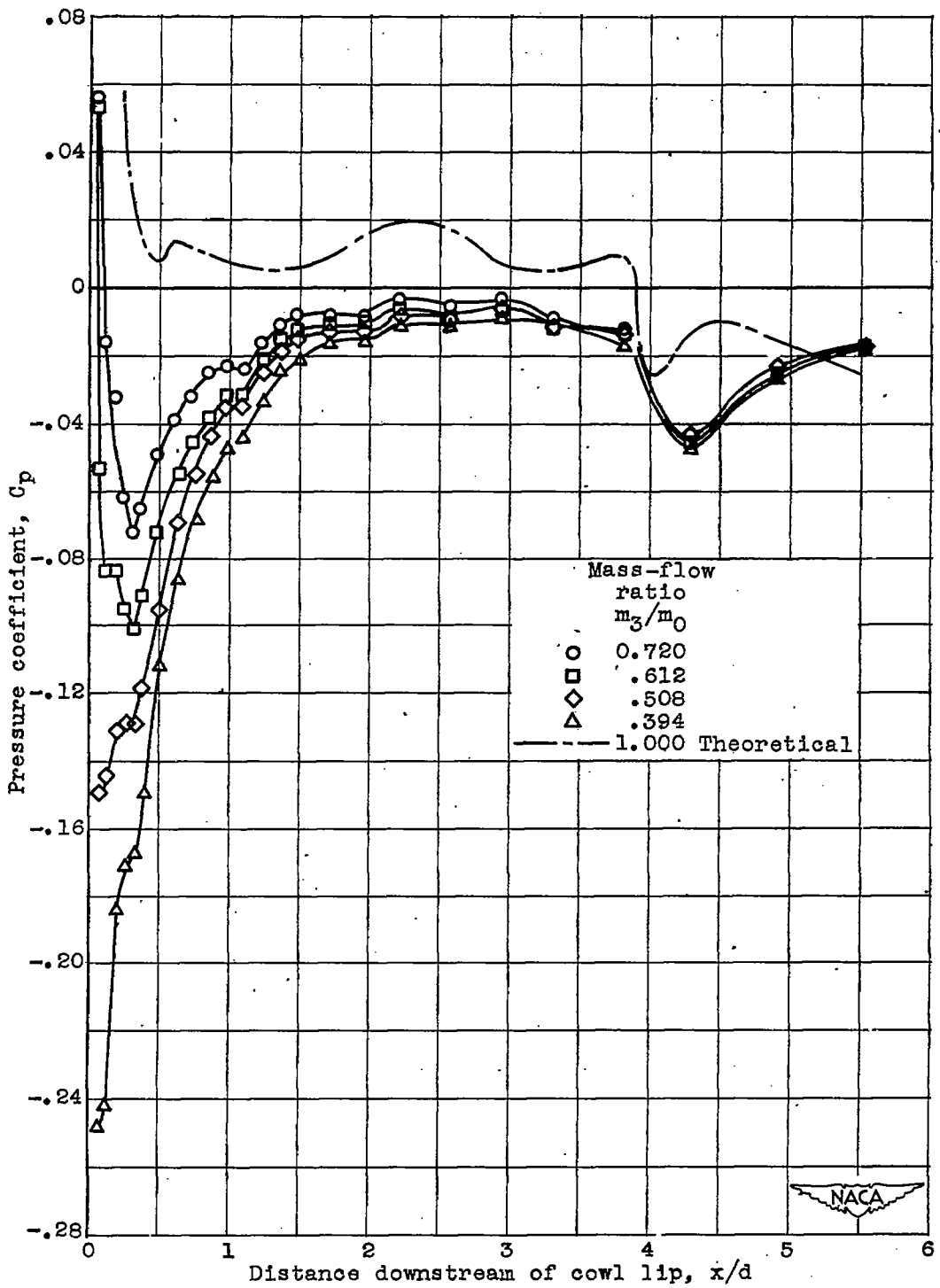
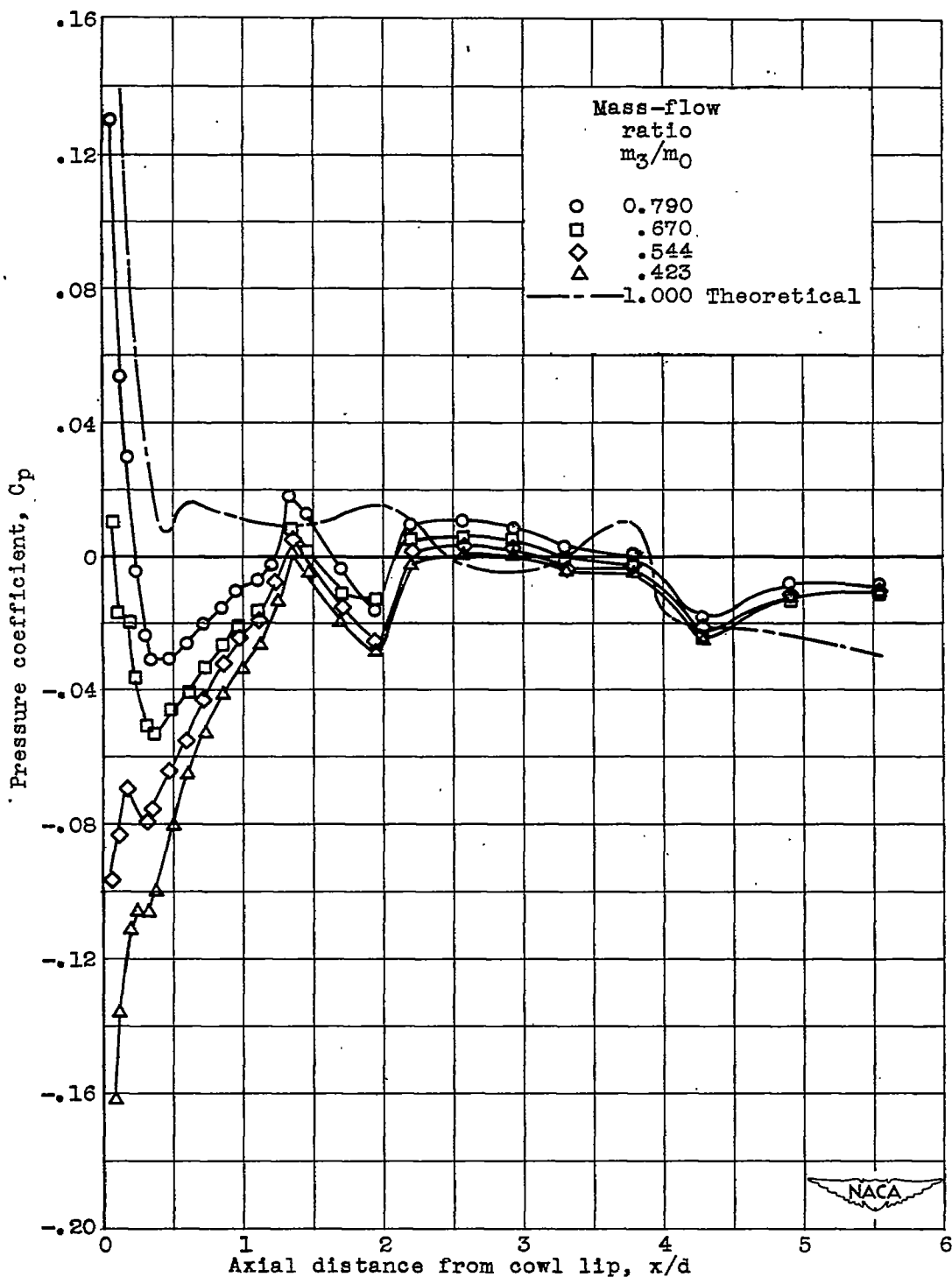


Figure 7. — Variation of pressure-drag coefficient with mass-flow ratio at zero angle of attack for three Mach numbers.



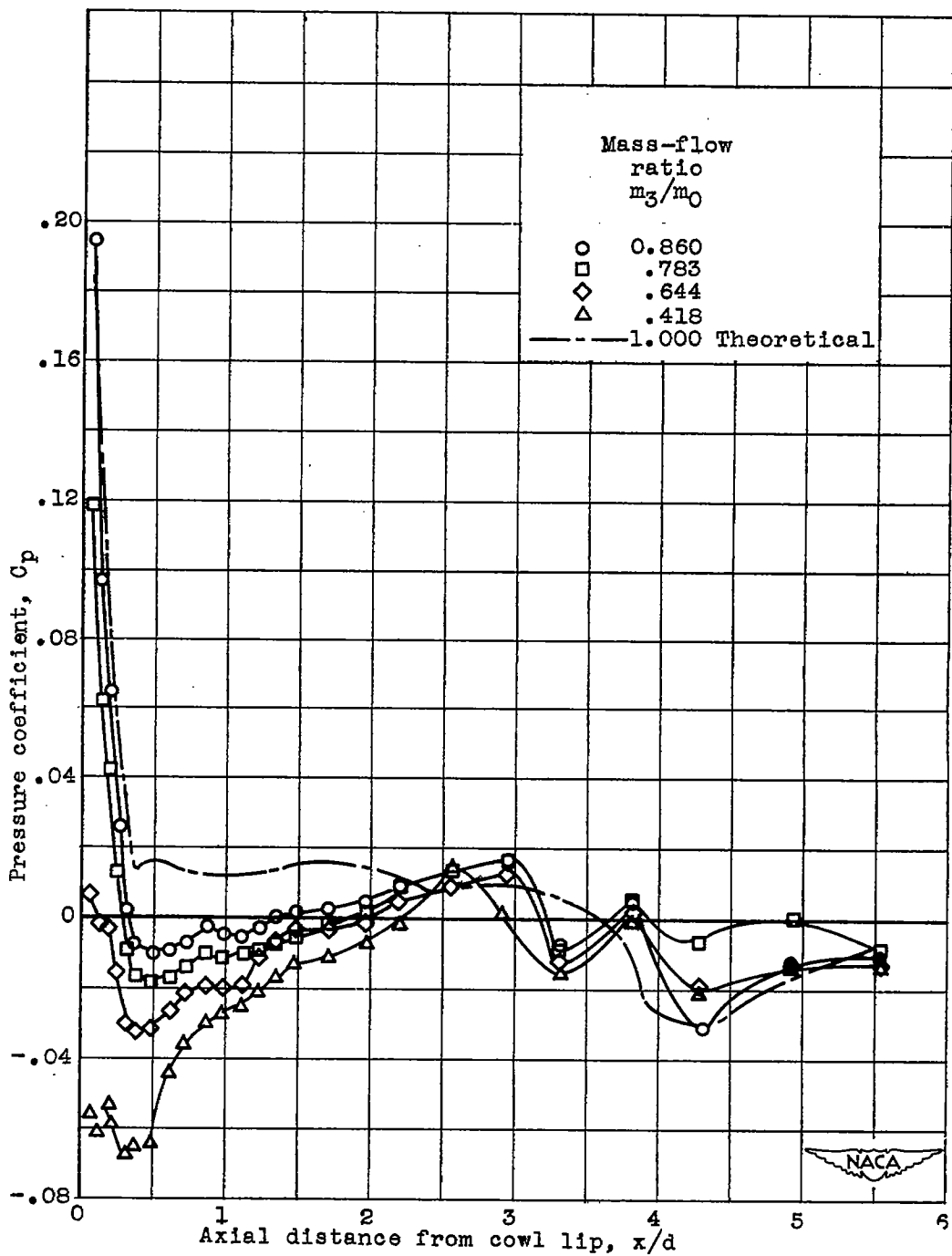
(a) Free-stream Mach number, 1.59.

Figure 8. - Axial variation of external pressure distribution along top surface of model at zero angle of attack for three Mach numbers.



(b) Free-stream Mach number, 1.79.

Figure 8. - Continued. Axial variation of external pressure distribution along top surface of model at zero angle of attack for three Mach numbers.



(c) Free-stream Mach number, 1.99.

Figure 8. - Concluded. Axial variation of external pressure distribution along top surface of model at zero angle of attack for three Mach numbers.

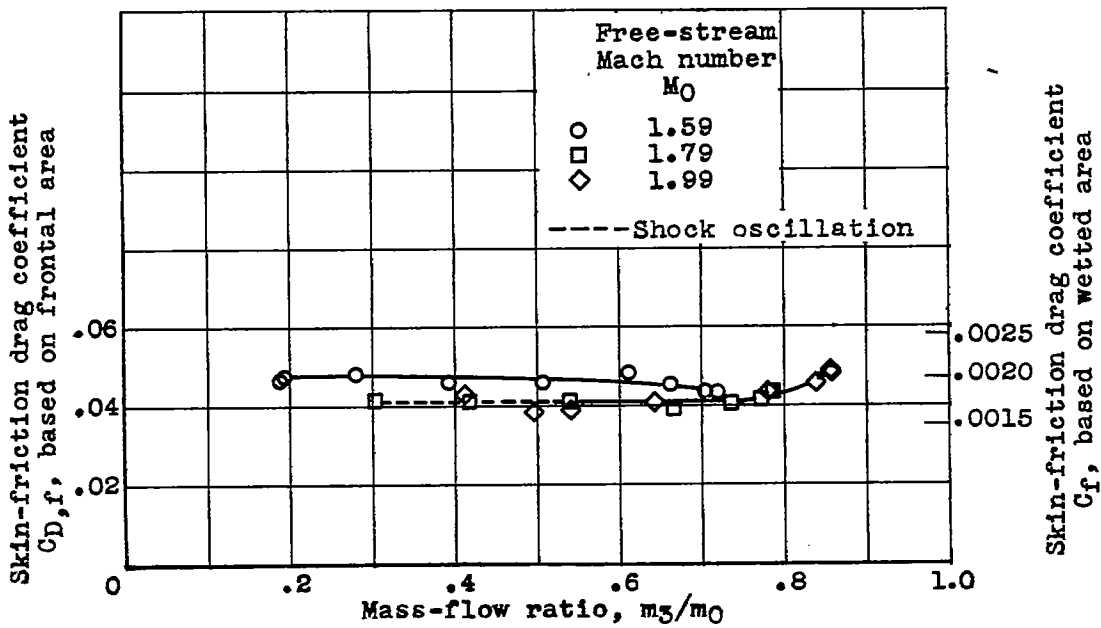


Figure 9. - Variation of skin-friction drag coefficient with mass-flow ratio at zero angle of attack for three Mach numbers.

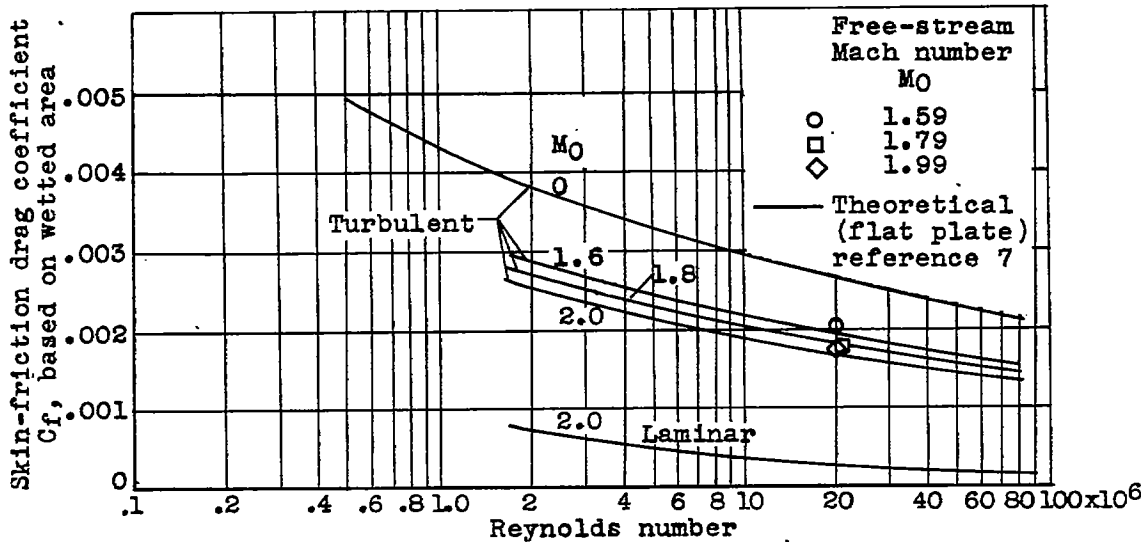


Figure 10. - Comparison of experimental skin-friction drag coefficient with two-dimensional compressible-flow theory at three Mach numbers.

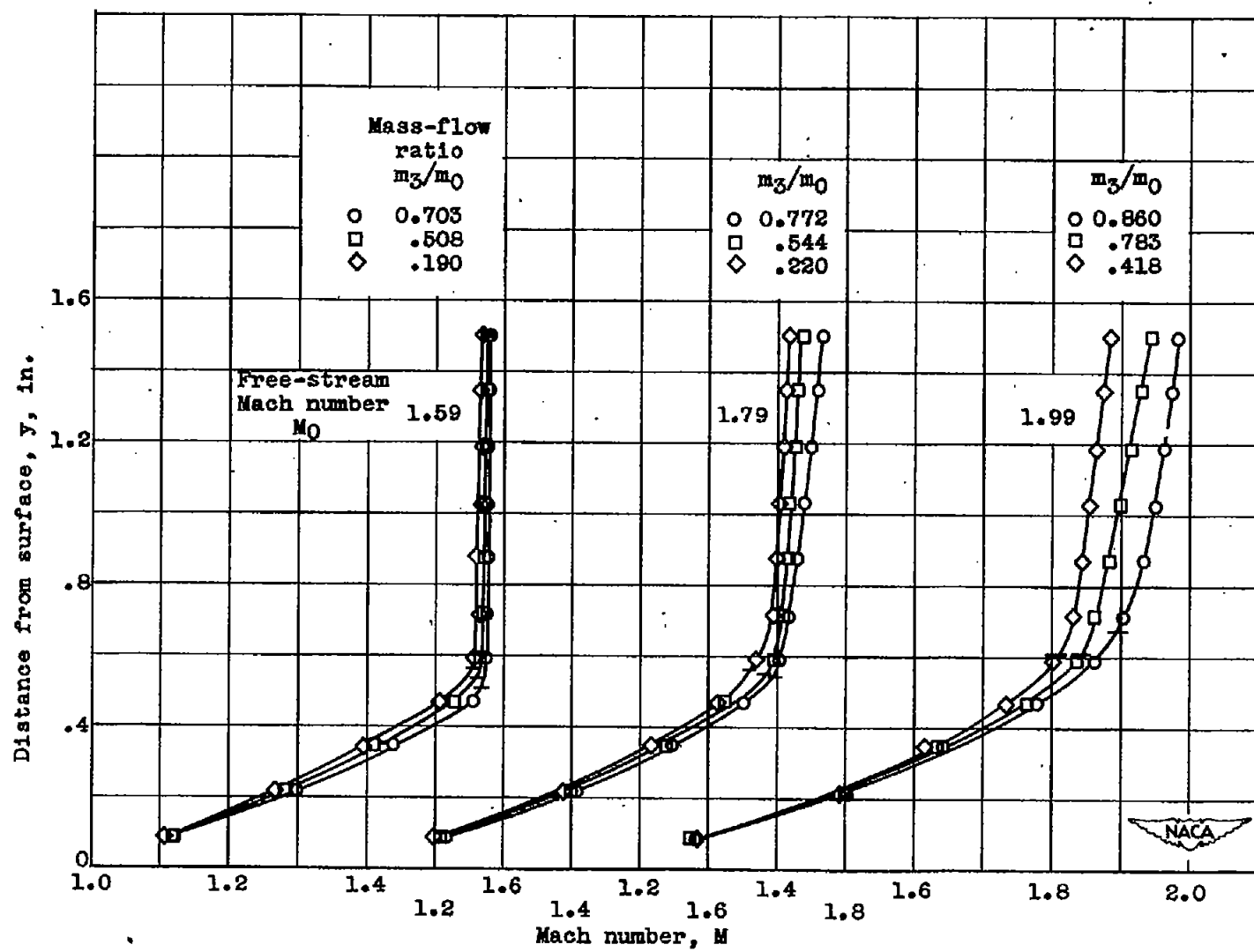


Figure 11. - Variation of Mach-number distribution in boundary layer at zero angle of attack for range of mass-flow ratios at three Mach numbers. Station 51.

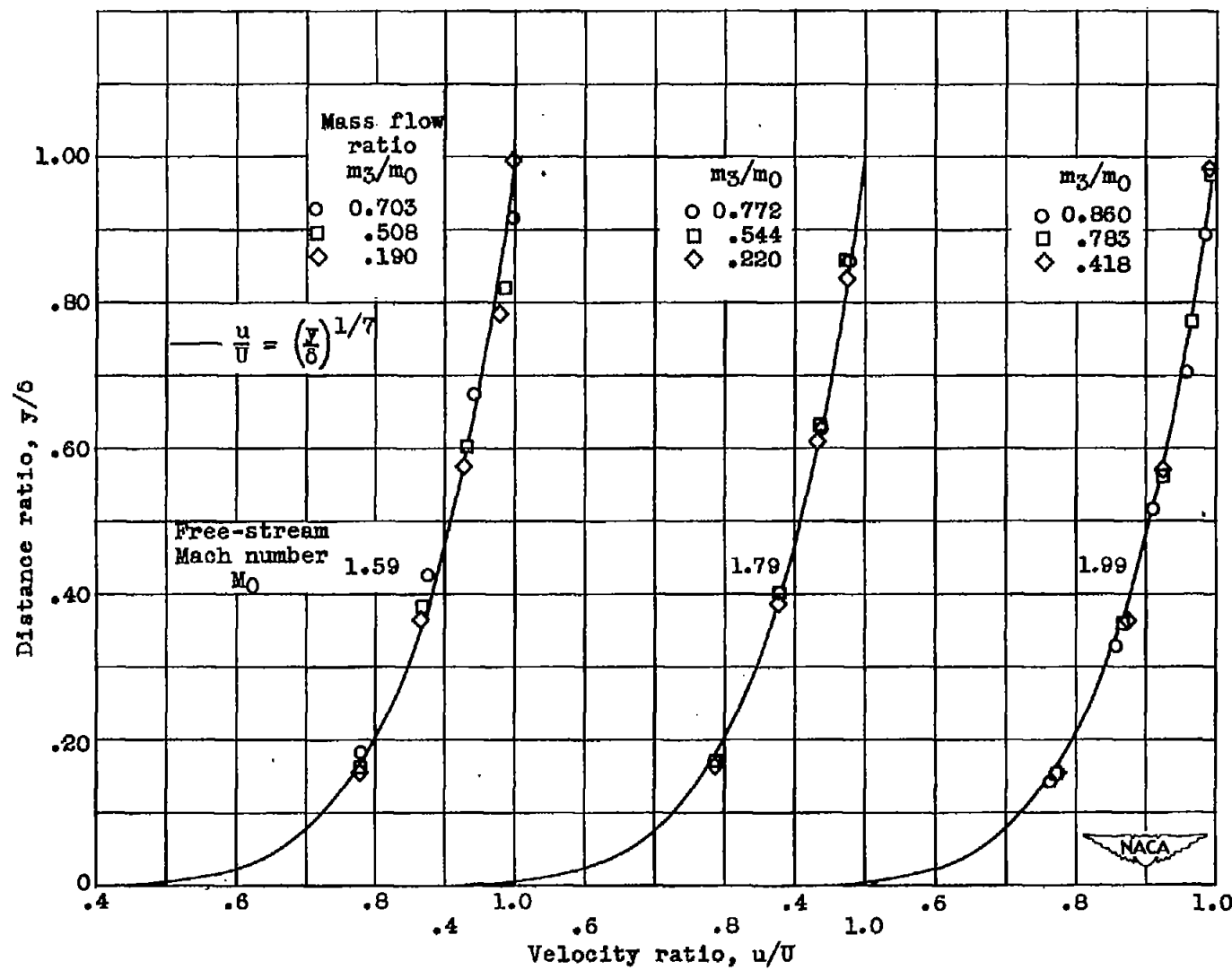


Figure 12. - Comparison of experimental and theoretical boundary-layer profiles at zero angle of attack for range of mass-flow ratios and three free-stream Mach numbers.

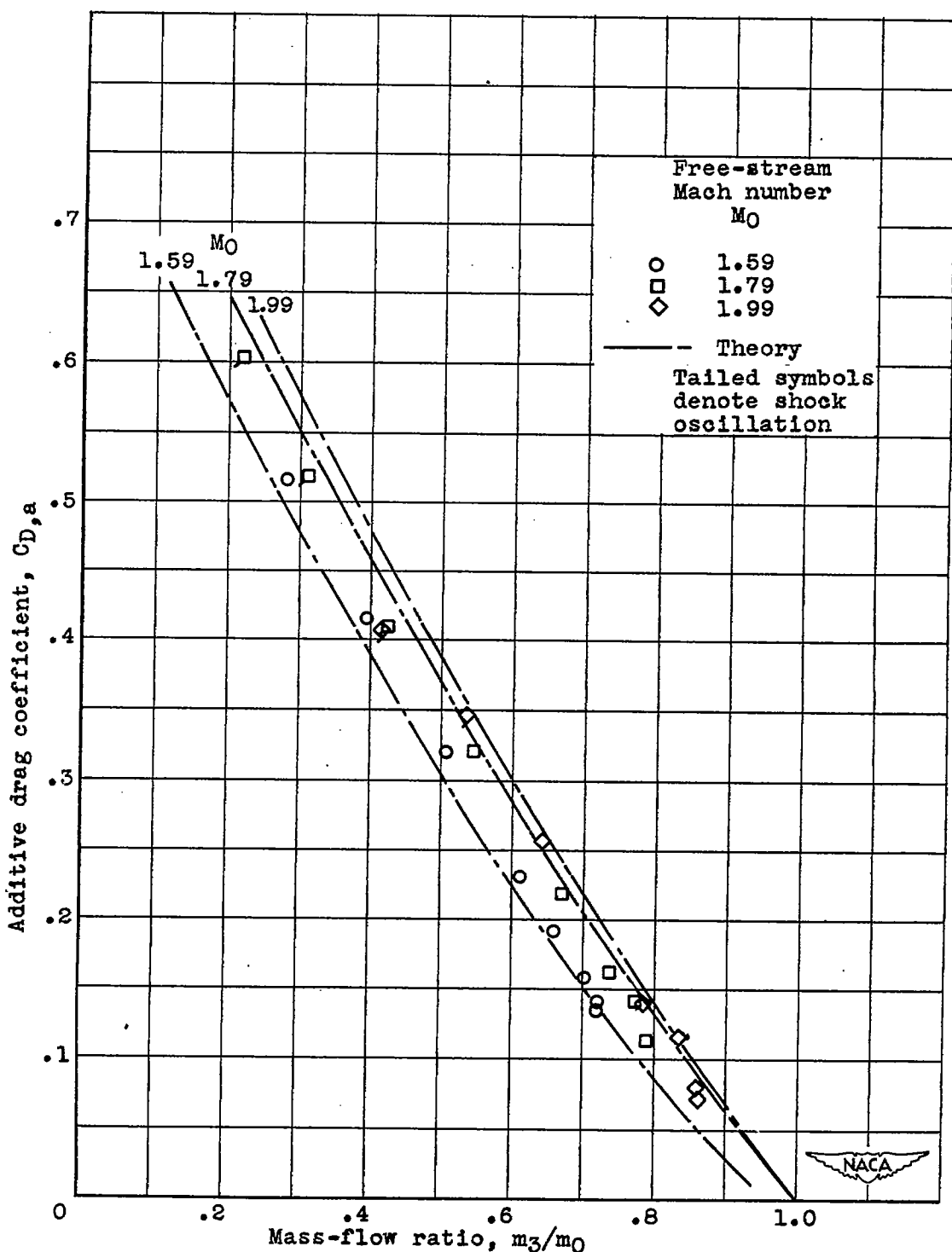
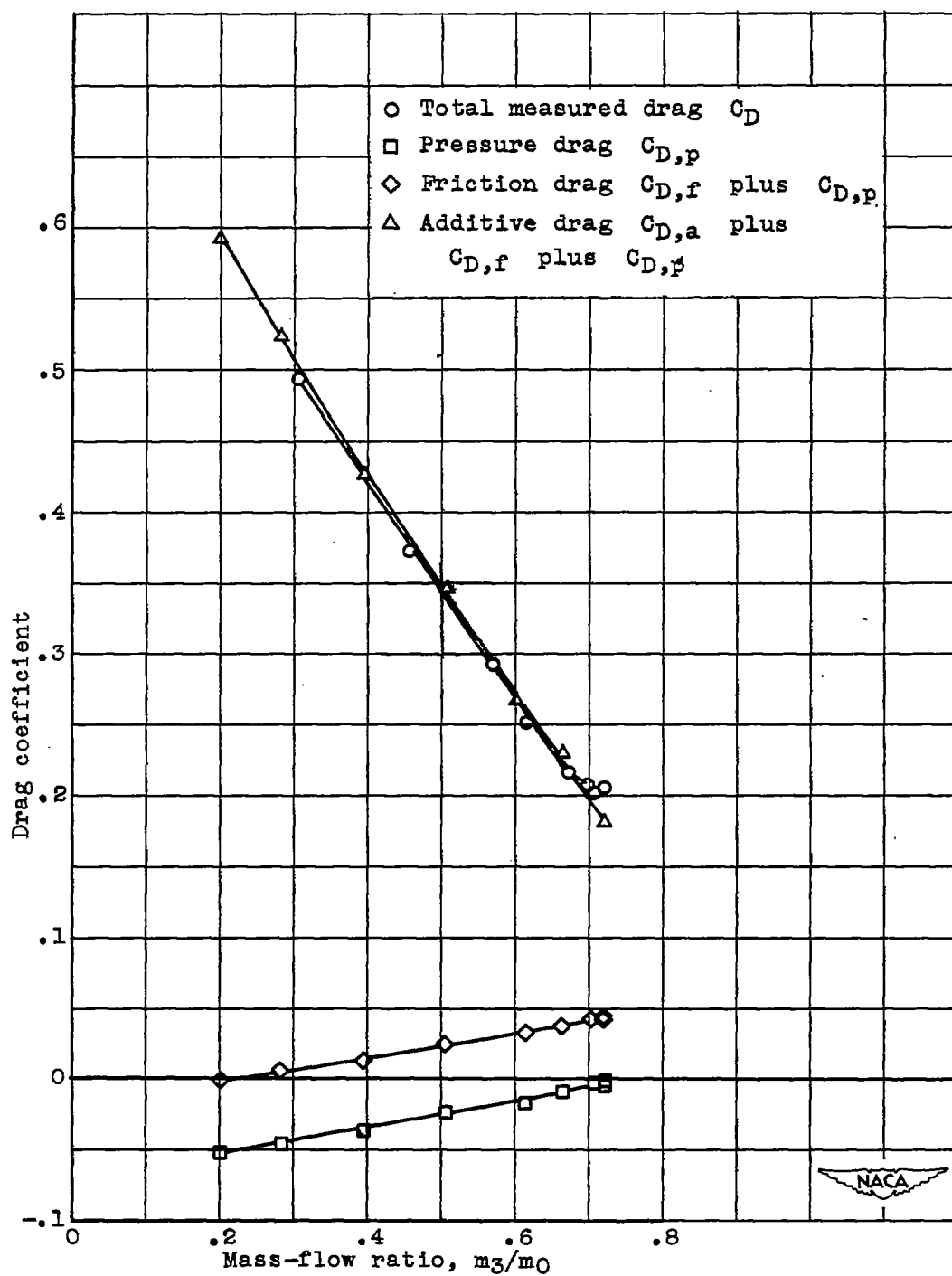
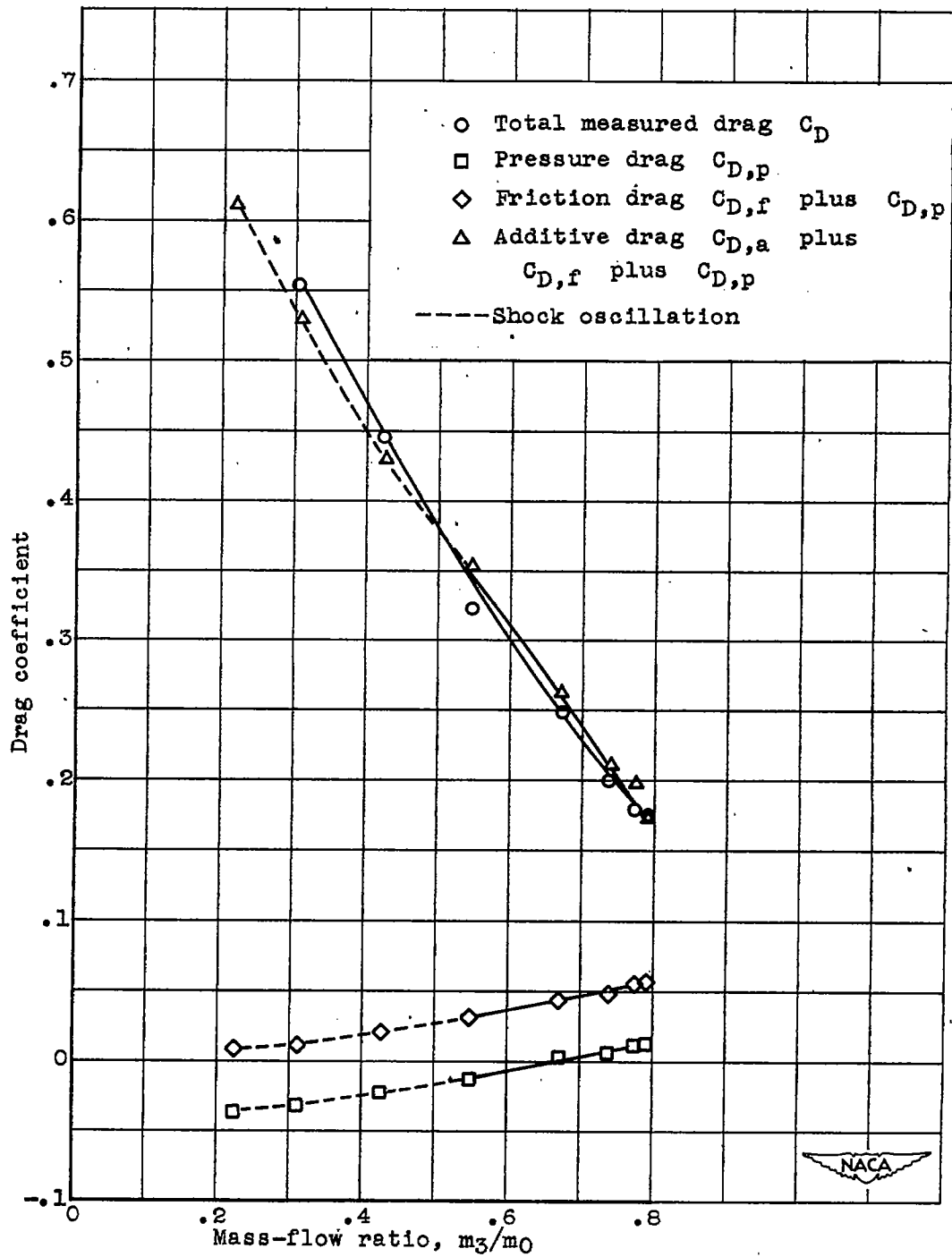


Figure 13. - Comparison of experimental additive drag coefficients with one-dimensional theory for range of mass-flow ratios at zero angle of attack for three Mach numbers.



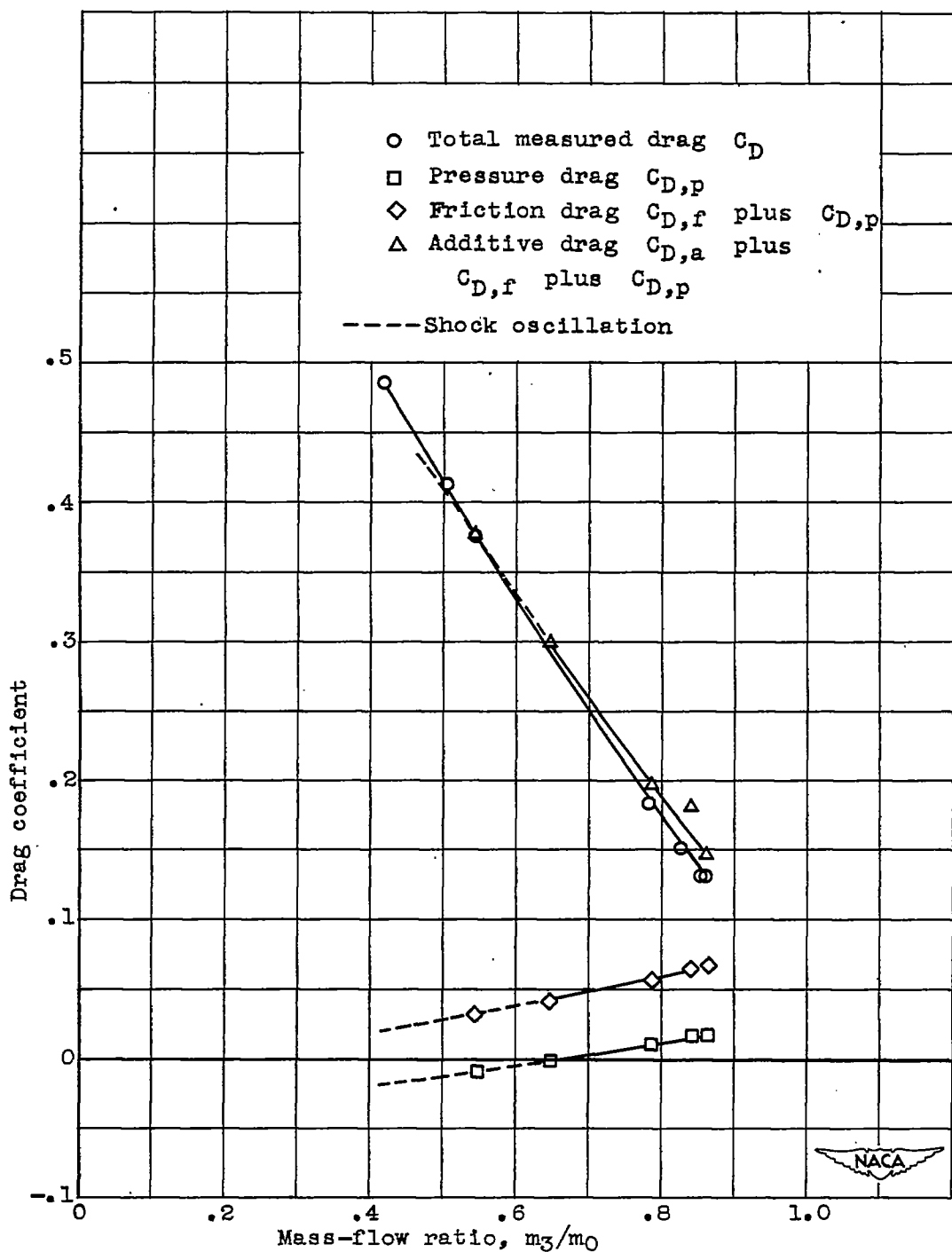
(a) Free-stream Mach number, 1.59.

Figure 14. - Variation of components of total-drag coefficient with mass-flow ratio at zero angle of attack for three Mach numbers.



(b) Free-stream Mach number, 1.79.

Figure 14. - Continued. Variation of components of total-drag coefficient with mass-flow ratio at zero angle of attack for three Mach numbers.



(c) Free-stream Mach number, 1.99.

Figure 14. - Concluded. Variation of components of total-drag coefficient with mass-flow ratio at zero angle of attack for three Mach numbers.

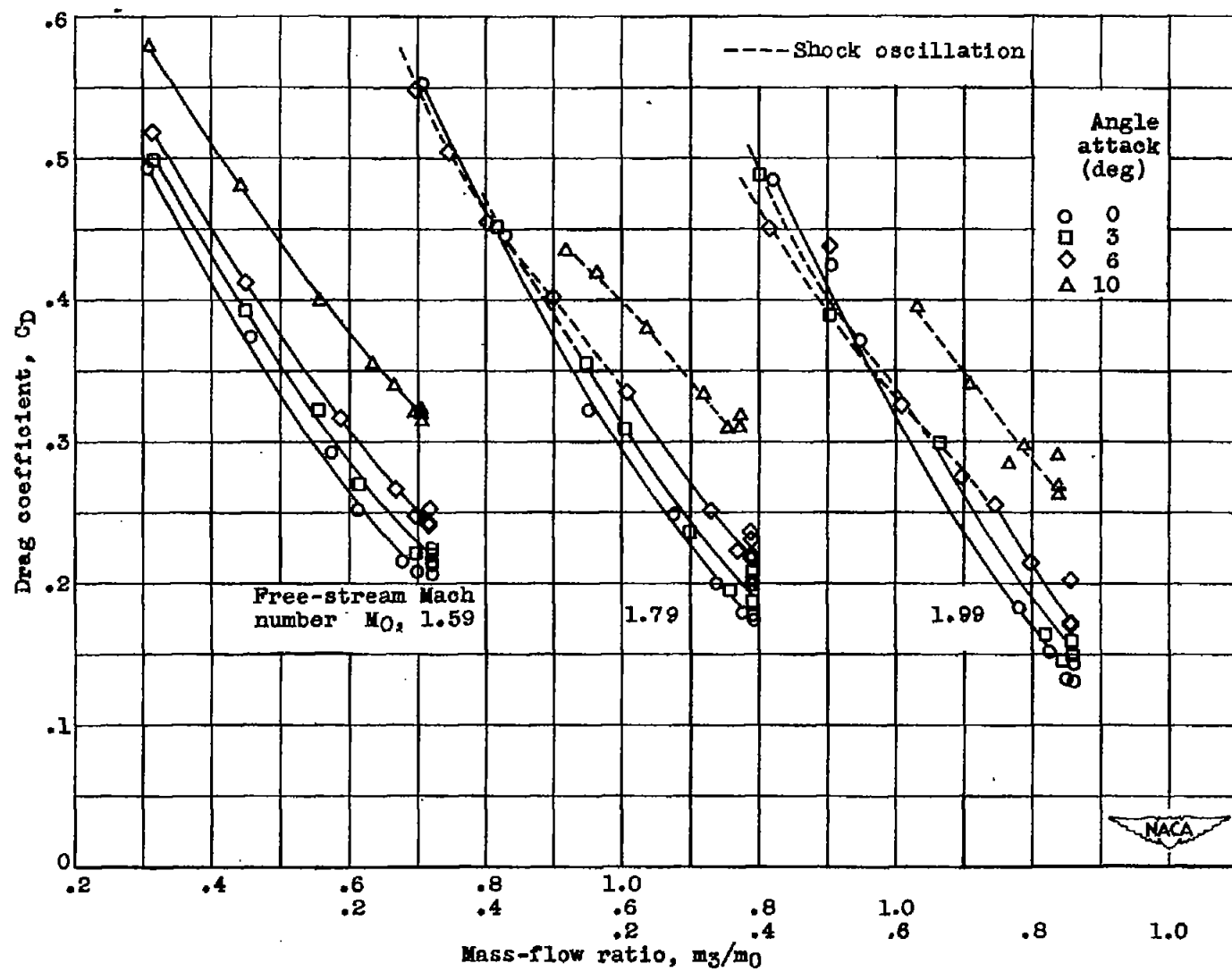


Figure 15. - Variation of total-drag coefficients with mass-flow ratio at four angles of attack for three Mach numbers.

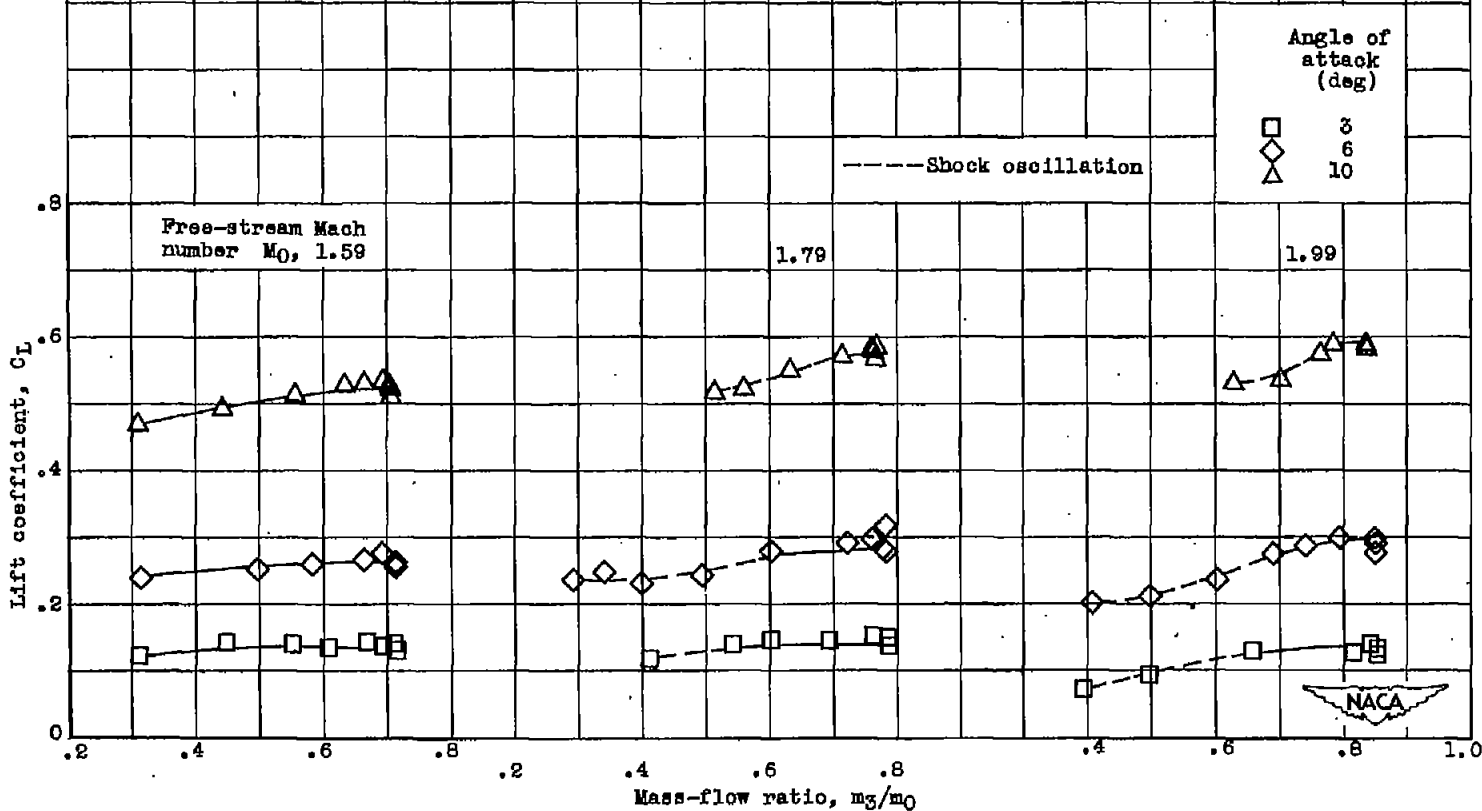


Figure 16. - Variation of external lift coefficients with mass-flow ratio at three angles of attack for three Mach numbers.

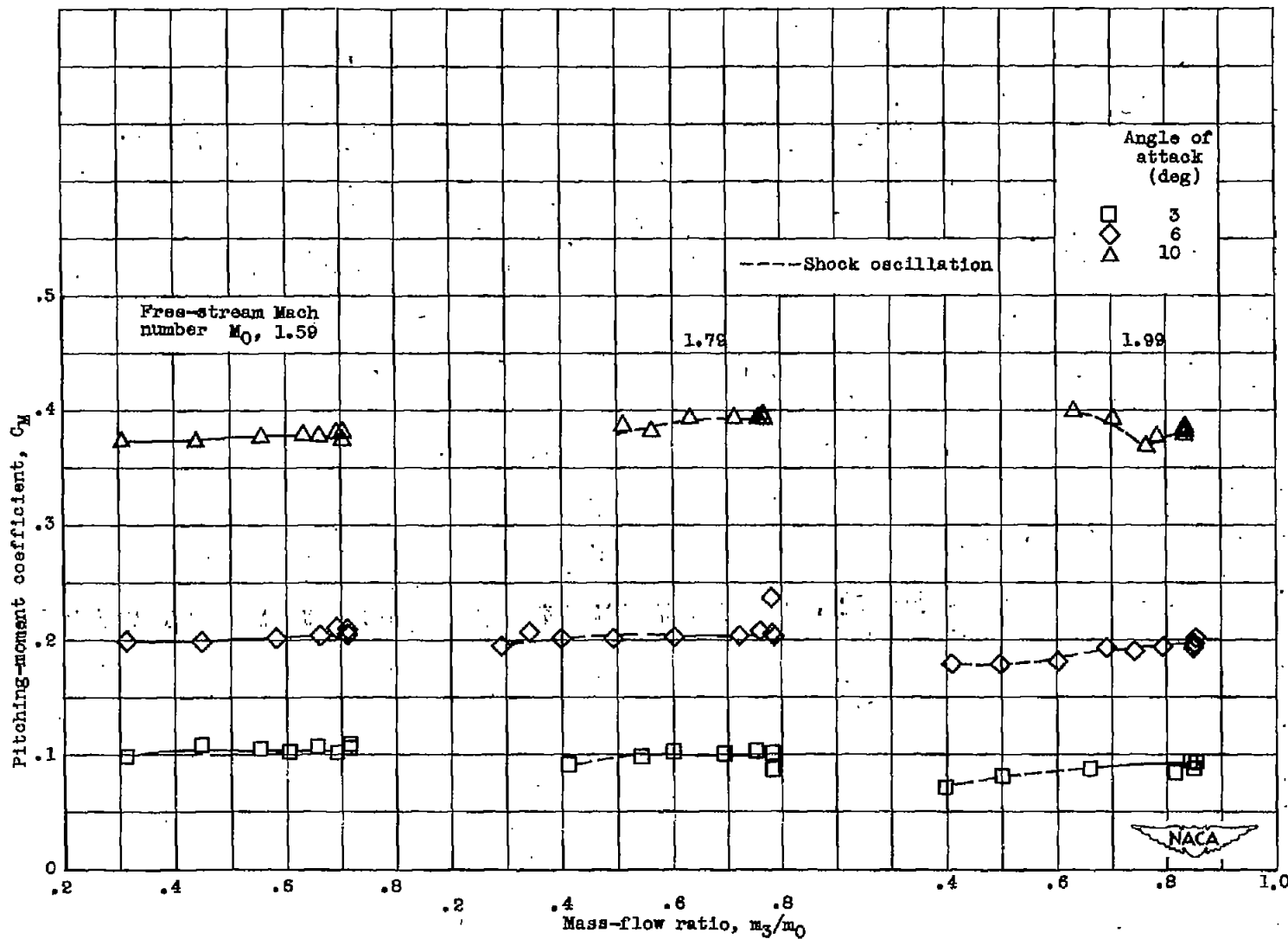


Figure 17. - Variation of external pitching-moment coefficients about base of model with mass-flow ratio at three angles of attack for three Mach numbers.

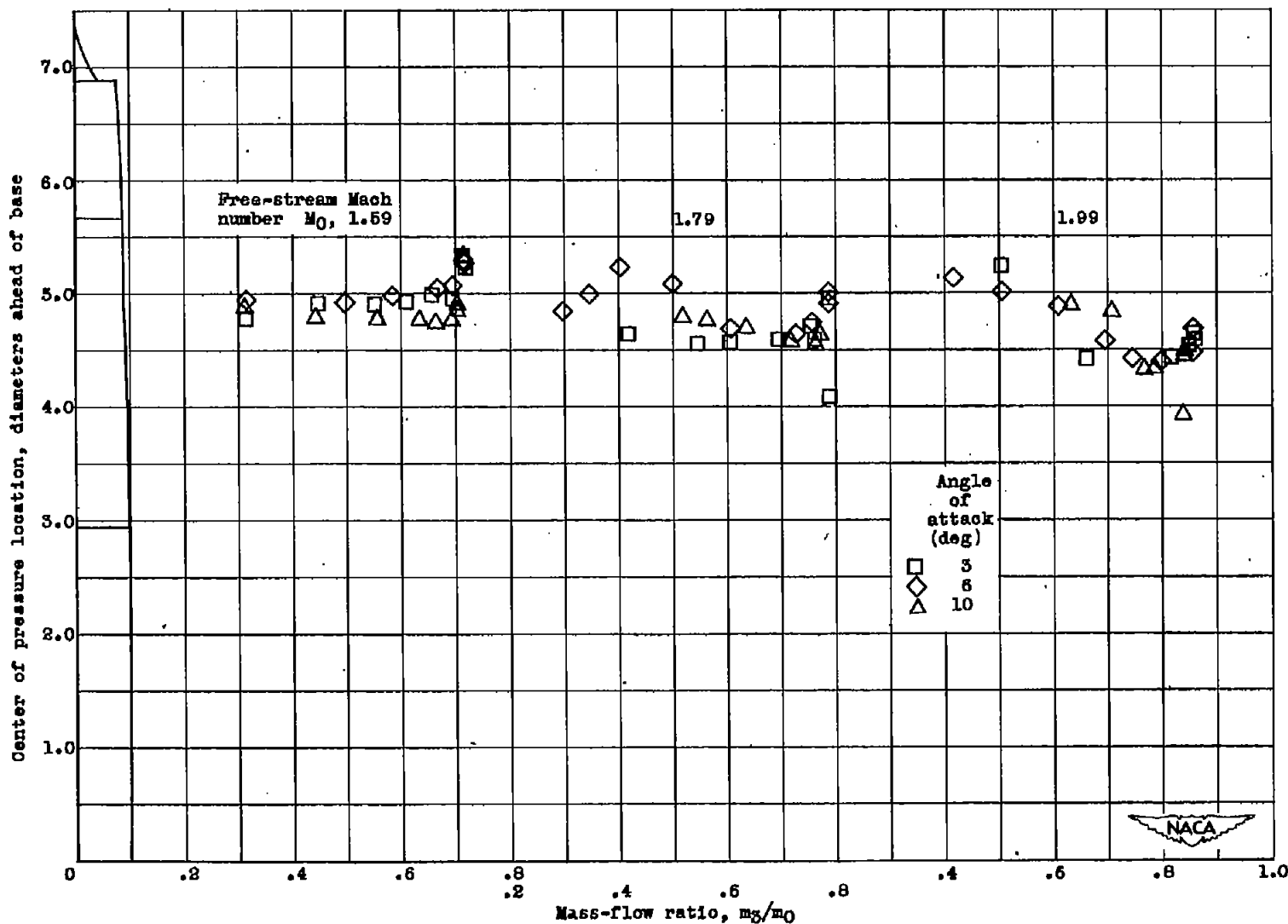


Figure 18. - Variation of center of pressure location with mass-flow ratio at three angles of attack for three Mach numbers.

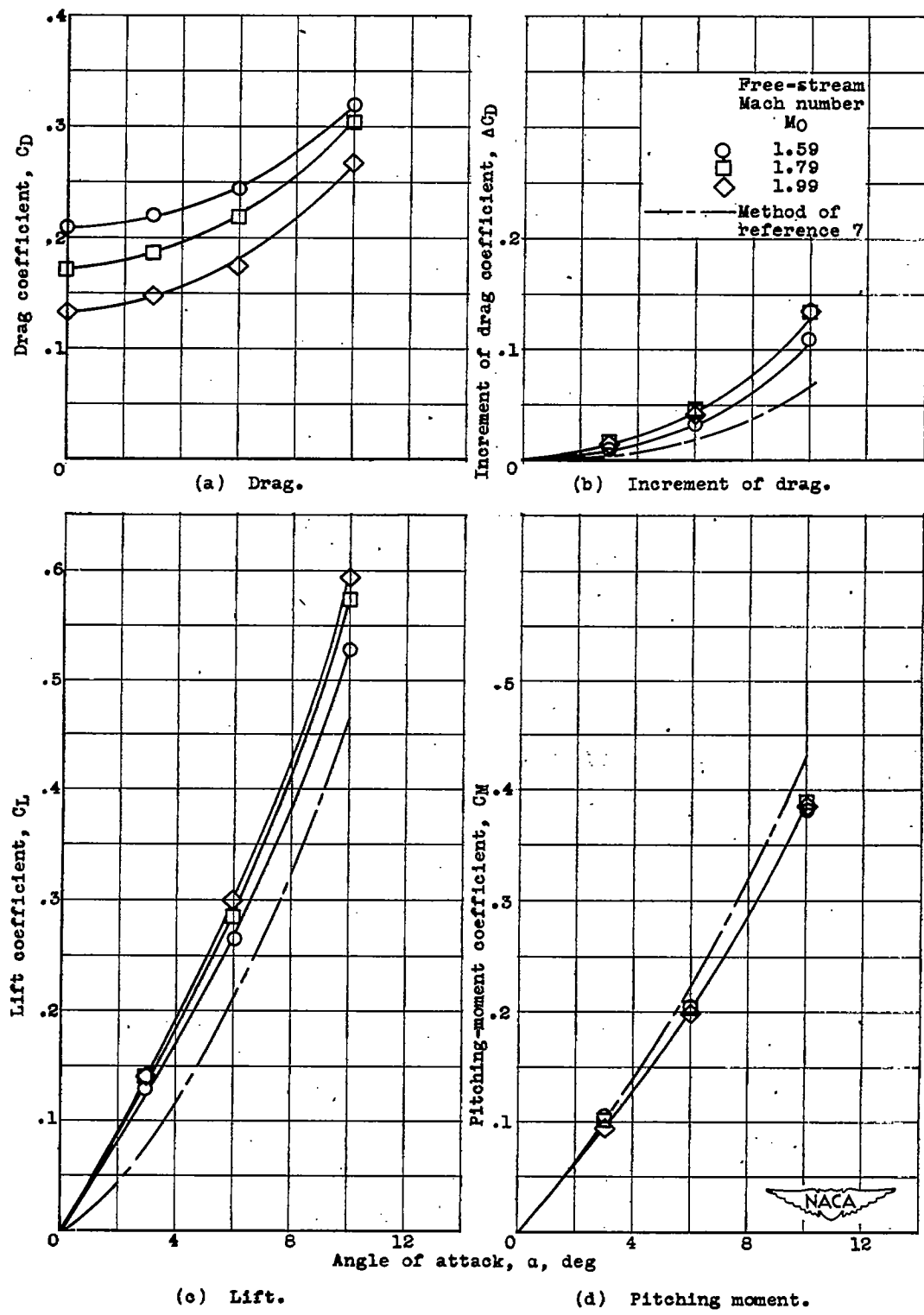


Figure 19. - Variation of drag, increment of drag, lift, and pitching moment with angle of attack at critical mass-flow ratios for three Mach numbers.

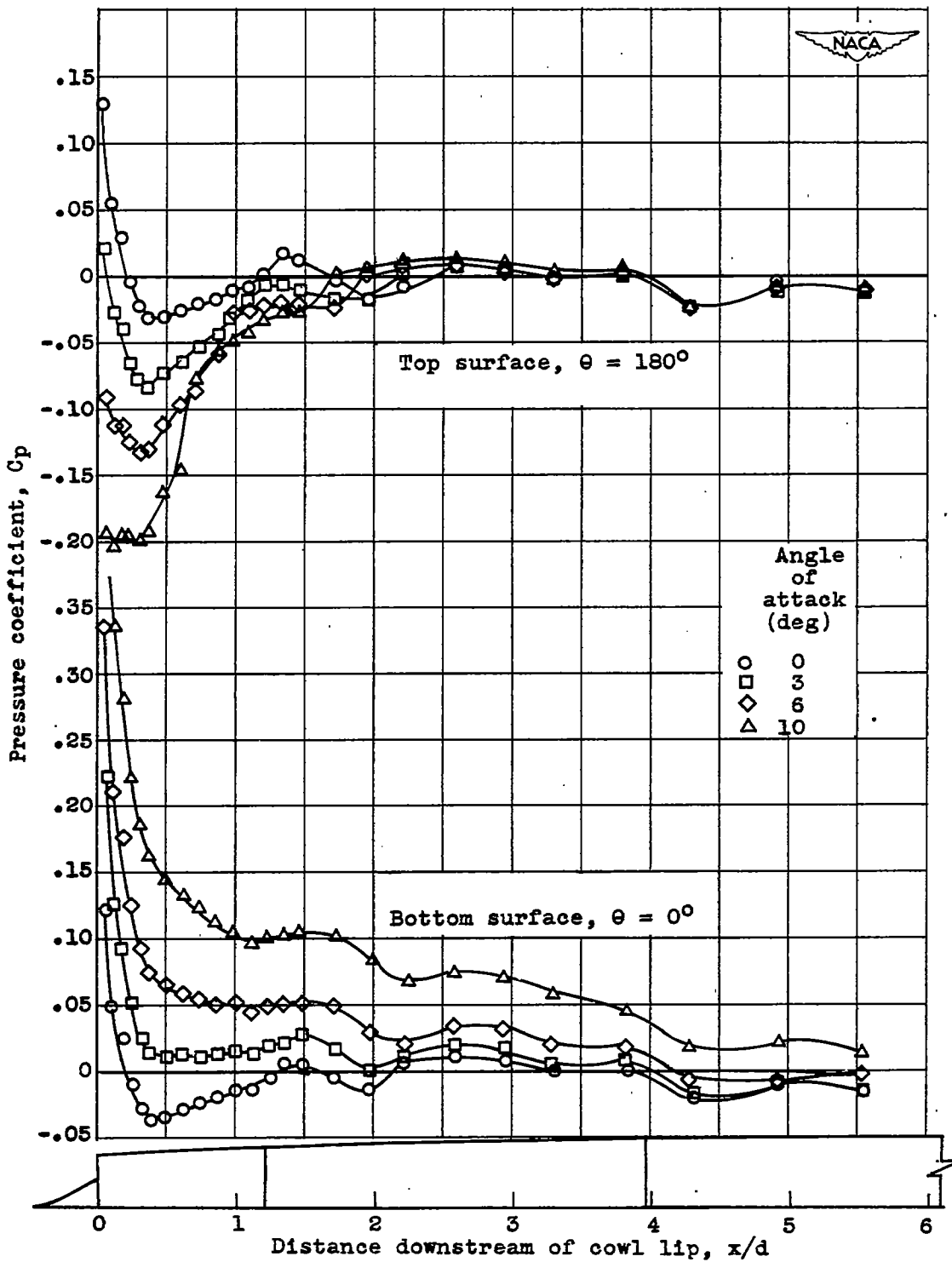
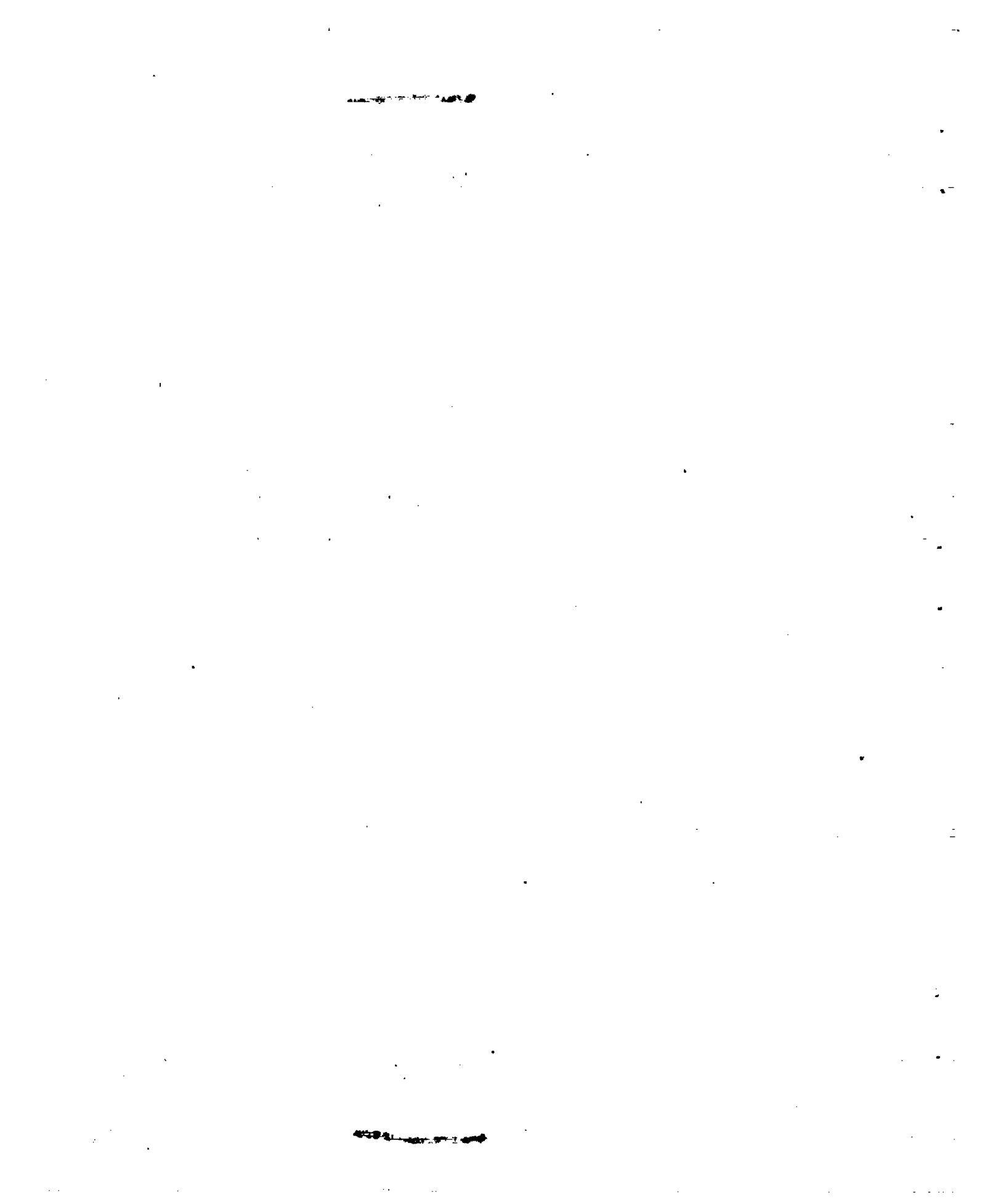


Figure 20. - Longitudinal variation of external-pressure coefficients at constant mass-flow ratio of 0.79 for four angles of attack.
Free-stream Mach number M_0 , 1.79.

CONFIDENTIAL





3

6

10

Angle of attack, deg

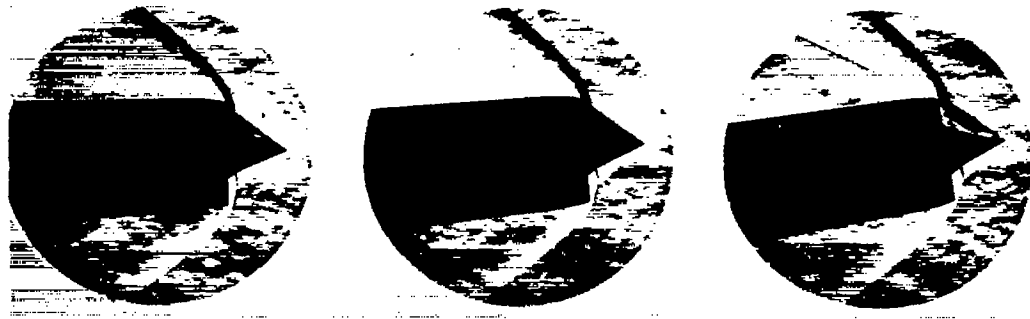
(a) Free-stream Mach number M_0 , 1.59.

3

6

10

Angle of attack, deg

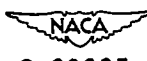
(b) Free-stream Mach number M_0 , 1.79.

3

6

10

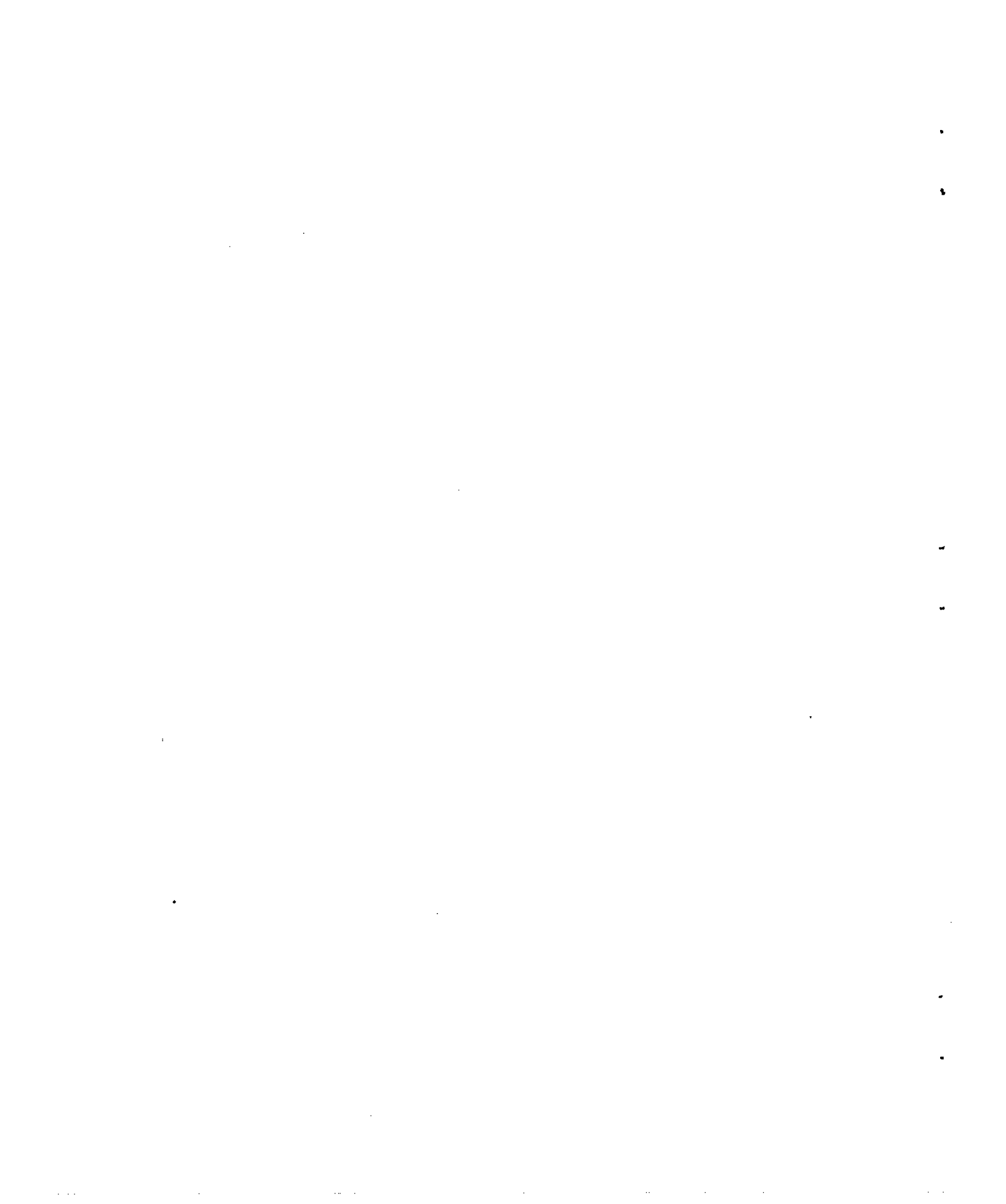
Angle of attack, deg

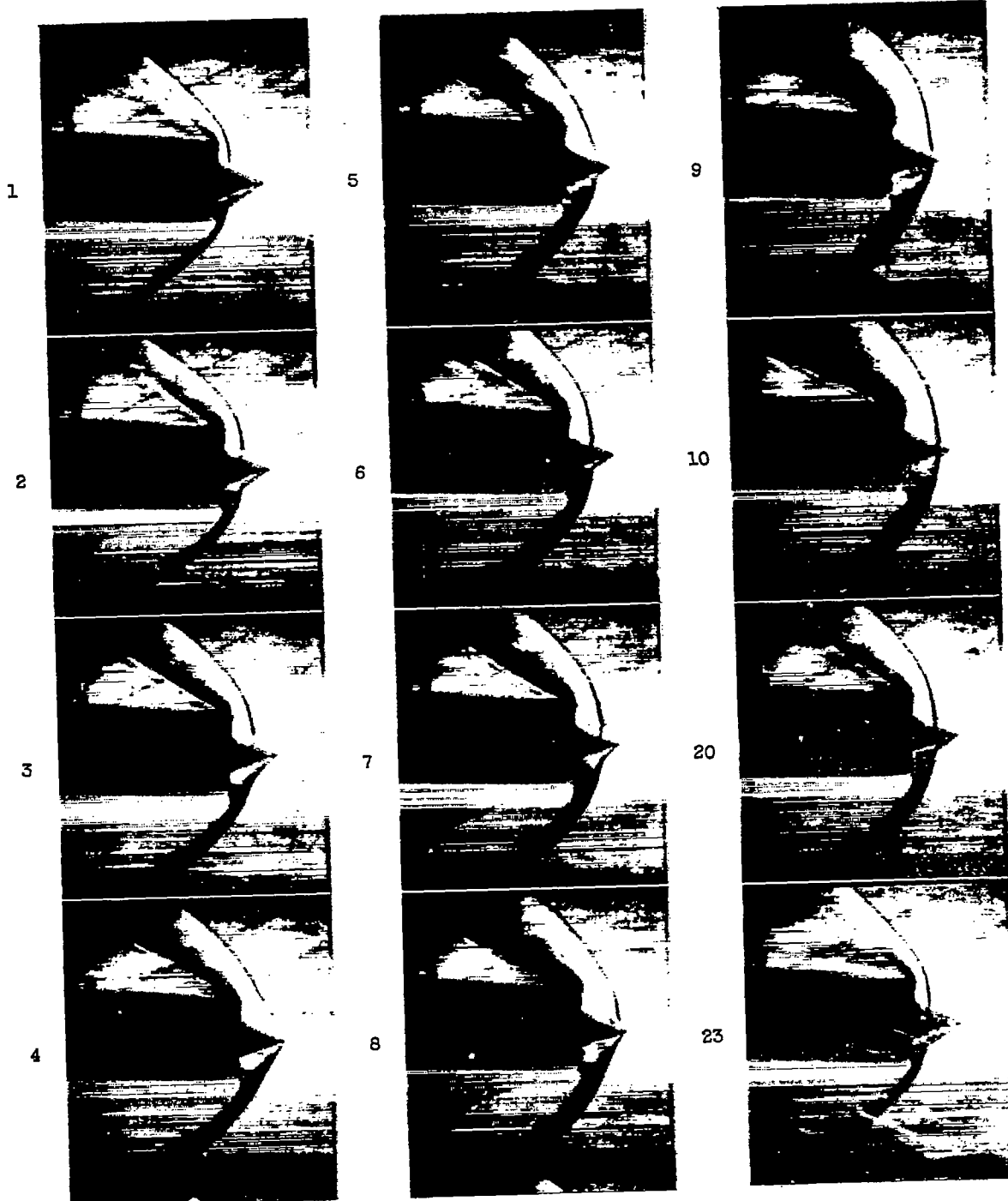
(c) Free-stream Mach number M_0 , 1.99.

C-26235

Figure 21. - Schlieren photographs of inlet at critical mass-flow ratios for three angles of attack and three free-stream Mach numbers.

CONFIDENTIAL



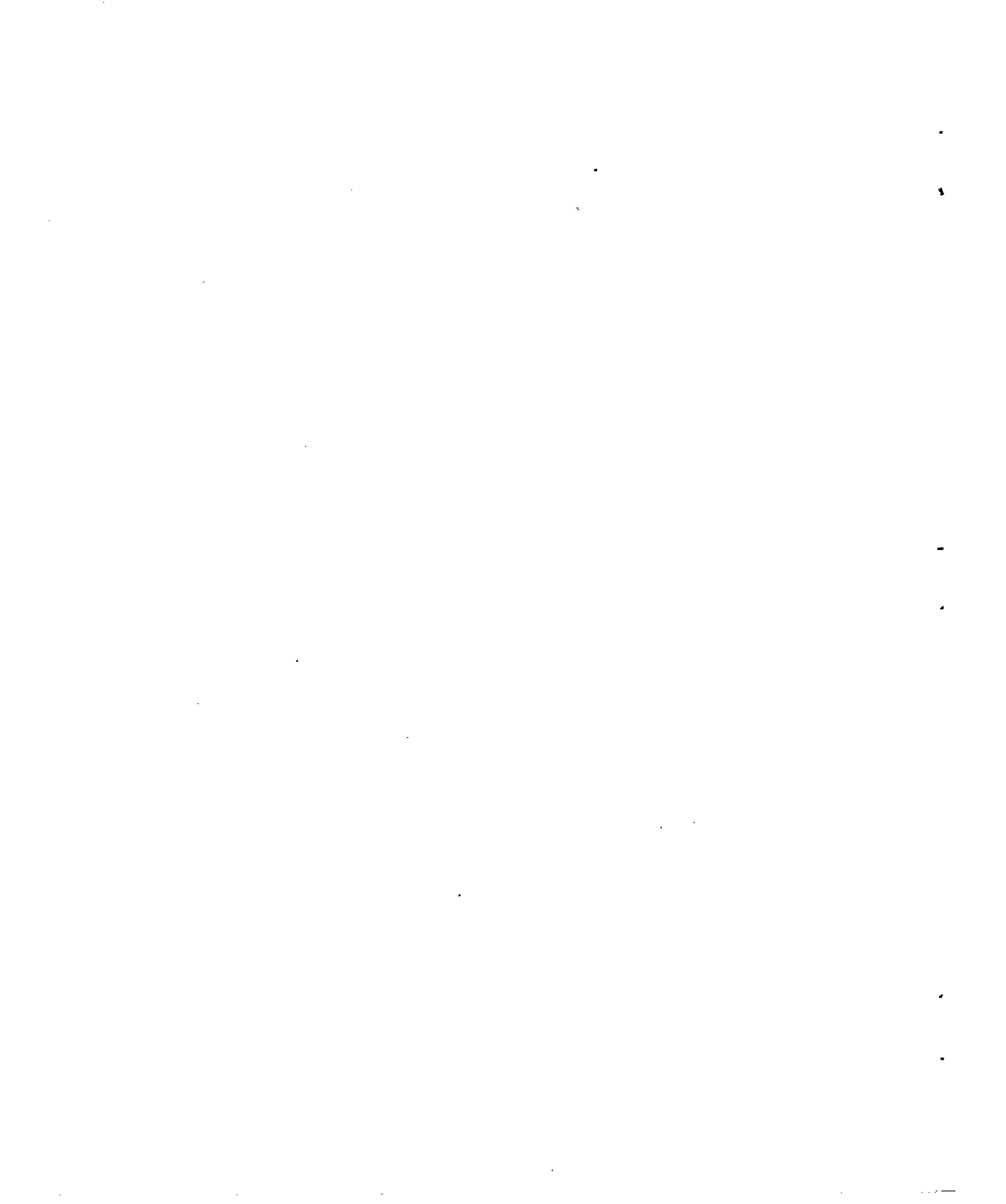
~~CONFIDENTIAL~~

NACA
C-26237

(a) Angle of attack, 0° ; mass-flow ratio, 0.418.

Figure 22. - High-speed schlieren photographs showing oscillation of bow wave. Free-stream Mach number, 1.99.

~~CONFIDENTIAL~~



(b) Angle of attack, 3° ; mass-flow ratio, 0.072.
C. 26238

Figure 22. - Concluded. High-speed schlieren photographs showing oscillation of bow wave. Free-stream Mach number, 1.99.

~~CONFIDENTIAL~~



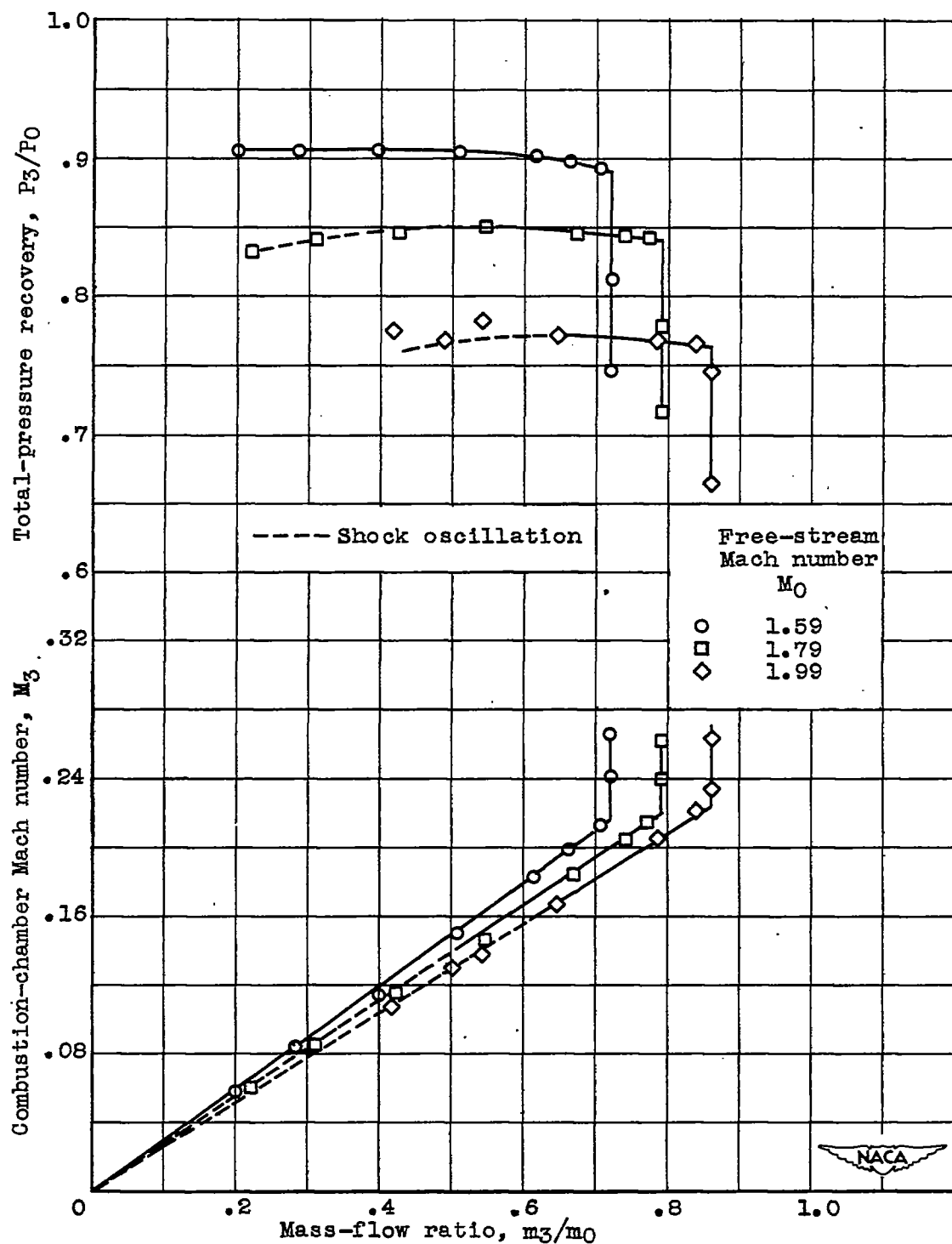


Figure 23. - Variation of total-pressure recovery and combustion-chamber Mach number with mass-flow ratio at zero angle of attack for three free-stream Mach numbers.

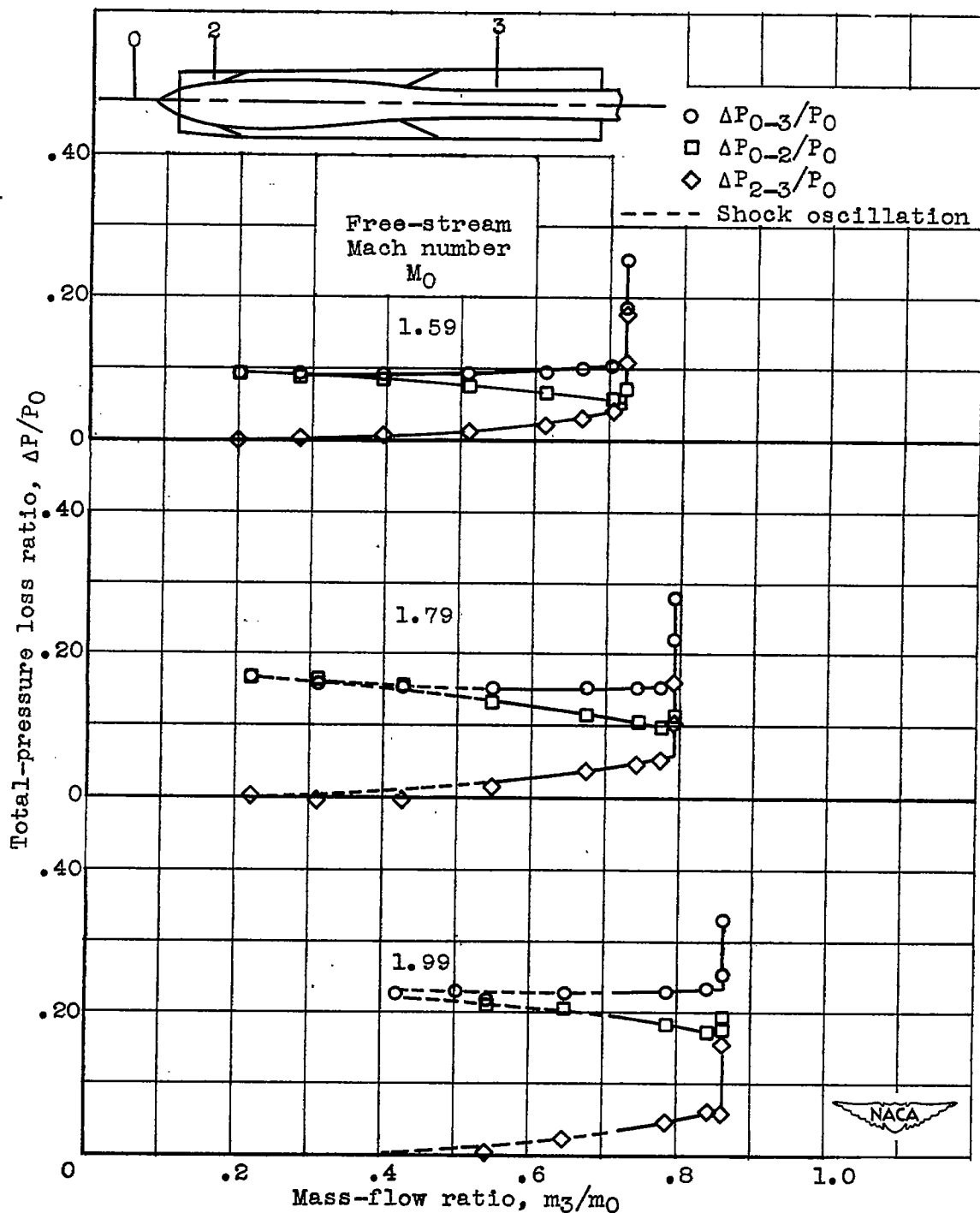


Figure 24. - Components of total-pressure loss at zero angle of attack for range of mass-flow ratios at three free-stream Mach numbers.

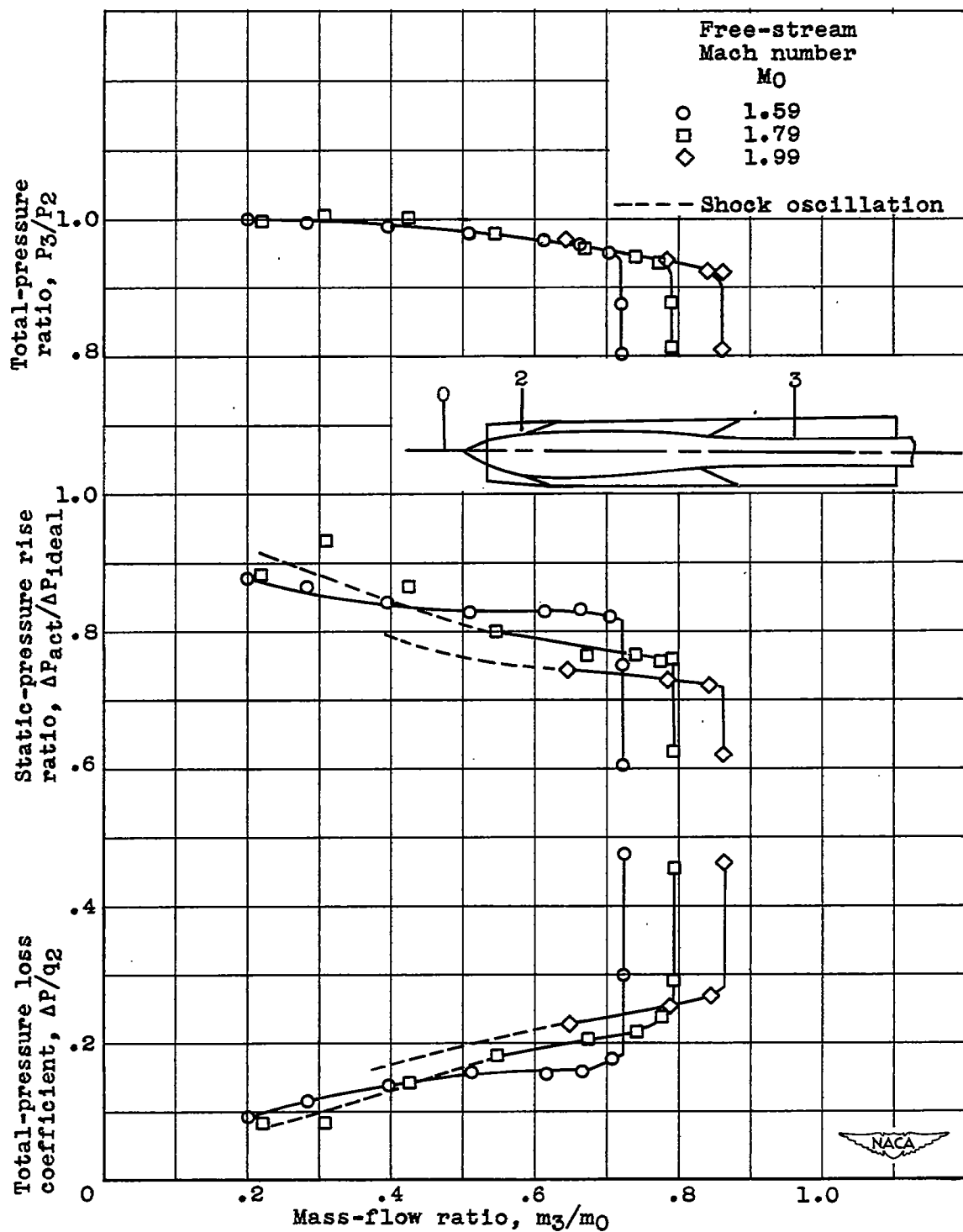


Figure 25. - Subsonic-diffuser characteristics at zero angle of attack for range of mass-flow ratios at three free-stream Mach numbers.

~~CONFIDENTIAL~~

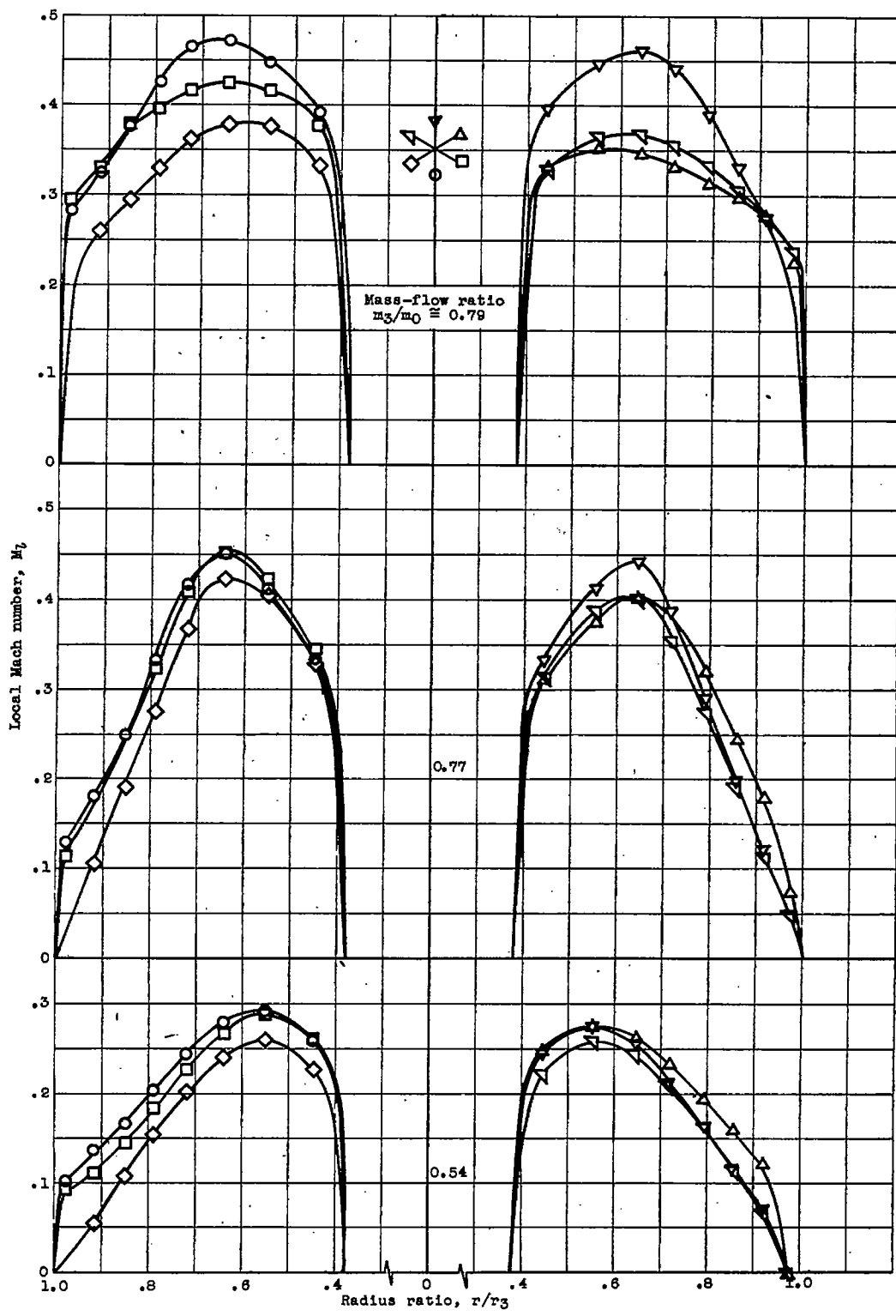
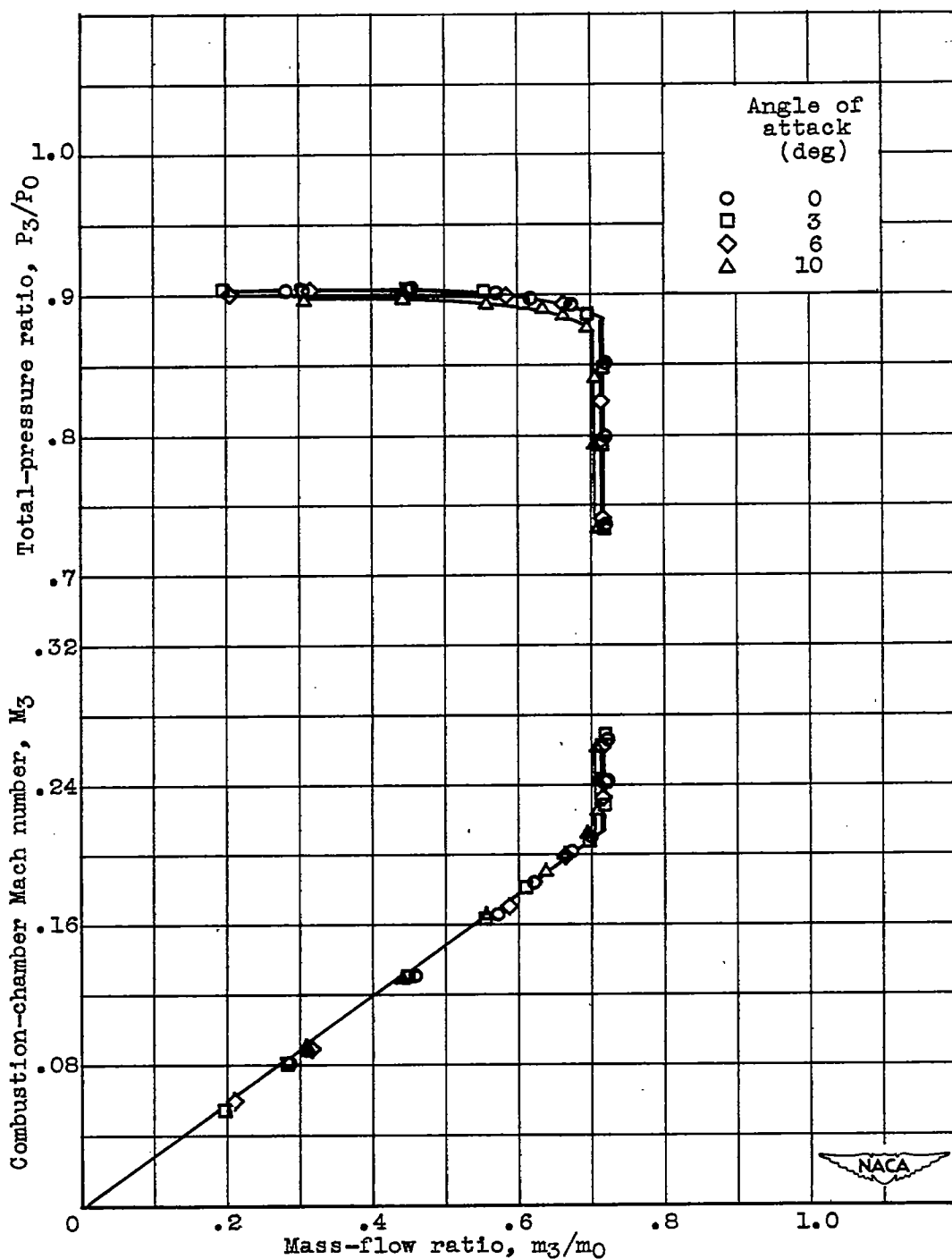


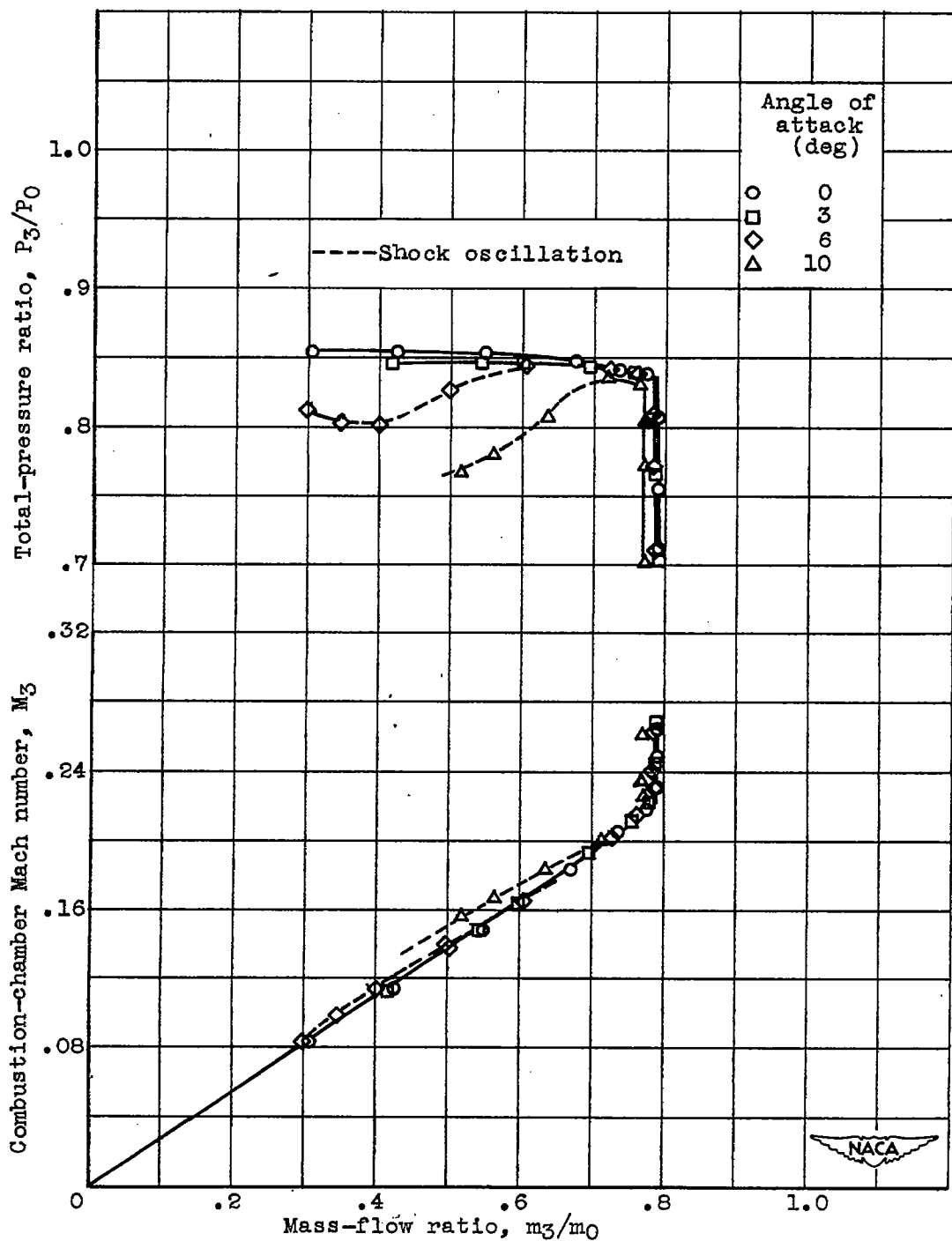
Figure 26. — Variation of Mach-number distribution at combustion-chamber inlet for several mass-flow ratios at zero angle of attack. Free-stream Mach number, 1.79.

CONFIDENTIAL



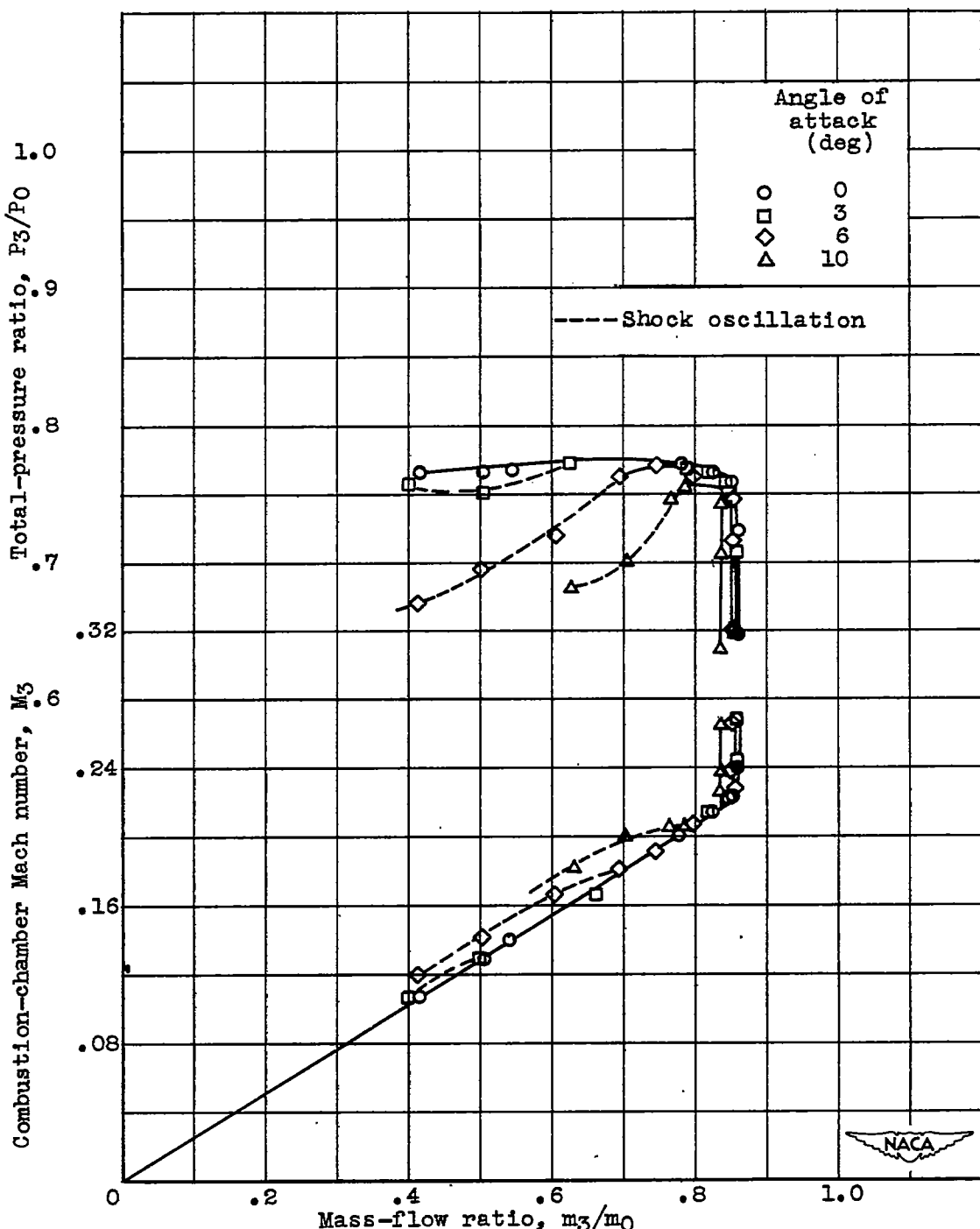
(a) Free-stream Mach number, 1.59.

Figure 27. - Variation of total-pressure recovery and combustion-chamber Mach number with mass-flow ratio at four angles of attack for three free-stream Mach numbers.



(b) Free-stream Mach number, 1.79.

Figure 27. - Continued. Variation of total-pressure recovery and combustion-chamber Mach number with mass-flow ratio at four angles of attack for three free-stream Mach numbers.



(c) Free-stream Mach number, 1.99.

Figure 27. - Concluded. Variation of total-pressure recovery and combustion-chamber Mach number with mass-flow ratio at four angles of attack for three free-stream Mach numbers.

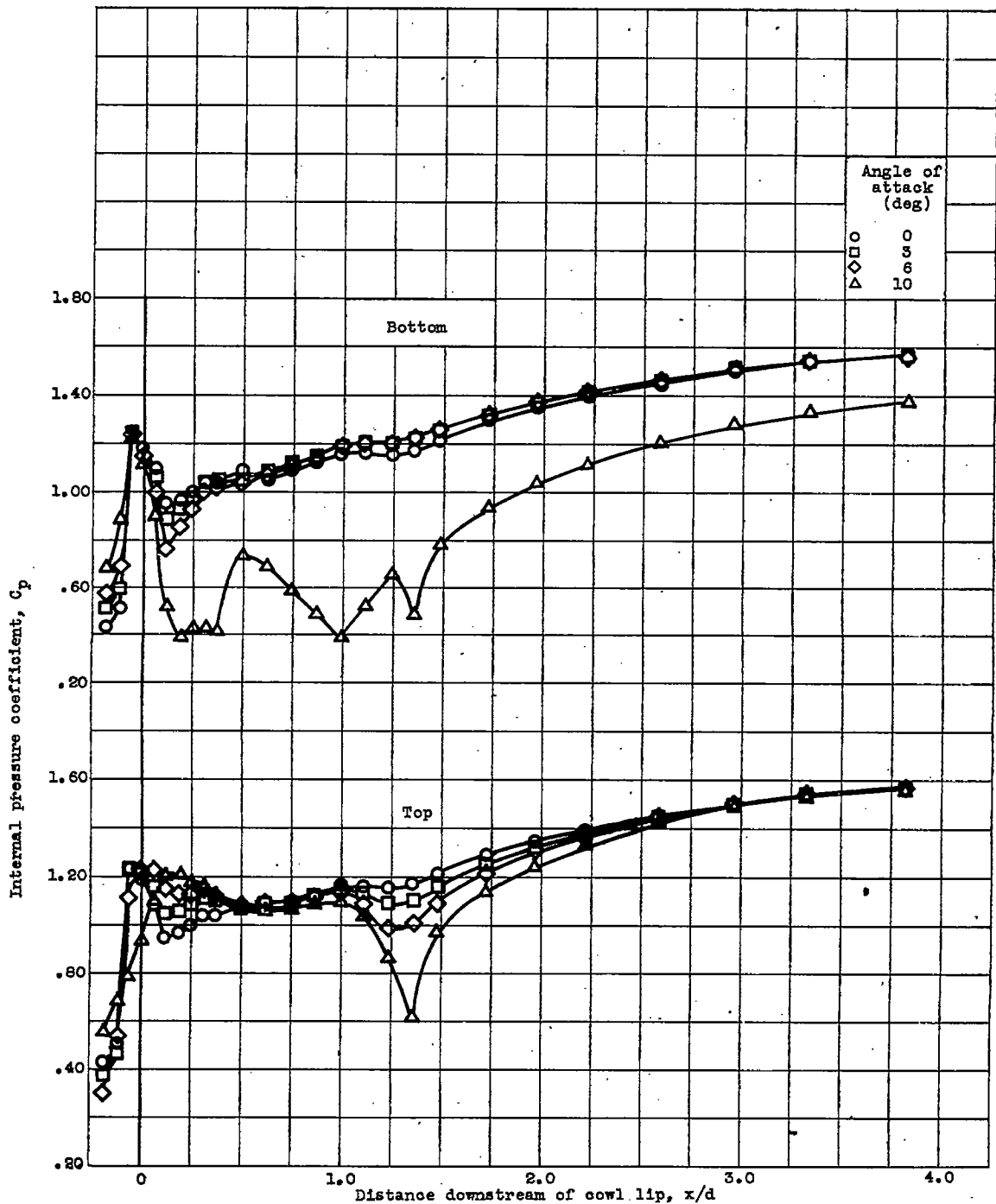


Figure 28. - Longitudinal variation of internal-pressure coefficient at constant mass-flow ratio of 0.77 for four angles of attack. Free-stream Mach number, 1.79.

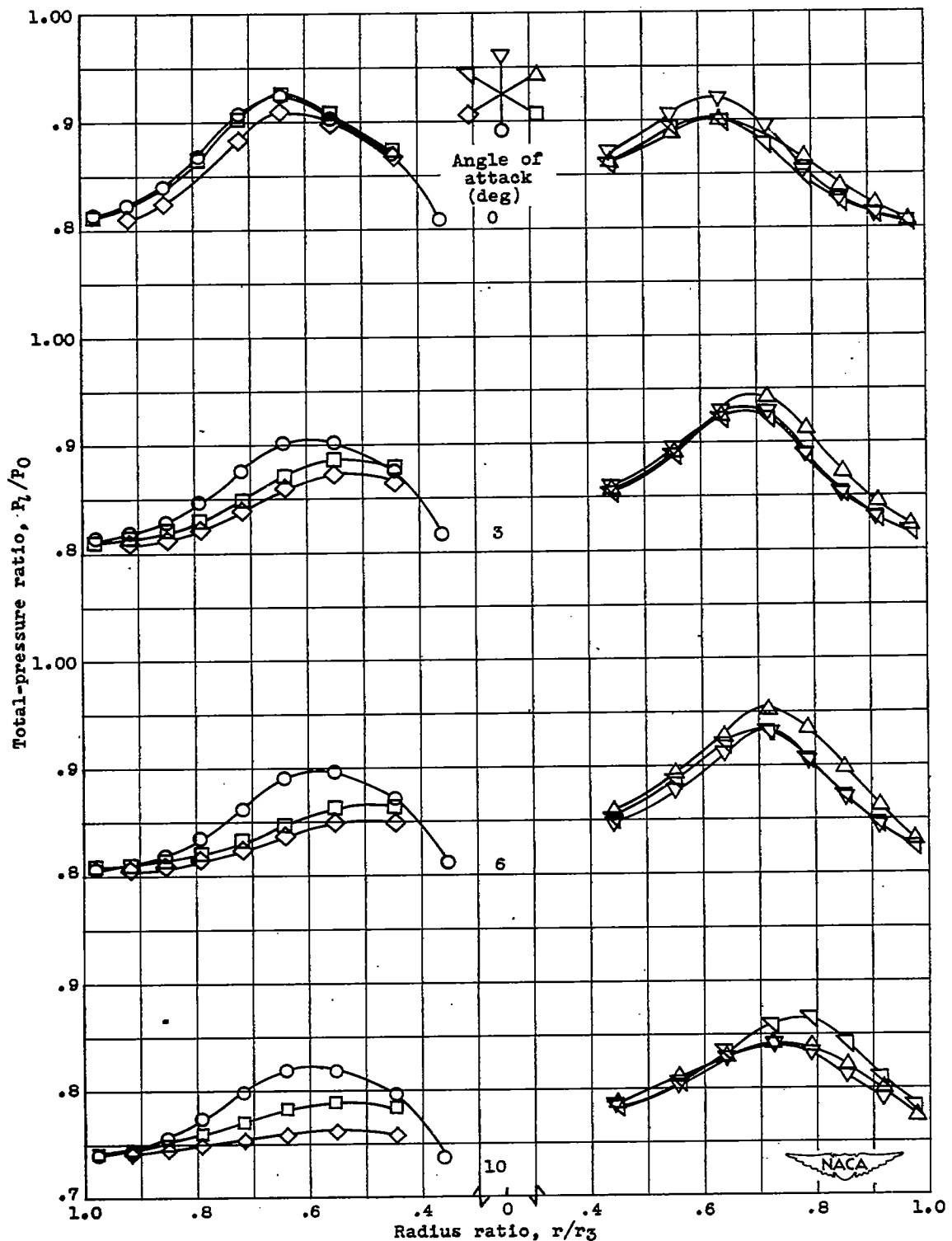


Figure 29. - Variation of total-pressure distribution at combustion-chamber inlet for constant mass-flow ratio of 0.77 and four angles of attack. Free-stream Mach number, 1.79.